

# Dynamic adhesion and friction mediated by supramolecular bonds

## Dissertation

zur Erlangung des Grades  
des Doktors der Naturwissenschaften  
der Naturwissenschaftlich - Technischen Fakultät  
der Universität des Saarlandes

von

Dipl.-Biophys. Johanna Blass

Saarbrücken

2016

Tag des Kolloquiums: 24.10.2016

Dekan: Prof. Dr. Guido Kickelbick

Mitglieder des Prüfungsausschusses:

Prof. Dr. Helmut Seidel

Prof. Dr. Roland Bennewitz

Prof. Dr. Karin Jacobs

Prof. Dr. Rainer Birringer

Dr. Thomas John

Die vorliegende Arbeit wurde am INM–Leibniz-Institut für Neue Materialien in Saarbrücken im Programmbereich *Nanotribologie* angefertigt. Ich danke dem Institut für die Möglichkeit zur Durchführung der Arbeit und bedanke ich mich bei Herrn Prof. Dr. E. Arzt, dem wissenschaftlichen Geschäftsführer des Instituts, für die fortwährende Unterstützung des Projektes. Ein großer Dank geht an meinem Betreuer, Herrn Prof. Dr. R. Bennewitz, für die vielen Diskussionen und Gespräche und das Vertrauen in meine Arbeit.

### **Eidesstattliche Versicherung**

Hiermit versichere ich an Eides statt, dass ich die vorliegende Arbeit selbstständig und ohne Benutzung anderer als der angegebenen Hilfsmittel angefertigt habe. Die aus anderen Quellen direkt oder indirekt übernommenen Daten und Konzepte sind unter Angabe der Quelle gekennzeichnet. Die Arbeit wurde bisher weder im In- noch im Ausland in gleicher oder ähnlicher Form in einem Verfahren zur Erlangung eines akademischen Grades vorgelegt.

Datum, Unterschrift

# Zusammenfassung

Die Kontrolle von adhäsiven Wechselwirkungen auf molekularer Ebene ist von besonderem Interesse im Forschungsfeld der Nanotechnologie. Im Rahmen dieser Arbeit wurde eine Oberflächenfunktionalisierung entwickelt, um die adhäsive Interaktion von Einzelmolekülen bis hin zu molekularen Ensembles zu untersuchen. Die Funktionalisierung basiert auf supramolekularen Bindungen, bestehend aus einem ditopen Konnektormolekül, das an zwei Cyclodextrin (CD) Moleküle bindet, wobei das eine CD-Molekül an die Spitze eines Rasterkraftmikroskops und das andere an eine glatte Siliziumoberfläche gebunden ist. Durch die Auswahl verschiedener Konnektormoleküle kann das dynamische Verhalten von Reibung und Adhäsion angepasst werden. Die Dynamik des Kontakts wird im Hinblick auf die Kinetik einer einzelnen Bindung sowie auf die Flexibilität der Anbindung untersucht.

Die Kontrolle von Adhäsion und Reibung wird mit Hilfe photosensitiver Konnektormoleküle erreicht, die sich durch einen externen Lichtstimulus schalten lassen. Um die Rauigkeit realer Kontakte zu überbrücken, wurden CD-Moleküle an Polymere angebunden, die ihrerseits an die Oberfläche und die AFM Spitze angebunden wurden. Die Ergebnisse dieser Arbeit tragen zu einem tieferen Verständnis der molekularen Prozesse von adhäsiver Reibung bei und zeigen eine Möglichkeit zur aktiven Kontrolle von Reibung und Adhäsion auf.



# Abstract

Understanding and controlling adhesive interactions on the molecular scale is one of the main challenges in the field of nanotechnology. A new surface functionalization was developed in this thesis for investigating the molecular origin of adhesive interactions from single molecular level to assemblies of multiple bonds. The surface functionalization is based on supramolecular bonds established by the inclusion of ditopic connector molecules into two cyclodextrin (CD) molecules, one attached to a tip of an atomic force microscope and the other attached to a flat silicon surface. By using different connector molecules, the dynamics in friction and adhesion can be tuned. The dynamics of the molecular system were studied with respect to single bond kinetics and the flexibility of the attachment.

The control of adhesion and friction was achieved by using photosensitive connector molecules which are sensitive to an external light stimuli. In order to enhance the applicability of the surface functionalization, the CD molecules were attached onto stiff polymers which can bridge the surface roughness of real contacts. The results of this thesis provide a deeper understanding of the molecular mechanisms underlying adhesive friction and open a new pathway for actively controlling friction and adhesion.





# Contributions of Co-Authors

This thesis is based on a collaboration between the Nanotribology group of Professor Roland Bennewitz at the INM - Leibniz Institute for New Materials and the Organic Macromolecular Chemistry group of Professor Gerhard Wenz at Saarland University. I would like to acknowledge the continuous support of Roland Bennewitz, Gerhard Wenz, and Marcel Albrecht in terms of financial funding, ideas and discussions through the entire scientific work. Details of the contribution of all co-authors to the individual chapters are acknowledged in the following. Chapter 2 and chapter 3 are published in peer reviewed journals in Ref.[1] and Ref.[2]. Further manuscripts based on chapter 4-7 are in preparation.

I acknowledge the Volkswagen Foundation for financial support through the program “Integration of Molecular Components in Functional Macroscopic Systems”.

## Published chapters

**Chapter 2** J. Blass, B. L. Bozna, M. Albrecht, J. A. Krings, B. J. Ravoo, G. Wenz, and R. Bennewitz. Switching adhesion and friction by light using photosensitive guest–host interactions. *Chemical Communications*, 51(10), 1830-1833, 2015.

Author contributions:

Jennifer Krings synthesized the photosensitive azobenzene connector molecule. AFM experiments were performed and analyzed by Johanna Blass. Marcel Albrecht was responsible for the synthesis of the silane and  $\beta$ -cyclodextrin molecules. Johanna Blass wrote the manuscript with contributions from Roland Bennewitz, Marcel Albrecht, Gerhard Wenz, Bart Jan Ravoo and Bianca L. Bozna. Research was directed by Roland Bennewitz, Gerhard Wenz and Bart Jan Ravoo. Authors acknowledge Devid Hero for the synthetic support in the preparation of some cyclodextrin derivatives.

**Chapter 3** J. Blass, B. L. Bozna, M. Albrecht, G. Wenz, and R. Bennewitz. Dynamic effects in friction and adhesion through cooperative rupture and formation of supramolecular bonds. *Nanoscale*, 7(17), 7674-7681, 2015.

Author contributions:

AFM experiments were performed and analyzed by Johanna Blass. Marcel Albrecht synthesized macromolecules. Johanna Blass wrote the manuscript with contribution from Roland Bennewitz, Gerhard Wenz, Marcel Albrecht and Bianca Bozna. Research was directed by Roland Bennewitz and Gerhard Wenz. Authors acknowledge Anand Jagota for fruitful discussion.

## In preparation

**Chapter 4** J. Blass, M. Albrecht, G. Wenz, and R. Bennewitz. Silane layer flexibility determines dynamic effects in friction and adhesion.

Author contributions:

Experiments were performed and analyzed by Johanna Blass. The chapter is written by Johanna Blass. Marcel Albrecht synthesized the macromolecules. Research was directed by Roland Bennewitz and Gerhard Wenz.

**Chapter 5** J. Blass, M. Albrecht, G. Wenz, and R. Bennewitz. *Cantilever stiffness determined the unbinding force of reversible bonds probed by force microscopy in thermal equilibrium.*

Author contributions:

AFM experiments were performed and analyzed by Johanna Blass. Marcel Albrecht and Jessica Brunke synthesized the CD-polymers. Marcel Albrecht and Yan Nan Zhang synthesized the ditopic PEG connector molecules. Marcel Albrecht also synthesized the cyclodextrin, silane and ditopic TEG connector molecules. The measurements and analysis of the single bond rupture force of the *polymer-polymer* system was performed by Franziska Emmerich. The chapter is written by Johanna Blass. Research was directed by Roland Bennewitz and Gerhard Wenz.

**Chapter 6** J. Blass, J. Brunke, F. Emmerich, C. Przybyski, Roland Bennewitz, G. Wenz, and M. Albrecht. Friction and adhesion of CD-polymers.

Author contributions:

Jessica Brunke and Johanna Blass contributed equally to this work. Marcel Albrecht and Jessica Brunke synthesized the CD-polymers. Marcel Albrecht was also responsible for the synthesis of the silane and  $\beta$ -cyclodextrin molecules. AFM experiments were performed by Johanna Blass and Franziska Emmerich. Cédéric Przybyski performed MALDI-TOF experiments of the CD-polymers. The chapter was written by Johanna Blass. Research was directed by Marcel Albrecht, Roland Bennewitz and Gerhard Wenz.

**Chapter 7** J. Blass, M. Albrecht, G. Wenz, and R. Bennewitz. Tuning friction and adhesion by changing supramolecular bond kinetics.

Author contributions:

AFM experiments were performed analyzed by Johanna Blass. Marcel Albrecht synthesized macromolecules. The chapter was written by Johanna Blass. Research was directed by Roland Bennewitz and Gerhard Wenz. Authors acknowledge the group of Prof. B. J Ravoo for providing the azobenzene connector molecule.

# Contents

<b>1</b>	<b>Introduction</b>	<b>1</b>
1.1	Supramolecular bonds . . . . .	3
1.1.1	Molecular components . . . . .	3
1.1.2	Kinetics of supramolecular bonds . . . . .	5
1.1.3	Bonds under force . . . . .	7
1.2	Atomic Force Microscopy . . . . .	12
1.2.1	Friction force microscopy . . . . .	13
1.2.2	Dynamic force spectroscopy . . . . .	14
1.2.3	Cantilever calibration . . . . .	17
<b>2</b>	<b>Switching friction and adhesion</b>	<b>21</b>
2.1	Introduction . . . . .	21
2.2	Results and Discussion . . . . .	21
2.3	Conclusion . . . . .	27
<b>3</b>	<b>Dynamic friction and adhesion</b>	<b>28</b>
3.1	Introduction . . . . .	28
3.2	Experimental section . . . . .	30
3.2.1	Instrumentation . . . . .	30
3.2.2	Synthesis of the ditopic connector . . . . .	30
3.2.3	Preparation of monolayer . . . . .	31
3.2.4	AFM measurements . . . . .	31
3.2.5	Data analysis . . . . .	32
3.3	Results . . . . .	32
3.4	Discussion . . . . .	36
3.5	Conclusion . . . . .	42
3.6	Supplementary Information . . . . .	43
<b>4</b>	<b>Attachment flexibility and adhesive interactions</b>	<b>45</b>
4.1	Introduction . . . . .	45
4.2	Experimental section . . . . .	47
4.3	Results . . . . .	48
4.4	Discussion . . . . .	51
4.4.1	Contact stiffness of differently aged silane layers . . . . .	51
4.4.2	Adhesion force on differently aged silane layers . . . . .	55

---

4.4.3	Dynamic effects in adhesion and friction on differently aged silane layers . . . . .	56
4.5	Conclusion . . . . .	57
4.6	Supplementary Information . . . . .	58
<b>5</b>	<b>System flexibility and bond rupture force</b>	<b>60</b>
5.1	Introduction . . . . .	60
5.2	Experimental section . . . . .	62
5.3	Results and Discussion . . . . .	63
5.3.1	Shape of the force-distance curves . . . . .	63
5.3.2	Effect of cantilever stiffness on single bond rupture force . . . . .	65
5.3.3	Impact of cantilever stiffness on adhesion of multiple bonds . . . . .	73
5.4	Conclusion . . . . .	75
<b>6</b>	<b>Friction and adhesion of CD-functionalized Polymers</b>	<b>76</b>
6.1	Impact of geometry and flexibility on friction and adhesion of CD-functionalized Polymers . . . . .	76
6.1.1	Introduction . . . . .	76
6.1.2	Experimental section . . . . .	78
6.1.3	Results . . . . .	79
6.1.4	Discussion . . . . .	83
6.1.5	Conclusion . . . . .	86
6.2	Time resolved thermal noise analysis of reversible polymer binding . . . . .	87
6.2.1	Introduction . . . . .	87
6.2.2	Results and Discussion . . . . .	90
6.2.3	Conclusion . . . . .	99
<b>7</b>	<b>Adhesive friction and bond kinetics</b>	<b>100</b>
7.1	Introduction . . . . .	100
7.2	Experimental section . . . . .	101
7.3	Results . . . . .	103
7.3.1	Loading rate dependence of adhesion . . . . .	103
7.3.2	Velocity dependence of friction . . . . .	106
7.3.3	Friction force and connector concentration . . . . .	108
7.4	Discussion . . . . .	110
7.4.1	Binding kinetics at the surface . . . . .	111
7.4.2	Loading rate dependence of adhesion . . . . .	112
7.4.3	Velocity dependence of friction . . . . .	115
7.5	Conclusion . . . . .	117
<b>8</b>	<b>Conclusions</b>	<b>118</b>
	<b>References</b>	<b>119</b>
	<b>Publications</b>	<b>119</b>

# Abbreviations

<b>Ad</b>	Adamantane
<b>AFM</b>	Atomic Force Microscope
<b>ATR</b>	Attenuated total reflection
<b>Azo</b>	Azobenzene
<b><math>\beta</math>-CD</b>	Monoamino- $\beta$ -cyclodextrin
<b>CDCl<sub>3</sub></b>	Chloroform-d
<b>CWT</b>	Continuous Wavelet Transform
<b>DFS</b>	Dynamic Force Spectroscopy
<b>ESI</b>	Electronic supplementary information
<b>DMSO</b>	Dimethyl sulfoxide
<b>Fc</b>	Ferrocene
<b>FT</b>	Fourier Transform
<b>LPD</b>	Liquid phase deposition
<b>ITC</b>	Isothermal Calorimetry
<b>IR</b>	Infrared
<b>N<sub>2</sub></b>	Nitrogen
<b>NMR</b>	Nuclear magnetic resonance spectroscopy
<b>PSD</b>	Power spectrum density
<b>PEG</b>	Polyethylene glycol
<b>RMS</b>	Root mean square
<b>SAM</b>	Self Assembles Monolayer
<b>SiO<sub>2</sub></b>	Siliconoxide
<b>TEG</b>	Tetraethylene glycol
<b>THF</b>	Tetrahydrofuran
<b>UV</b>	Ultraviolet
<b>VIS</b>	Visible
<b>VPD</b>	Vapor phase deposition



# 1 Introduction

Controlling friction and adhesion at the nanoscale is one of the challenges in the field of nanotechnology. The interaction of small contacts in the nanometer range plays a key role in the fabrication of artificial systems such as electronic [3], optical [4] and medical devices [5]. The continuous miniaturization of components requires new techniques for manipulating systems with a length scale of several nanometers. With decreasing length scale, surface properties gain importance over bulk properties promoting the field of surface science. New surface science techniques were developed in order to analyze, understand, and control the interaction of small surface contacts. A powerful surface science technique is the Atomic Force Microscope (AFM) which allows the investigation of surface properties such as adhesion and friction with molecular resolution as well as the manipulation of single molecules [6]. By means of AFM it was possible to investigate adhesive systems in nature which serve as model systems for controlling surface properties on the nanoscale. Examples of such systems are the adhesion of mussels to various kinds of surfaces [7] or the dynamics of single molecule interactions [8]. In nature, many adhesive systems are composed of assemblies of supramolecular (non-covalent) bonds [9]. Inspired by nature, much effort has been put into the construction of artificial systems based on monolayers of supramolecular binding sites [10]. The construction of artificial systems is motivated by both, the understanding of molecular recognition processes and the designing of new materials for future technologies. An interaction involving a multiplicity of bonds can exhibit a higher affinity than just the sum of all interactions due to the cooperative interaction of individual bonds. Cooperativity in this context refers to the physical interaction between independent bonds and not to the chemical interaction where one ligand can change the binding affinity of a receptor towards the next ligand as it is described in Ref.[11]. The phenomenon of physical cooperativity is referred to as multivalency effect [12] and describes the different kinetics of monovalent and multivalent interactions. The underlying mechanisms and the consequences of multivalency for the dynamics of adhesive interaction are not yet fully understood.

This thesis describes the development of a macromolecular toolkit to control adhesive interactions and to investigate the molecular mechanisms underlying the dynamic effects of adhesion and friction. This macromolecular toolkit is developed in cooperation with the group of Prof. Wenz at the Saarland University. The molecular system is based on monolayers of cyclodextrin (CD) molecules which form specific supramolecular bonds with a variety of guest molecules that are included into the hydrophobic cavity of the CD molecules in aqueous solution. The adhesive interaction between two CD-coated surfaces is established by ditopic connector molecules which bear an hydrophobic end group on either side of a short glycol chain. One hydrophobic end group forms an inclusion complex with a CD molecule on one surface, the other end group is included in a CD attached to the opposing surface. The advantage of this system lies in its versatility. Binding strength and kinetics of the individual bonds can be adjusted by solely changing the connector molecule without changing the surface functionalization. The molecular interactions are probed by means of AFM in order to obtain single molecular resolution as well as to investigate the dynamics of a multiple bond contact.

An overview of the most important concepts of this thesis are provided in the following. The molecular components of the system and the kinetics of supramolecular bonds under force are described. Furthermore, a brief introduction to the modes of measurement in AFM is provided.

In the **second chapter**, the successful application of the molecular toolkit for controlling adhesion and friction by external stimuli is demonstrated. The adhesive interaction between the AFM tip and surface is established by photoresponsive connector molecules synthesized in the group of Prof. Ravoo at the University of Münster.

**Chapter 3** is the central chapter of this thesis. In this chapter, we address the fundamental question if adhesive friction and adhesion are alike or not by investigating their dynamic effects with respect to the kinetics of single bonds and effects of multivalency.

The impact of flexibility of the cyclodextrin attachment on the dynamics of adhesion and friction is systematically studied in **chapter 4**.

In **chapter 5** we demonstrate that the stiffness of the force probe determines the single bond rupture force rather than the molecular linker stiffness.

As a step towards applications, stiff polymers were synthesized and attached to surfaces. The polymers carry several CD molecules and can bridge gaps between rough surfaces. In **chapter 6** the impact of the configuration of polymer attachment on adhesion is investigated.



In **chapter 7**, the versatility of our molecular toolkit approach was utilized to study the effect of individual bond kinetics on the dynamic cooperative effects in adhesion and friction.

In **chapter 8**, a summary of the main results of this thesis is provided.

## 1.1 Supramolecular bonds

Supramolecular interactions play a key role in many biological systems such as the movement and attachment of single-cell organisms, intracellular transport and infections [13] or specific antigen-antibody recognition in the immune system [8]. In contrast to covalent bonds, supramolecular bonds are reversible and consist of two or more components where one component is included into the other [14]. The complexation reaction can be driven by a variety of forces such as electrostatic interactions including ion-dipole, dipole-dipole and hydrogen bonding or less specific and often weaker effects such as van der Waals forces and the hydrophobic effect [14]. Due to their specificity and reversibility, supramolecular bonds are used in artificial systems in order to provide specific recognition [15], designing self-healing polymers [16] or studying cooperative interaction of several individual bonds [17].

An example of a artificial supramolecular bond is the host-guest interaction between cyclo-oligosaccharides and their guest molecules which are used as complexing agents for weak hydrophobic interactions in aqueous solution [18]. In this theses, cyclodextrin inclusion complexes are used in order to establish adhesive interaction between two cyclodextrin functionalized surfaces. The macromolecular components are synthesized by the group of Prof. Wenz localized at the Saarland University, if not stated differently. In the following, the molecular components of the surface functionalization are described.

### 1.1.1 Molecular components

The surface functionalization is based on cyclomalto-oligosaccharides (cyclodextrins) which are attached to a flat silicon surface in a two step process. First, a silane layer consisting of 3-isothiocyanatopropyl-triethoxysilane molecules is attached to the surface. The molecules of the layer expose an reactive group towards the solution. Details of the silane layer formation and its impact on adhesive interactions are provided in chapter 4. In a second step, monoamino- $\beta$ -cyclodextrin molecules (CDs) are attached to the silane layer by forming

a thiourea bond between the amino group of the CD and the isothiocyanat group of the silane molecule.

Cyclodextrin molecules are chemically stable and consist of six to eight circularly-arranged sugar units which form a hydrophobic cavity of 4.7 Å-8.4 Å in their center which includes hydrophobic guest molecules. The number of sugar units is reflected by the indicator  $\alpha$ ,  $\beta$ ,  $\gamma$  where  $\alpha$  stands for the smallest molecule and  $\gamma$  for the largest. In this study,  $\beta$ -Cyclodextrins are used as host molecules with an average cavity diameter of 6.25 Å (see Fig.1.1(a)). The inclusion reaction is driven by the hydrophobic effect including entropic and enthalpic contributions. The enthalpy change dominates the inclusion reaction of cyclodextrins and is caused by the penetration of the guest molecules into the CD cavity [19]. During penetration six to seven hydrogen bonds are displaced from the cavity and hydrogen bonds are formed between the host cavity and the guest molecule. The minor entropy change is caused by the loss of the hydration shell which surrounds the host molecule [19].

We investigate cyclodextrin inclusion of three different guest molecules, adamantane, ferrocene and azobenzene, which differ in binding strength and kinetics (see Fig.1.1(b)). The adamantane end group exhibits the highest binding affinity with  $\beta$ -CD, followed by the azobenzene group with a lower binding affinity and the ferrocene group with the lowest binding affinity. The photosensitive azobenzene guest molecule was synthesized in the group of Prof. Ravoo at the University of Münster and can be switched between two states by an external light stimulus. The effect of the switching process on adhesion and friction is investigated in chapter 2.

The guest molecules carry two hydrophobic end groups which are connected via a short glycol chain. Due to their ditopic design the guest molecules can connect two CD-functionalized surfaces by forming an inclusion complex with one CD on either surface. The short chain should exclude that one connector molecule complexes with two CDs of the same surface leading to a passivation of the surface. For comparison, a long polyethylene glycol chain with two hydrophobic end groups was used to gain information about the complexation reaction when using a flexible molecular linker. We demonstrate in chapter 5 that the flexibility of the linker molecule does not affect the rupture force of a single complex.

The complexation reaction proceeds in aqueous solution. In order to enhance the water solubility of the connector molecules, a positive charge or a piperazine ring were included into the short glycol chain, respectively. The positive amino group in the chain of the adamantane and ferrocene connector is located close to the hydrophobic end group and is

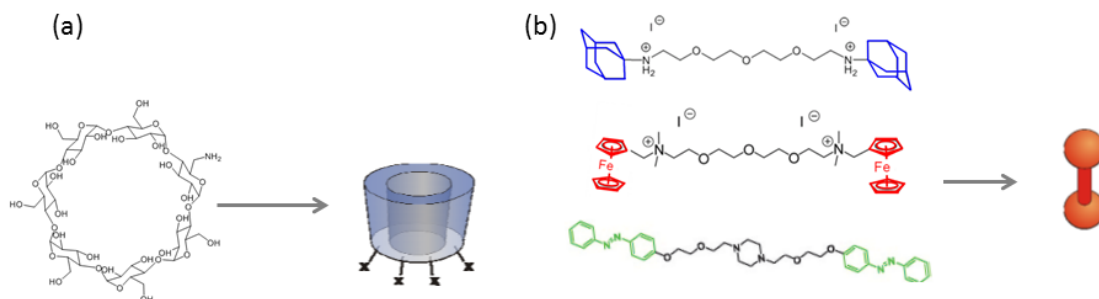


Figure 1.1: Chemical structure and schematic drawings of (a) monoamino- $\beta$ -CD and (b) the ditopic connector molecules from top to bottom: adamantane, ferrocene and azobenzene.

expected to slightly lower the binding affinity of the connector molecule [20].

In line with their ability to connect opposing surfaces, the ditopic guest molecules will be referred to as connector molecules within this study. The supramolecular complex formed by two  $\beta$ -CDs and one connector molecule will be addressed as bond in the following. The binding affinity and reaction kinetics of the different bonds are subject of this study and are investigated by means of AFM. Concepts of the intrinsic dissociation rates of supramolecular bonds and of dissociation under force are provided in the following sections.

### 1.1.2 Kinetics of supramolecular bonds

In aqueous environment, cyclodextrin molecules form inclusion complexes with their hydrophobic guests. Due to thermal activation the inclusion complex breaks and rebinds up to several thousand times per second. The dynamic equilibrium can be described by the following reaction



where  $k_{\text{on}}^0$  and  $k_{\text{off}}^0$  are the reaction rates of the forward and backward reaction. The parameter A represents the unbound state of independent host and guest molecules and B stands for the bound state of a host-guest complex (see Fig.1.2(a)). The stability of the complex is driven by enthalpy as well as by entropy [19] and can be described by the binding constant  $K = k_{\text{on}}/k_{\text{off}}$  which is typically in the order of  $10^3 - 10^5 \text{ mol}^{-1}$  for  $\beta$ -CD complexes [21]. The strongest known inclusion complex is formed between  $\beta$ -CDs and adamantanyl derivatives [19]. The complex stability is mostly determined by the off-rate since the on-

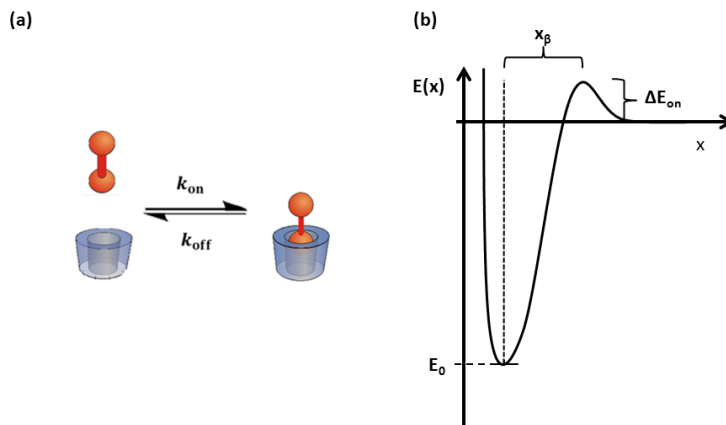


Figure 1.2: (a) Scheme of the host-guest reaction with the characteristic reaction rates  $k_{\text{on}}$  and  $k_{\text{off}}$ ; (b) Scheme of the energy landscape of a simple host-guest bond. The bond potential is described as a one-well potential with the width  $x_\beta$ , the depth  $E_0$  and the excitation energy  $\Delta E_{\text{on}}$ .

rate is diffusion limited and in the order of  $10^9$  ( $\text{mol}^{-1}\text{s}$ ) for most guest molecules [22]. The off-rate is specific for each guest molecule as it is determined by the energy landscape of the respective bonds. For host-guest interactions between a cyclodextrin and their guests the energy profile exhibits one global minimum  $\Delta G_0$  (s. Fig.1.2(b)). The width of the energy barrier  $x_\beta$  is typically in the range of  $0.1 - 1$  nm [8]. The energy barrier can be overcome by thermal activation leading to the force scale  $f_\beta = k_B T / x_\beta$ . In thermal equilibrium the bond exhibits a characteristic life time of the respective supramolecular bond  $\tau = 1/k_{\text{off}}^0$  which can span from  $\mu\text{s}$  to several years. In friction and adhesion measurements, a force is applied to the bond which lowers the life time of such bonds by orders of magnitude such that slow systems can be investigated on the time scale of an AFM [8].

The time scales are different for supramolecular bonds. The lifetime of  $\beta$ -CD complexes is rather small and in the order of milliseconds which is faster than the time scale of an AFM measurement. We will demonstrate in chapter 3 that our ditopic cyclodextrin inclusion complexes are probed in thermodynamic equilibrium which was demonstrated in previous studies for monotopic cyclodextrin complexes [23].

### 1.1.3 Bonds under force

Whenever two surfaces come in mutual contact, bonds are formed resulting in an attractive force preventing the surfaces from separation or sliding. The respective forces depend on the number and strength of the bonds which are determined by the time scale of bond formation and rupture. In this section, the dynamic behavior of single and of multiple bonds under force is addressed separately for adhesion and friction.

#### Adhesion

The dynamics of reversible bonds were first described by Bell [24] and later Evans and Williams developed a model to describe the kinetics of single and later multiple bonds under force [8]. The dynamics of single molecules are discussed in the beginning of this paragraph and a description of multiple bonds follows in the second part.

**Single bonds** The lifetime of a single bond can be lowered by applying an external force. Bell predicted that the rate of dissociation increases exponentially with the applied force

$$k_{\text{off}} = k_{\text{off}}^0 e^{\frac{f \times x_{\beta}}{k_{\text{B}} T}} = k_{\text{off}}^0 e^{\frac{f}{f_{\beta}}} \quad (1.2)$$

where  $k_{\text{off}}^0$  is the thermally activated off rate when no force is applied and  $x_{\beta}$  is the width of the energy barrier between the bound and unbound state. The parameter  $f_{\beta} = k_{\text{B}} T / x_{\beta}$  describes the force scale of the inclusion reaction.

In dynamic force spectroscopy experiments the force is applied by pulling on one binding partner that is attached to an AFM tip while the other is attached to a flat substrate. Assuming a pulling direction along the reaction coordinate, the force ramp acting on the bond is the product of effective contact stiffness and pulling velocity. The effective contact stiffness is the resulting spring constant of the molecular spring  $k_{\text{mol}}$  and the cantilever spring  $k_{\text{c}}$  coupled in series  $k_{\text{eff}} = k_{\text{mol}} \times k_{\text{c}} / (k_{\text{mol}} + k_{\text{c}})$ . The applied force causes a tilt of the energy landscape such that the barrier between the bound and unbound state is lowered [24]. The lower energy barrier results in a higher off-rate compared to thermal equilibrium. For slow pulling velocities, the bond is loaded with a slowly increasing force until it unbinds thermally at a force only slightly higher than in thermal equilibrium. For high pulling rates, the bond is loaded fast which does not give the bond the same time to detach thermally. Hence, higher loading rates result in a higher rupture force. Evans proposed a linear increase of the most probable rupture force  $f^*$  with the logarithm of the

pulling rate  $r$  [8]

$$f^* = \frac{k_B T}{x_\beta} \ln \left( \frac{r x_\beta}{k_{\text{off}} k_B T} \right) = f_\beta \ln \left( \frac{r}{k_{\text{off}} f_\beta} \right). \quad (1.3)$$

A large number of studies on different molecular systems has confirmed this logarithmic rate dependence [25, 26, 27]. In contrast, no rate dependence of the single bond rupture force was observed for cyclodextrin inclusion complexes [23, 17]. The high reaction rates of CD inclusion complexes compared to the time scale of a pulling experiment lead to a continuous un- and rebinding of the bond resulting in a thermal equilibrium situation. This finding was in agreement with the theory of Friddle et al. who demonstrated that a plateau force develops for low loading rates caused by the harmonic potential of the cantilever [28]. In case of supramolecular bonds with reaction rates faster than the response time of the cantilever, three loading force regimes were introduced: the monostable regime, fast rebinding and kinetic unbinding regime (see Fig.1.3). For low loading forces, when the distance between tip and surface is small, the presence of the AFM tip enhances the rebinding of broken bonds resulting in a monostable regime (see Fig.1.3A). For intermediate loading forces, a second minimum is created outside the potential well of the molecular bond. The energy barrier between the two potential wells is low so that a rebinding of bonds is still probable (see 1.3B).

At a certain force  $f$ , the binding  $k_{\text{on}}$  and unbinding rates  $k_{\text{off}}$  are given by [29]

$$k_{\text{off}} = k_{\text{off}}^0 \exp \left[ \frac{1}{k_B T} \left( f x_\beta - \frac{1}{2} k_c x_\beta^2 \right) \right] \quad (1.4)$$

$$k_{\text{on}} = k_{\text{off}}(f) \exp \left[ \frac{1}{k_B T} \left( \Delta G - \frac{f^2}{2k_C} \right) \right] \quad (1.5)$$

where  $x_\beta$  is the location of the energy barrier and  $f/k_c$  represents the displacement of the force probe potential.  $\Delta G$  is the binding energy in thermodynamic equilibrium of the complexing reaction obtained for example in Isothermal Calorimetry Measurements (ITC). The rupture occurs at the force  $f_{\text{eq}}$  when the off-rate exceeds the on-rate. At this distance, the potential energy stored in the cantilever spring equals the binding energy of the bond potential  $\Delta G = f_{\text{eq}}^2/(2k_C)$  so that [29]

$$f_{\text{eq}} = \sqrt{2k_C \Delta G}. \quad (1.6)$$

In reality, single-bond contacts are rare and much effort has put into the preparation of single molecule experiments. In real contacts, multiple bonds cross the interface which has

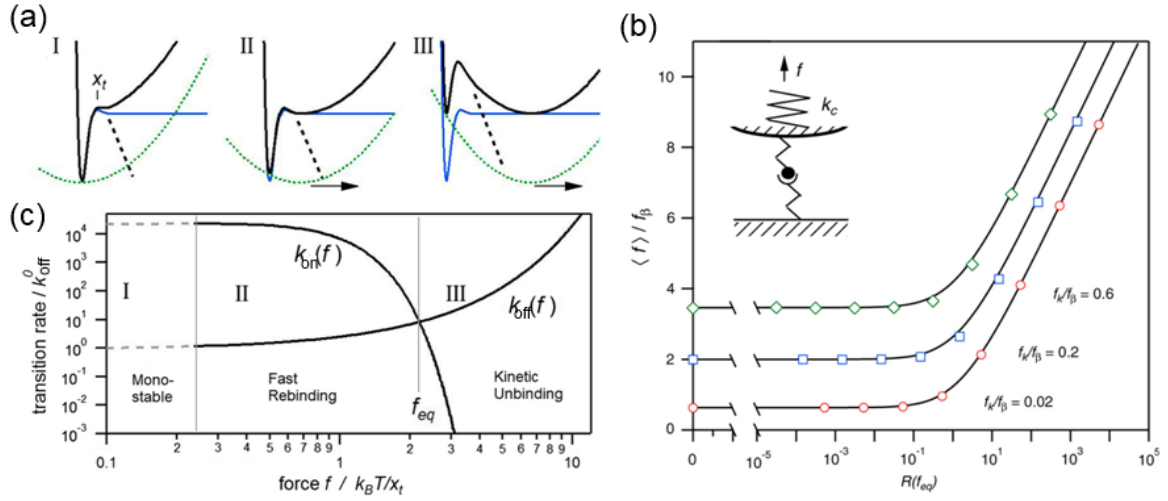


Figure 1.3: (a) Sketch of the 1D energy landscape in the monostable (I), fast rebinding (II) and kinetic unbinding (III) regime. The blue solid line reflects the bond potential, the dotted green line the harmonic potential of the force probe and the black line is the superposition of both. (b) The transition rates in the unit of  $k_{off}^0$  are given as a function of loading force scaled to the force scale  $f_\beta$ . The interception of both between regime II and III reveals the equilibrium rupture force  $f_{eq}$ . In (c) the rate dependence of the most probable rupture force ( $\langle f \rangle$ ) is shown where a specific plateau develops for each cantilever stiffness at low loading rates. For high loading rates, a linear increase proportional to the  $\ln(R)$  is shown. The figure is adopted from Ref.[29].

an dramatic effect on the dynamics of the overall system.

**Multiple bonds** In contrast to single bonds, the situation of multiple bond contacts is more complex since the bonds may interact cooperatively. Cooperativity in this context refers to the collective behavior of bonds and does not include chemical interactions of neighboring binding sites. Previous studies have shown that the dynamics of the overall system change dramatically when several bonds are involved [17, 8]. There are two limiting cases which are understood so far: all bonds are arranged in parallel or all bonds are attached in series. If all bonds are parallel, the lifetime of the overall system is increased by several orders of magnitude in comparison to a single bond because the probability that all bonds unbind simultaneously decreases with an increasing number of bonds. This effect is known as the multivalency effect [17]. Consistently, the probability to find all bonds formed simultaneously decreases with an increasing number of bonds resulting in a rupture force slightly lower than  $N \times f_\beta$  [8]. Williams developed a model to predict

the most probable rupture force which is highly loading rate dependent in the far from equilibrium regime [30]

$$F_{\text{zipper}} = f_{\beta} \left[ \ln \left( \frac{r_f}{f_{\beta} k_{\text{off}}} \right) + \ln(N) \right] \quad (1.7)$$

with the parameters  $r_f$  as loading rate and the number of bonds  $N$ . A zipper like attachment leads to a subsequent peeling of single bonds which only slightly affects the off-rate compared to a single bond resulting in a similar rupture force [30]

$$F_{\text{parallel}} \propto f_{\beta} N \left[ \ln \left( \frac{r}{f_{\beta} k_{\text{off}}} \right) - \ln \left( \frac{F_{\text{parallel}}}{f_{\beta}} \right) \right]. \quad (1.8)$$

The case of the AFM tip is more complex since the bonds are attached on different heights leading to an non-equal load shearing. A multiple bond model that covers the non-equal load shearing was developed recently by Guerra et al. [31] in response to our study of dynamics of friction and adhesion mediated by supramolecular bonds in chapter 3.

## Friction

A force is required when sliding two surfaces against each other which is referred to as the friction force. The friction force can be divided into the static friction force which prevents the surfaces from moving and the dynamic friction force which acts against the movement of sliding. The friction force on the molecular scale is commonly described by the Prandl-Thomlinson model that depicts the tip and surface as a single-asperity contact that jumps from one energy minimum to the next [32]. In the adhesive friction regime the energy dissipation is mainly caused by the reversible rupture of multiple molecular bonds. Similar to the multiple bond rupture in adhesion, Filippov et al. introduced a friction model including the multiple bond kinetics [33]. The thermally activated rupture and rebinding of interfacial bonds is limited by the activation energy barrier  $\Delta E_{\text{off}}$  and  $\Delta E_{\text{on}}$  and the respective time scales  $k_{\text{off}}^0$  and  $k_{\text{on}}^0$ . During sliding, each bond is stretched resulting in a force which lowers the activation barrier  $\Delta E_{\text{off}}$ . The bonds can be modeled by elastic springs bridging the two surfaces as shown in Fig.1.4 with a stiffness  $k_{\text{bond}}$  and equilibrium length  $l_0$ . The motion of the top plate with a mass  $M$  along the coordinate  $x$  with the velocity  $v$  can be described by the following differential equation [33]

$$M\ddot{x} + \eta\dot{x} + F_b + k_C(x - vt) = 0. \quad (1.9)$$



where  $\eta$  is the damping coefficient and  $F_b$  equals the sum of the interfacial bonds  $F_b = \sum q_i f_i^x$ . A bond bridges the interface only when it is attached to both surfaces which is reflected in the parameter  $q_i$  that can be in the bound state ( $q_i = 1$ ) or unbound state ( $q_i = 0$ ). In the bound state, one bond causes the elastic force  $f_i = k_{\text{bond}}(l_i - l_0)$  where  $l_i$  is the length of the bond under force. Filippov et al. describe three different velocity regimes: the low-velocity sliding regime, stick-slip motion and high-velocity sliding regime. They introduced the parameter  $k_{\text{bar}}$  which reflects the rate of decrease of the energy barrier  $\Delta E_{\text{off}}$  initiated by the stretching of the bond  $k_{\text{bar}} = k_{\text{bond}} v x_\beta / k_B T$ . At a critical velocity  $v_c$ , the rate of decrease  $k_{\text{bar}}$  equals the thermally activated off-rate  $v_c = k_{\text{off}} k_B T / (k_{\text{bond}} x_\beta)$ . In the low-velocity regime, the thermally activated bond dissociation dominates which implies the fact that the off-rate is faster than the decrease of energy barrier  $v < v_c$ . Simulations revealed no correlation between the individual rupture events corresponding to the near equilibrium regime [33]. In the intermediate velocity regime,  $v \geq v_c$ , the thermal activated unbinding competes with the stretching induced rupture resulting in a chaotic stick-slip behavior due to the cooperative rupture of multiple bonds. For high sliding velocities, when the contact time is too short to allow rebinding of bonds, a transition to a smooth sliding without stick-slip is observed which is dominated by the viscous damping term  $F = \eta v$ . In this model, contact time effects play a crucial role in friction experiments. Beyond the time scale of (un)binding of supramolecular bonds, there are further interactions which cause an increase of the static friction force. Li et al. have shown that there is a linear increase of the static friction force as a function of the logarithmic contact time in the range of 0.1 s to 100 s [34]. They relate this aging effect to the formation and strengthening of chemical bonds such as hydrogen bonds, van der Waals interaction and the formation of new covalent bonds.

In summary, models are available for dynamic adhesion and friction forces including the kinetics of single bonds. It is important to note that the model in adhesion is valid only for cooperativity effects where all bonds are arranged in parallel. In case of an AFM tip the situation is more complex since the bonds are attached on different heights due to the curvature of the tip apex. When this thesis project started, no model existed describing both, the dynamic effects in friction and adhesion for bonds attached on different heights. Our results on dynamic effects in friction and adhesion have triggered a simulation study which was recently published in Ref. [31].

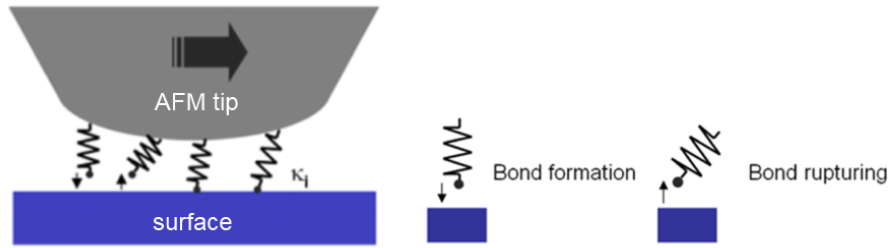


Figure 1.4: Sketch of bond formation and rupture between an AFM tip and surface during sliding. Graphic adapted from Ref.[35].

## 1.2 Atomic Force Microscopy

Atomic Force Microscopy (AFM) belongs to the scanning probe techniques where a sharp tip scans a sample surface in order to obtain topography information or gain information about the tip-surface interaction. The AFM was developed by Binnig, Quate and Gerber in 1986 [36] and was introduced as a combination of scanning tunneling microscopy and stylus profilometry. High resolution is provided by an atomically sharp tip that is attached to a flexible cantilever which is mounted on a piezo stage. A scheme of the instrument is provided in Fig.1.5. The tip-surface interactions leads to a bending of the cantilever beam either in the direction of the surface (attractive forces) or in the opposite direction (repulsive forces). In most instruments, the bending of the cantilever is optically traced by a light beam which is reflected from the cantilever backside onto a photo detector. By using a four segment detector, torsional  $[(A+C)-(B+D)]$  and vertical bending  $[(A+B)-(C+D)]$  of the cantilever can be quantified. The information about the vertical bending of the cantilever is applied to a feedback loop which allows the control of the cantilever height with picometer resolution. The precise control allows the non-destructive investigation of soft samples which is particularly important in the field of biology or macromolecular chemistry. Besides the classical imaging modes, the AFM can operate in the dynamic force spectroscopy mode where it approaches towards and retracts from the surface in order to quantify tip-surface interactions.

In this chapter we provide experimental details for friction force microscopy and force spectroscopy which are the most relevant modes in this study. A detailed description of the other operation modes of an AFM can be found in the Ref.[37].

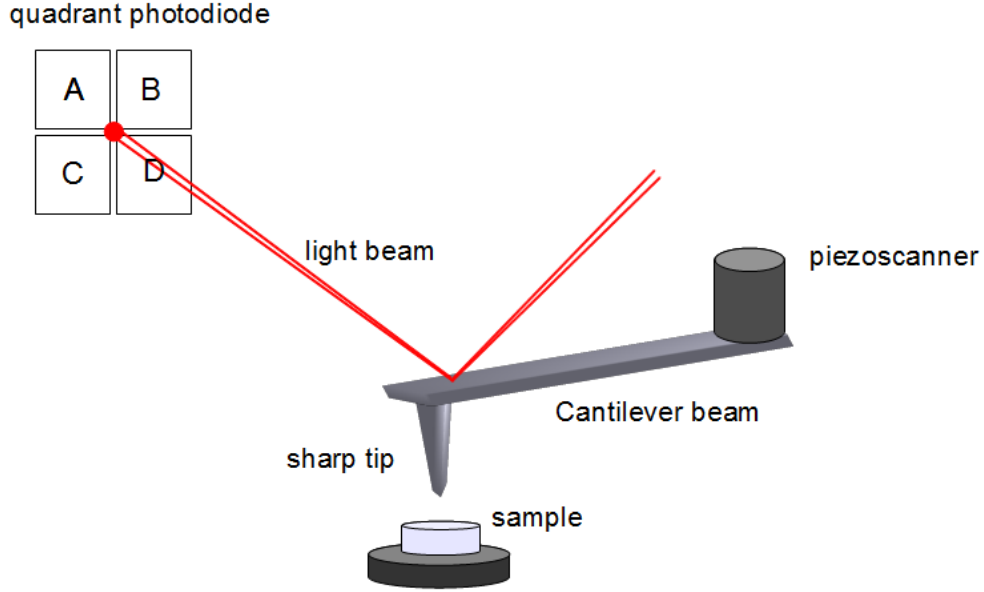


Figure 1.5: Scheme of an AFM with optical detection of the tip-sample interaction via a four segment detector.

### 1.2.1 Friction force microscopy

The friction force between the AFM tip and surface can be quantified in a friction loop when scanning forward and backward across the sample. A schematic drawing of a friction loop is provided in Fig.1.6. The lateral movement is carried out perpendicular to the cantilever axis in order to avoid a buckling of the cantilever and to record the normal and torsional bending of the cantilever independently. The adhesive interactions between tip and surface cause a torsion of the cantilever which can be detected as the lateral force signal on the photo detector. The hysteresis between the lateral force of the trace and retrace reveals the dissipated energy which is directly related to the mean friction force  $\bar{f}_1$ . The friction force refers to the mean lateral force and can be derived from the lateral deflection of the cantilever within the friction loop

$$\bar{f}_1 = \frac{\bar{f}_1^{\text{trace}} - \bar{f}_1^{\text{retrace}}}{2}. \quad (1.10)$$

In this study, the adhesive friction regime is investigated so that other effects such as surface wear or topography effects were minimized. In order to avoid these contributions, the normal load is kept below 1 nN and a small scanning area of 50 nN was chosen which is large enough to represent a sufficient number of molecules but small enough to avoid

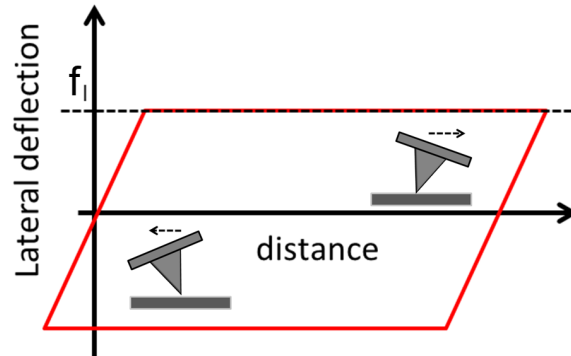


Figure 1.6: Sketch of a friction loop,  $f_l$  indicates the mean friction force. The insets indicate the direction of torsion of the AFM tip during scanning.

topographical effects such as roughness or surface contamination. The gains of the tip height feedback loop were kept low in order to avoid a readjustment of the normal force due to cross-talk between the lateral and normal signal e.g. during stick-slip events.

The dynamic effects in friction were investigated by varying the scanning speed in the range of 10 nN/s to 1000 nN/s. The velocity range was limited by instrumental effects such as drift for lower velocities and by viscous effects between the cantilever and the surrounding liquid when scanning fast. During a dynamic friction experiment, the velocity was first increased and subsequently decreased in order to exclude systematic errors caused by drift or ageing effects within a measurement series.

Friction and adhesion experiments in this study were performed in a droplet of about 500  $\mu\text{L}$  instead of a commonly used liquid cell. The droplet has the advantage that no contamination from mounting the sample such as glue, or residues on the components of the liquid cell are dissolved in the liquid. Further experimental details are provided in the experimental section of each chapter.

## 1.2.2 Dynamic force spectroscopy

The dynamics of adhesive interactions between an AFM tip and surface in normal direction can be investigated in force spectroscopy measurements. The force versus the separation distance can be assessed in force-distance curves (f-d curve) where the AFM tip is approached to and retracted from the surfaces. A scheme of the vertical deflection signal of a f-d curve is given in Fig.1.7.

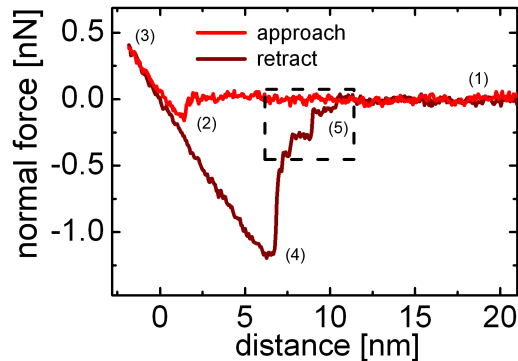


Figure 1.7: Example of a force-distance curve, the dotted area depicts the rupture of single and multiple bonds. The numbers refer to prominent points in the f-d curve and are described in the text.

In the beginning of a f-d curve, tip and surface are well separated so that no surface force is acting on the AFM tip. At this distance, the vertical deflection signal is set to zero (1). During approach, the distance between tip and surface decreases and often a snap-in occurs several nanometers above the surface (2) indicating long-range attractive forces. In the repulsive regime tip and surface are in direct contact until a defined setpoint is reached (3) and the cantilever is retracted from the surface. In this study, the setpoint is kept below 1 nN in order to avoid tip wear and surface damage. Due to attractive forces, the cantilever remains at the surface until the restoring force of the cantilever exceeds the adhesion force and a snap-off occurs (4). This maximum force is referred to as the pull-off force in this study. During retraction several rupture events can be detected when using a compliant cantilever (5). In single force spectroscopy experiments, the last rupture event reveals information about the rupture force of a single molecular complex [23]. The resolution of rupture events depends on the stiffness of the cantilever. For soft cantilevers, a high sensitivity goes along with a high noise level and a high inertia leading to slow response times of the cantilever. Cantilevers with a high stiffness exhibit a lower noise level and lower inertia but cannot resolve single rupture events due to their low sensitivity. In this study, rather soft cantilevers with a stiffness of 0.1 N/m to 0.35 N/m are used in order to achieve high sensitivity at a reasonable noise level for observing single pull-off events.

In the last step, tip and surface are separated and the cantilever remains in its relaxed position (1). The relaxed position of the retract part of a f-d cycle is commonly used as a baseline of the force measurement which can cause some misinterpretation of the data.

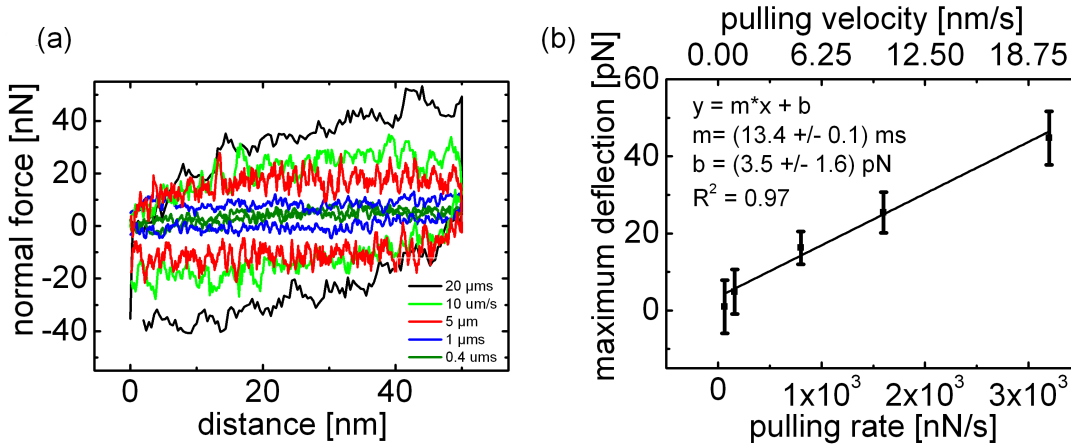


Figure 1.8: (a) Vertical deflection of force-distance cycles in water,  $100 \mu\text{m}$  above the surface with cantilever stiffness of  $0.17 \text{ N/m}$ ; (b) average maximum deflection in relation to resting position, the error bar represents the standard deviation of 10 cycles.

For high velocities, approach and retract curve do not overlap due to viscous friction effects between the cantilever and liquid environment. The contribution of hydrodynamic drag was quantified when moving the cantilever in water  $100 \mu\text{m}$  above the surface. The cantilever was moved  $50 \text{ nN}$  up and down in  $z$ -direction with different velocities and the force trace was recorded (see Fig.1.8(a)). Starting at  $0 \text{ nN}$ , the vertical deflection increases slowly until a saturation regime with a maximum deflection is reached. The slow increase is caused by the feedback loop which slowly rises the velocity. If the feedback loop is switched off, the velocity increases rapidly, leading to a force peak caused by cantilever inertia. The hysteresis between approach and retract scan increases with driving velocity indicating that energy is dissipated during the movement of sliding. In order to quantify the hydrodynamic drag for the different velocities, the maximum deflection in the static regime was plotted versus the pulling rate which is the product of driving velocity and cantilever stiffness (Fig.1.8(b)). A linear correlation between viscous friction and pulling rate was observed. The impact of hydrodynamic drag becomes significant when measuring small pull-off forces in the piconewton range with a high velocity above  $10 \text{ nm/s}$ . In order to avoid a significant impact of viscous drag, the loading rate was kept below the critical velocity. For higher loading rates, the respective force has to be added to the pull-off force.

### 1.2.3 Cantilever calibration

The bending of the cantilever in normal and lateral direction is revealed as a voltage signal from the photo detector. The voltage signal can be transferred into a force signal by using the following equations

$$F_n = S_n \cdot k_n \cdot U_n \quad (1.11)$$

and

$$F_l = S_l \cdot k_l \cdot U_l \quad (1.12)$$

The sensitivity  $s$  and the spring constant  $k$  of the cantilever in normal and lateral direction have to be determined. In case of the normal direction, the sensitivity is directly assessable from force-distance cycles recorded on a hard surface  $S_n = \frac{U_n}{\Delta z} = \frac{U_n}{F_n/k_n}$ . The slope of the repulsive regime indicates the sensitivity of the cantilever in normal direction  $S_n$ . The sensitivity in the lateral direction can be derived from the normal sensitivity [38]

$$S_l = \frac{3}{2} \cdot \frac{h}{l} \cdot S_n. \quad (1.13)$$

The manufacturing process of silicon cantilevers leads to thickness variations of the cantilever beam which lead to different spring constants. To guarantee the comparability of experiments, each cantilever has to be calibrated. In this study, the Sader method [39] was used to determine the force constants in normal and lateral direction. Due to the indirect calibration of the lateral force constant, the wedge method [40] was used additionally in friction measurements. In the following the Sader and wedge methods are presented in more detail.

#### Sader Method

With the Sader method the normal and lateral spring constants of a cantilever beam can be determined by measuring the unloaded resonance frequency  $f$ , and the quality factor  $Q$  of the normal and torsional thermal oscillation. By knowing the density of the environment  $\rho$ , length  $l$  and width  $w$  of the cantilever, the normal spring constant  $k_n$  is given by [39]

$$k_n = 0.1906 \rho w^2 l Q_z f_z \Gamma_i^z(f_n) \quad (1.14)$$

where  $\Gamma_i^z = \Omega \Gamma_{\text{circ}}^z$  is the imaginary component of the product of the hydrodynamic equation  $\Gamma_{\text{circ}}^z$  for cantilevers with rectangular cross sections and the correction function  $\Omega$  [41]. In

order to calculate the torsional spring constant, equation (1.14) has to be modified as follows [39]

$$k_t = 0.1592\rho w^4 l Q_t f_t^2 \Gamma_i^t(f_t). \quad (1.15)$$

The subscript  $t$  refers to the torsional version of the parameter introduced in equation (1.14). For small deflections the lateral spring constant can be calculated from the torsional spring constant by considering the height of the tip

$$k_l = \frac{k_t}{h^2} \quad (1.16)$$

To calibrate the normal and torsional spring constants of the cantilevers used in this study, an online calibration tool was used offered by the authors of Ref.[39] on the webpage of Prof. John E. Sader (<http://www.ampc.ms.unimelb.edu.au/afm>).

### Wedge Method

The wedge calibration method is an experimental approach to directly calibrate the lateral sensitivity  $\alpha$  of AFM force probes

$$F_l = \alpha U_1. \quad (1.17)$$

The protocol used in this study was introduced by Wang et al. [40] based on the method described by Varenberg et al. [42]. In the experimental part, the calibration grid TGG11, Micromash, Russia-Estonia with etched pyramids of certain slope angles (see Fig.1.9(a)) is scanned with different normal loads. The scanning direction has to be perpendicular to the facets and the gains have to be adjusted so that the cantilever adapts to the topography of the surface. In Fig.1.9(b), the interaction between AFM tip and surface are shown when sliding uphill and downhill across the facets. The force acting on the cantilever is composed of the contact load, friction force and adhesion force and are balanced by the normal load, lateral force and the torsional moment. The acting forces are reflected in the torsional bending of the cantilever for the respective scanning direction recorded in a force-distance loop as shown in Fig.1.9(c). The average between the uphill and downhill scan on the sloped facets, indicated as midpoint in Fig.1.9(c), defines the offset  $\Delta_0(M, \Theta)$ . The difference between forward deflection and midpoint on the sloped facets is reflected in the half width  $W_0(M, \Theta)$ . The offset and half width parameters have to be corrected by the offset of the flat facets. The corrected half width  $W_0^0$  is proportional to the sum and the offset  $\Delta_0^0$  is proportional to the difference between the torsional moments uphill  $M_u$



and downhill  $M_d$ . Moreover,  $W_0^0$  and  $\Delta_0^0$  increase linearly with the normal [40]

$$W_0^0(M, \Theta) = \frac{M_u - M_d}{2\beta} = S_W F_{\text{load}} + l_W$$

$$\Delta_0^0(M, \Theta) = \frac{M_u + M_d}{2\beta} = S_\Delta F_{\text{load}} + l_\Delta$$

The parameter  $\beta$  is defined by the proportionality factor  $\alpha$ , the height of the AFM tip  $h$  and the thickness of the cantilever beam:  $\alpha = \frac{\beta}{h+t/2}$  [40]. The y-intercepts  $l_W$  and  $l_\Delta$  do not contribute to the friction coefficient.

In order to obtain the proportionality factor  $S_W$  and  $S_\Delta$ , the sample is scanned on different normal loads. The corrected half width and offset on the sloped facets  $\Delta_0^0(M, \Theta)$  and  $W_0^0(M, \Theta)$  are plotted in Fig.1.9(d) versus the applied normal load. The linear fit to the data reflects the gradients  $S_W$  and  $S_\Delta$  which are required to calculate the conversion factor  $\alpha$  from  $\beta$  and the friction coefficient  $\mu$  by using the following equations [40]

$$S_W = \frac{h + t/2}{\beta} \frac{\mu}{\cos^2\Theta - \mu^2 \sin^2\Theta}$$

$$S_\Delta = \frac{h + t/2}{\beta} \frac{\mu^2 \sin\Theta \cos\Theta + \sin\Theta \cos\Theta}{\cos^2\Theta - \mu^2 \sin^2\Theta}.$$

The error of the wedge method is stated by the authors of the publication with 10 % [40].

The calibration measurements for the wedge method were performed in air. In this thesis, adhesion and friction are investigated in aqueous solution. Due to the different refractive indexes  $n$  of water and air, a correction factor has to be applied for the experiments in liquid [43]

$$S_1^{\text{liquid}} = S_1^{\text{air}} \frac{n_{\text{air}}}{n_{\text{liquid}}}. \quad (1.18)$$

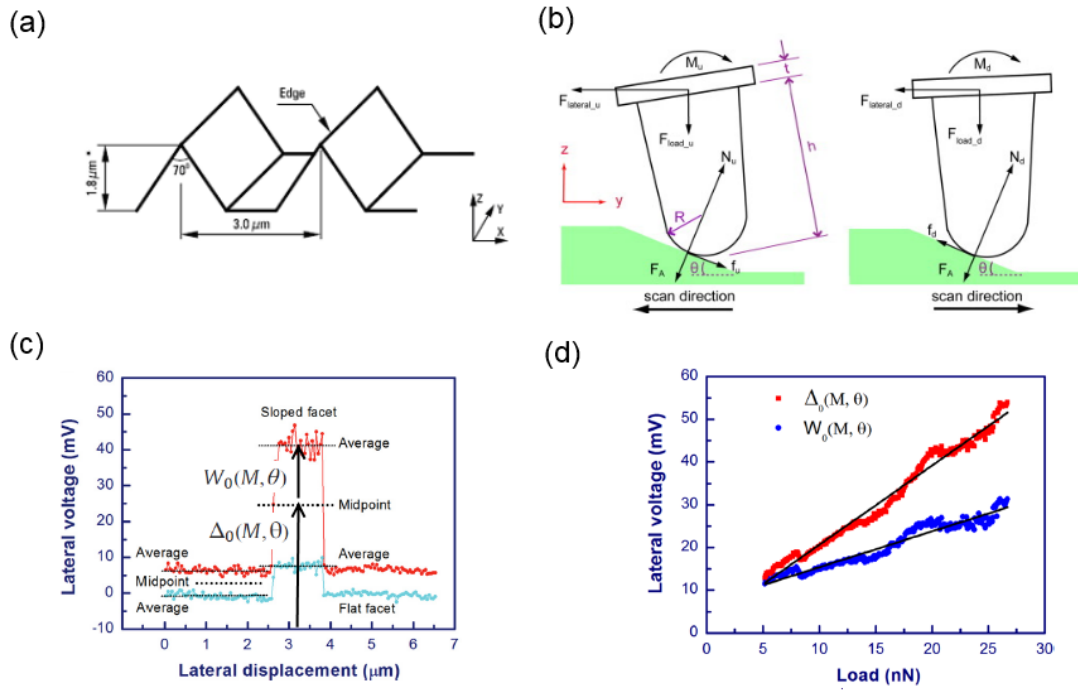


Figure 1.9: (a) Calibration grid TGG11 containing etched pyramids with a height of  $1.8 \mu\text{m}$  and a spacing of  $3 \mu\text{m}$ , the opening angle  $\alpha$  is  $70^\circ$ . The graphic (a) is obtained from Micromash, Russia-Estonia. (b) Lateral deflection when scanning across the etched pyramids of the sample, the half width  $\Delta_0(M, \Theta)$  and offset and  $W_0(M, \Theta)$  reflect the slope of the uncorrected data in (c). (d) Shows the lateral deflection corrected by the offset observed on the flat terrace. The images (b) - (c) are adapted from Ref.[40].

# 2 Switching adhesion and friction by light using photosensitive guest-host interactions

## 2.1 Introduction

Surfaces with switchable adhesion or friction characteristics present a new field of research and promise great potential in the field of adhesives or tribological systems controlled by external stimuli. Self-assembled monolayers are one promising approach to provide surfaces with switchable functions, examples being the switching of wettability [44] or of nanomechanical properties [45, 46, 47, 48]. In this field, azobenzene-derived systems are of special interest as azobenzene has been shown to change its configuration instantly but reversibly by irradiation with ultraviolet (UV) and visible (VIS) light, respectively [49, 50, 51], without generating any side products [52]. Thus, azobenzenes have been used in supramolecular assemblies [53], in covalent functionalization of metal surfaces [52], or for the switching of bioactivity by controlling the binding of azobenzene modified glycoconjugates to cyclodextrin monolayers [54]. Atomic force microscopy (AFM) allows to study mechanical properties of surface-linked azobenzene-derivatives at the single molecule level [55].

## 2.2 Results and Discussion

In this letter, we present a novel surface functionalization based on cyclodextrin assemblies with photo switchable friction and adhesion characteristics mediated by ditopic azobenzene connector molecules in solution. Azobenzene moieties can be isomerized reversibly from *trans* to *cis* states by irradiation with light at 365 nm and from *cis* to *trans* at 455 nm.

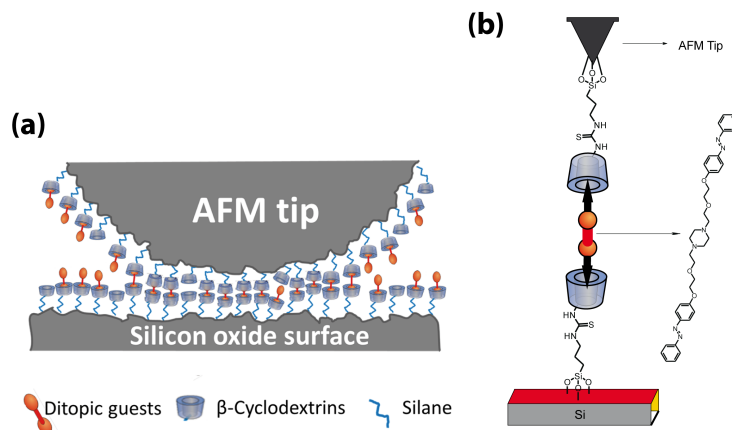


Figure 2.1: (a) Schematic representation of the experiment. Tip and surface are functionalized by  $\beta$ -cyclodextrin molecules. Both end groups of ditopic guest connector molecules form complexes with  $\beta$ -cyclodextrin molecules at tip and surface, resulting in adhesion and friction. (b) Molecular structures of the compounds.

The rod like trans state of the azobenzene is apolar and binds efficiently into the cyclodextrin cavities whereas the bent cis form is much more polar and sterically hindered from complexation [56]. Force measurements by AFM are sensitive enough to detect single host-guest interactions. These interactions have been studied in detail for various guests in cyclodextrin (CD) hosts [23, 57, 58, 17, 59]. We use AFM to study the molecular mechanisms underlying friction and adhesion. A  $\beta$ -cyclodextrin ( $\beta$ -CD) monolayer is attached to both the oxidized silicon tip of the AFM and the oxidized silicon wafer substrate, see the scheme in Fig.2.1(a). The attachment is realized by first tethering a silane adlayer with isothiocyanate groups in tetrahydrofuran to the silicon oxide surfaces. The  $\beta$ -CD molecules carry an amine functionality [21] which is able to form a stable thiourea bond by reaction in water with the isothiocyanate groups at the surfaces. Attractive interactions between the  $\beta$ -CD molecules at tip and surface arise from complexation of ditopic guest connector molecules, see Fig2.1(b). The synthesis of the ditopic guest molecules and their photo-responsive complexation with cyclodextrin molecules has been described elsewhere [56]. Typical association constants for trans-azobenzene derivatives with  $\beta$ -CD are of the order of  $2.5 \times 10^3 \text{ M}^{-1}$  [60], while the binding affinity of cis-azobenzene is too small for quantification. For the binding of azobenzene in  $\beta$ -CD monolayers an association constant of  $5.8 \times 10^3 \text{ M}^{-1}$  has been reported [54]. The ditopic connector molecules carry two hydrophobic end groups which form a specific non-covalent bond between two opposing  $\beta$ -CD cavities via hydrophobic interactions.

All force microscopy experiments were performed at room temperature, using a jpk NanoWizard3 AFM and a rectangular silicon cantilever with a nominal force constant of 0.2 N/m. Normal force measurements were calibrated following the methods introduced by Sader and co-workers [39]. Lateral force measurements were calibrated using the wedge method in air [40] (sample TGG01 from Micromash, Sofia, Bulgaria) and applying the correction factor for experiments in liquid introduced by Tocha et al.[43] A typical example for a force-distance curve is shown in Fig.2.2(a). The force between tip and surface is recorded while the AFM cantilever is approached to and retracted from the surface. Two stepwise increases of the attractive force are observed when the tip apex approaches the surface, indicating a molecular snap-into-contact through complexation events. The rupture of  $\beta$ -CD – azobenzene complexes occurs in multiple steps during the retraction of the AFM cantilever from the surface. Each force drop reflects the rupture of multiple or single complexes. To determine the characteristic rupture force for an individual complex, the distribution of the last force drops, labelled Frupture in Fig.2.2(b), is plotted as a histogram in Fig.2.2(c). Only the last rupture event of each curve is considered to ensure that the cantilever is fully relaxed after the rupture event. The histogram exhibits multiple maxima with equidistant spacing corresponding to the rupture of a single complex, parallel rupture of two complexes etc. The maxima lie at multiples of  $61 \pm 10$  pN, which is the characteristic rupture force for a single complex. In an ongoing study of ditopic guest connector molecules with adamantane end groups we have found a single complex rupture force of  $82 \pm 10$  pN. The lower rupture force for the azobenzene connector is consistent with the lower binding constant for complexes of azo derivatives with  $\beta$ -CD of  $K = 2.5 \times 10^3 \text{ M}^{-1}$  [60] as compared to the one for adamantane derivatives with  $\beta$ -CD of  $K = 4.6 \times 10^4 \text{ M}^{-1}$  [61].

Previous force microscopy studies with various monotopic guests have reported rupture forces ranging from 39 to 102 nN where adamantane guests form the strongest complexes with cyclodextrin molecules [23]. The maximum of the histogram indicates the most probable force to rupture one of two complexes connected in series, while the most probable force to rupture one single azobenzene –  $\beta$ -CD complex would probably be a little higher. The influence of the connector molecules and of their light-induced isomerization on the maximum pull-off force (1.8 nN in the example in Fig.2.2(a)) is summarized in Fig.2.3. Control experiments were performed in ultrapure water. Connector molecules were diluted in dimethyl sulfoxide (DMSO) and added to the ultrapure water in a ratio of 1:10, resulting in 10  $\mu\text{M}$  concentration. Each histogram reflects the distribution of pull-forces from

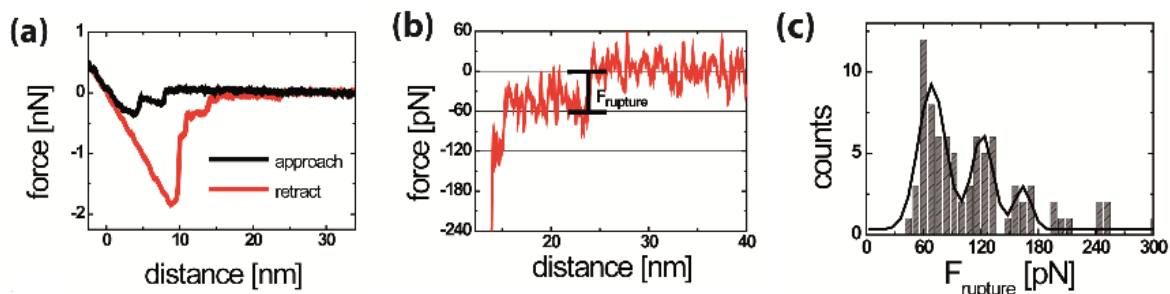


Figure 2.2: (a) Representative force-distance curve recorded in the guest connector solution. Formation of non-covalent bonds can be observed upon approach, a high pull-off force and the subsequent rupture of multiple complexes are observed during retraction. (b) Detail of the retract curve in (a), showing the last rupture event and the related force drop  $F_{\text{rupture}}$  (c) Histogram showing the distribution of  $F_{\text{rupture}}$ . The solid line represents the sum of Gaussian curves fitted to the peak.

1200 force-distance curves (pulling rate  $1 \mu\text{m/s}$ , maximum load  $0.5 \text{ n/N}$ ) recorded in 70 minutes. The histograms show the significant effect of the ditopic connector molecules on the adhesion force.

In the control experiment, non-specific tip-sample interactions result in a narrow distribution of pull-off forces around  $0.35 \text{ nN}$ . After adding the guest molecules the spectrum of adhesion forces becomes much wider with pull-off forces between  $0.5$  and  $1.5 \text{ nN}$ , some even up to  $2.5 \text{ nN}$ . Irradiation with the light of a UV LED (peak intensity at  $367 \text{ nm}$ ,  $10.5 \text{ nm}$  width) results in a decrease of pull-off forces to the values of control experiment. By subsequent irradiation with VIS light (broad-spectrum white light LED with peak intensities at  $454 \text{ nm}$  and  $553 \text{ nm}$ ) the system was switched back to the high adhesion state with pull-off forces ranging again from  $0.3$  to  $2.5 \text{ nN}$ . While the low pull-off force values around  $0.3 \text{ nN}$  observed in the control experiment are not observed after initially adding the connector molecules, they are observed after the sequence of UV and VIS irradiation. The transition of azobenzene end groups from the cis to the trans state under VIS irradiation may not be complete and, therefore, non-specific interactions may arise from competition of ditopic complex formation with only partially isomerized connector molecules. Only a low concentration of guest molecules in the water-DMSO solution ( $10 \mu\text{M}$ ) is required to achieve these significant effects on adhesion. About 60 complexes contribute to adhesion. This rough upper bound estimate can be made by taking the product of the maximum packing density of  $\beta\text{-CD}$  molecules of  $0.33 \text{ nm}^{-2}$  and an estimated contact area derived from the

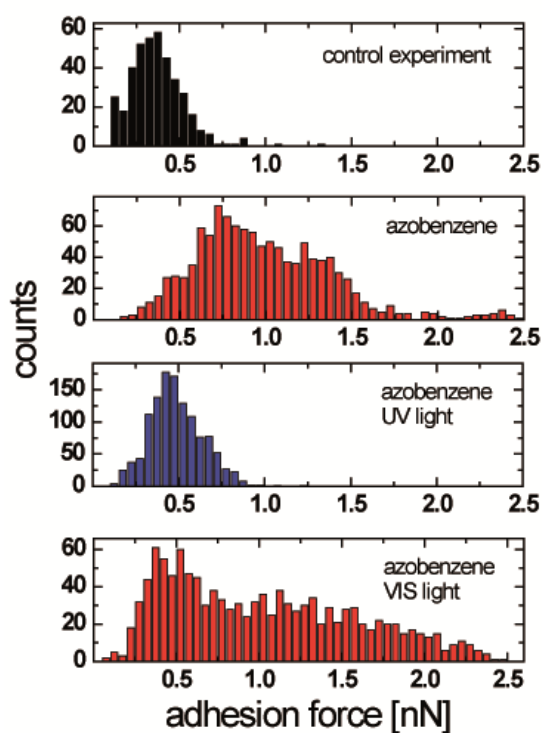


Figure 2.3: Histograms of pull-off forces recorded in a series of experiments for a  $\beta$ -CD functionalized AFM-tip and surface in a control experiment in pure water, in a solution of azobenzene connector molecules, after irradiation with UV light (367 nm), and after irradiation with VIS (454 nm) light.

tip radius of  $200 \text{ nm}^{-2}$  and by assuming that most  $\beta$ -CD molecules are complexed. While changing the light stimuli, the AFM-tip was retracted about  $3 \mu\text{m}$  from the surface, resulting in a time gap of less than five minutes between each series of force-distance curves. The results presented here were achieved with illumination of tip and sample from the side. Quantitatively similar results were obtained for a borosilicate glass substrate functionalized in the same way, where tip and sample were illuminated through the substrate. The molecular complex formation and its switching by light stimuli also lead to a significant friction contrast. The result of a series of friction force microscopy experiments is summarized in Fig.2.4. The friction force is determined from the torsional bending of the AFM cantilever when the tip slides in contact with the surface [62]. In this configuration, friction can be switched reversibly by a factor of more than two by irradiation with UV and VIS light. The friction force decreases upon UV irradiation almost to the value of the control experiment without azobenzene connector molecules. The measurements were performed by scanning lines of  $50 \text{ nm}$  back and forth, i.e. several times the estimated contact diameter, in 1 second. The normal load was kept at a low value of  $0.5 \text{ nN}$  in order to minimize non-specific and deformation contributions to the friction signal. The AFM tip was retracted for 1 minute while switching the irradiation wavelength. Typical lateral force traces are shown in Fig.2.4(b) for a control in pure water and for irradiation with UV and VIS light in the guest molecule solution. The complex formation by the guest connector molecules under VIS irradiation does not only cause higher average friction, but also changes the characteristic appearance of the lateral force traces.

While the non-specific interactions in the control experiments lead to a smooth lateral force curve with some minor fluctuations, the rupture and rebinding of guest-host complexes produces irregular stick-slip motion of the AFM tip which is revealed as saw-tooth characteristic of the lateral force. Typical force drops in the stick-slip force trace have values scattering around  $250 \text{ pN}$ , comparable to the force drops observed in the force-distance curves in Fig.2.2(a) when multiple non-covalent bonds were broken. The friction process can thus be described in the following way. The AFM tip is stuck in place by multiple non-covalent bonds, while the lateral force is built up by the pulling of the cantilever. When the lateral force reaches a threshold value, one or usually multiple bonds are broken and the tip slips to a new position where a different configuration of non-covalent bonds leads to a further sticking phase. This process is continuously repeated, as each new position of the tip leads to rebinding with new  $\beta$ -CD molecules at the surface. The force trace recorded in guest molecule solution under UV irradiation reveals significantly lower



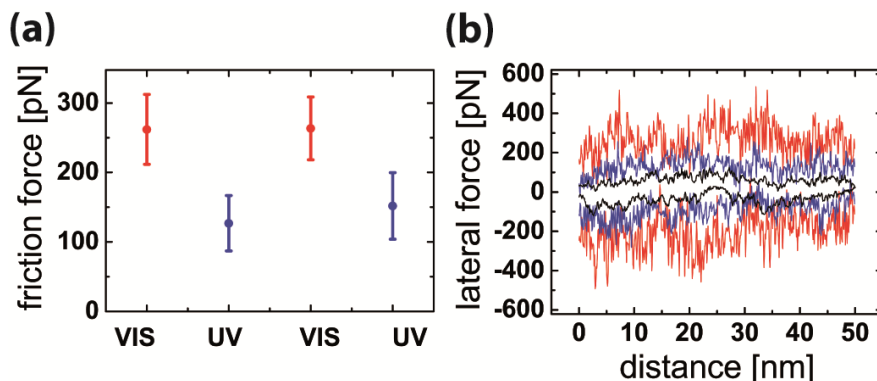


Figure 2.4: a) Light-responsive friction between  $\beta$ -CD functionalized AFM-tip and silicon surface in azobenzene connector molecule solution. The friction force is calculated as the average lateral force during one forward and one backward scan over 50 nm. The error bars represent the standard deviation of 512 scan lines. (b) Typical lateral force traces for forward and backward scan in pure water as control experiment (black line) and in azobenzene connector molecule solution during irradiation with VIS light (red) and UV light (blue).

average friction than that recorded under VIS irradiation, but exhibits some signatures of the stick-slip characteristic, reflecting that even under UV irradiation a fraction of about 20% of the connector molecules is still in the trans-state and contribute to the molecular binding process [63].

## 2.3 Conclusion

In conclusion, we present a novel surface functionalization of host monolayers with switchable friction and adhesion properties mediated by photoresponsive connector molecules. At the molecular level, the rupture force of an individual host-guest complex formed by  $\beta$ -cyclodextrin molecules and the two azobenzene end groups of the connector molecule is  $61 \pm 10$  pN. The pull-off force between functionalized AFM tip and silicon surface can be switched by irradiation with UV and VIS light a factor of five, similarly the friction can be switched by a factor of two. The novel surface functionalization is a first example to demonstrate active control of adhesion and friction by means of macromolecular surface functionalization and guest-host chemistry. The molecular design of our approach allows for different guest connector molecules binding the same surface functionalization, offering a great variability in the molecular control of friction and adhesion.

# 3 Dynamic effects in friction and adhesion through cooperative rupture and formation of supramolecular bonds

## 3.1 Introduction

Friction is the dissipative force acting in sliding contacts. Contributions to friction arise from the plastic or viscoelastic deformation of the contacting bodies and from surface adhesion. This distinction has been the basis of successful scientific investigation into friction phenomena, in particular since Bowden and Tabor's studies on plasticity and adhesion in metallic contacts by an ensemble of molecular bonds [64], which has been introduced in a model based on force-dependent off rates and aging-related on rates by Filippov et al. [33]. We follow a molecular toolkit concept, where adhesion between the contacting surfaces is caused by supramolecular host-guest interactions in aqueous environment. The novelty of our system lies in its versatility achieved by the symmetric functionalization of the opposing surfaces by assemblies of host molecules. Various ditopic connector molecules with two guest end groups form a specific supramolecular bond between the CDs on the two surfaces leading to adhesion and friction. Our study addresses the adhesion and friction dynamics of a group of supramolecular complexes attached to a microscopic asperity, realized by the tip of an atomic force microscope (AFM) (see Fig.3.1). The curved shape of the AFM tip leads to a non-equal load sharing between the bonds which is a key aspect in the discussion of the results. This situation is more complex than the equal load sharing described in previous studies and reflects the situation at the interface between rough surfaces.

Supramolecular interactions, in particular the inclusion of hydrophobic groups into the cavities of cyclodextrin molecules, have been employed for the development of a variety

of molecular materials, ranging from supramolecular structures [18] and molecular print boards [58] to self-assembling macroscopic blocks of gels [15]. At the single complex level, atomic force microscopy has revealed the force which inclusion complexes can sustain, typically of the order of several tens of piconewton [23, 58]. Due to the high binding and unbinding rates of inclusion complexes, single molecule force experiments typically probe the system in thermal equilibrium leading to no observable dependence on the force loading rate [58]. Macroscopic measurements of adhesion recorded in thermal equilibrium result in values for the work of adhesion which are proportional to the density of bonds and to the free energy found for single molecule detachment experiments [65]. The situation can become different when the force sustained by multiple inclusion complexes. The kinetics change dramatically and lead to significant rate-dependent adhesion when the several bonds contribute equally to the interaction [17]. Such effects of multivalency play an important role in supramolecular chemistry [11] and beyond in biological adhesion and recognition [12].

The results of this study quantify the friction caused by multiple inclusion complexes. They reveal the conditions under which the complexes, which share the external force non-equally due to attachment to a curved surface, exhibit multivalency effects in adhesion. The bond failure in our system is characterized by a cooperative behavior as described by Evans and Williams [8] and Filippov et al. [33]. Such physical cooperative behavior is encountered even in the absence of a chemical cooperativity in the sense of effects of binding in adjacent receptors, and may then also called non-cooperative multivalency [17].

We have functionalized the surfaces of AFM tips and silicon wafer substrates by dense monolayers of  $\beta$ -cyclodextrin ( $\beta$ -CD) molecules. Adhesion and friction between tip and surface, probed by normal and lateral force vs. distance curves, arise from complexation of the two adamantane end groups of the ditopic connector molecules into the cavities of opposing  $\beta$ -CD molecules. The design of a ditopic system allows the quantification of non-specific interactions between the opposing surfaces in direct control experiments. Moreover, different connector molecules can bind to the same surface functionalization which allows to control friction and adhesion using switchable connector molecules [2] or to adapt to surface roughness by varying the lengths of the connectors. In this study, we use a connector molecule with adamantyl end groups because of its high binding constant and the well-known molecular kinetics for the monotopic guests [17, 61]. For sake of simplicity, we will refer to the specific interaction between one connector molecule and two opposing  $\beta$ -CDs as bond throughout the manuscript and ask the reader to keep in mind

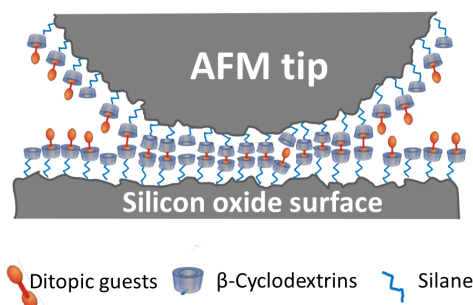


Figure 3.1: Schematic representation of a  $\beta$ -CD hosts monolayer attached to an AFM tip and silicon wafer. Hydrophobic interactions lead to inclusion of the connector molecules into the hosts and to the tip-sample interaction.

the non-covalent, supramolecular nature of the bond.

## 3.2 Experimental section

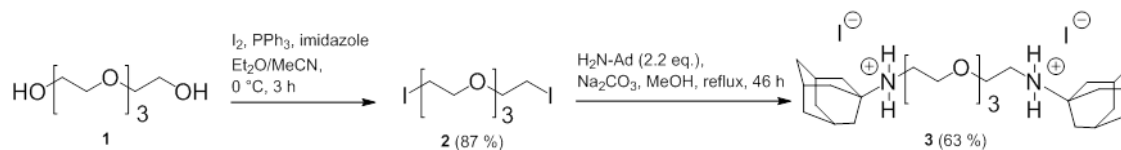
### 3.2.1 Instrumentation

Isothermal titration calorimetry (ITC) was performed on a Nano ITC2G from TA Instruments at 25°C.  $^1\text{H}$  and  $^{13}\text{C}$  NMR spectra were recorded on a Bruker Magnet System 400 MHz Ultra shield plus ( $^1\text{H}$ : 400.00 MHz) using  $\text{CDCl}_3$  at 25°C. The solvent signals were used as internal standards. The program MestReNova 6.0.2 was used for data processing and deconvolution of the spectra. The following abbreviations were used for multiplicities: **s** for singlet, **t** for triplet. Overlapping signals and multiplets were labeled with **m**, broad singlets with **bs**.

### 3.2.2 Synthesis of the ditopic connector

1, 11-Diiodo-3,6,9-trioxoundecane (5 mmol, 2.070 g, synthesized according to Ref. [66]) and 1-aminoadamantane (11 mmol, 1.663 g) were dissolved in dry methanol (20 mL). Sodium carbonate (20 mmol, 2.1 g) was added and the mixture was stirred at reflux temperature for 46 h. After filtration of the solid the solvent was evaporated and the residue was purified by column chromatography ( $\text{SiO}_2$ , dichloromethane : methanol 15 : 1). The product was obtained as a white solid (2.25 g, 63 %).

$^1\text{HNMR}$  ( $\text{CDCl}_3$ , 400 MHz):  $\delta$  8.35 (bs, 4 H,  $\text{NH}_2\text{-H}$ ), 4.00 (t,  $J = 4.6$  Hz, 4 H), 3.68

Figure 3.2: Synthesis of the ditopic connector **3**.

(m, 8 H), 3.16 (t,  $J = 4.6$  Hz, 4 H), 2.16 (m, 6 H), 2.07 (m, 12 H), 1.67 (m, 12 H) ppm.

$^{13}\text{C}$ NMR ( $\text{CDCl}_3$ , 100 MHz):  $\delta$  70.3, 69.7, 65.5, 58.5, 39.7, 38.2, 35.3, 28.9 ppm.

IR(ATR): 2907, 2851, 1611, 1453, 1362, 1307, 1074  $\text{cm}^{-1}$ .

### 3.2.3 Preparation of monolayer

As substrates commercial available Si (111) wafers were used (Si-Mat, Kaufering, Germany) which were first cleaned using piranha solution (3:2 mixture of sulfuric acid and hydrogen peroxide) to remove organic contamination, rinsed with ultrapure water and dried with  $\text{N}_2$ . Subsequently the samples were kept for two hours in the silane solution (0.1 vol.% of 3-isothiocyanatopropyl-triethoxysilane, diluted in tetrahydrofuran (THF)). The silane 3-isothiocyanatopropyl-triethoxysilane was synthesized according to Ref.[67]. After a washing procedure with THF and water the wafer remained in 1 mM solution of mono(6-deoxy-6-amino)- $\beta$ -CD diluted in water over night at room temperature. All samples were freshly prepared for the AFM measurements and stored in water. The silicon AFM tips (Nanosensors(TM) PPP-Cont AFM Probes, NanoandMore, Wetzlar, Germany) were functionalized in the same way.

### 3.2.4 AFM measurements

All AFM measurements were performed with a Nanowizard 3 setup (JPK Instruments, Berlin, Germany) in water or connector solution at room temperature. A connector molecule concentration of 10  $\mu\text{M}$  was chosen in order to work in the saturation regime of the Langmuir curve (see Supplementary Information for more details). Silicon cantilevers with nominal normal spring constant of 0.2 N/m and typical lateral spring constants of 50 N/m have been calibrated using the thermal noise analysis. Lateral force measurements were calibrated using the wedge method in air [40] (sample TGG01 from Micromash, Sofia, Bulgaria) and applying the correction factor for experiments in liquid introduced by Tocha et al. [43]. To avoid surface damage and unspecific contributions to the friction

force the maximum normal force was kept below 0.5 nN. The shown adhesion values were obtained on at least three different surface positions, more than 100 force-distance curves each. Friction experiments were performed with low feedback gains by scanning perpendicular to the axis of the cantilever.

### 3.2.5 Data analysis

For the force spectroscopy analysis the implemented Data Processing software (JPK instruments, Berlin, Germany) was used. Each force curve was examined either for the maximum pull-off force or the last rupture, depending on the experiment. The results were plotted in a histogram and the most probable rupture force was obtained by a Gaussian curve fitted to the data.

## 3.3 Results

The synthesis of the ditopic connector **3** was performed in a straightforward approach (Fig.3.2) starting from commercially available materials. In the first step tetraethylene glycol was directly converted into the corresponding diiodo compound using  $\text{PPh}_3$ , imidazole, and iodine [66]. Subsequent substitution reaction with 1-aminoadamantane resulted in the formation of the ditopic connector **3** as its diammonium iodide salt as indicated by a characteristic signal of the ammonium protons in  $\text{CDCl}_3$  at 8.35 ppm. Based on its ionic structure product **3** is well soluble in water which is essential for our molecular toolkit approach. The ditopic connector **3** forms an 1:2 inclusion complex with  $\beta$ -CD. The binding constant  $K = 11300 \text{ M}^{-1}$  equivalent to a binding free energy  $\Delta G = -23.1 \text{ kJ/mol}$  and a binding enthalpy of  $\Delta H = -39.4 \text{ kJ/mol}$  was determined by ITC in aqueous solution (see supplementary information for details). These values compare well with values for the corresponding monotopic 1-adamantylammonium  $\Delta G = -22.2 \text{ kJ/mol}$  and  $\Delta H = -20.1 \text{ kJ/mol}$  [68] indicating independent complexation of both adamantane groups.

The molecular interactions contributing to friction and adhesion were studied by means of AFM. A  $\beta$ -CD monolayer was attached to the AFM tip and substrate in a two step process. In the first step, a silane adlayer with an isothiocyanate group was self assembled on the silicon oxide surface [69]. Subsequently, the  $\beta$ -CD molecules which carry an amine

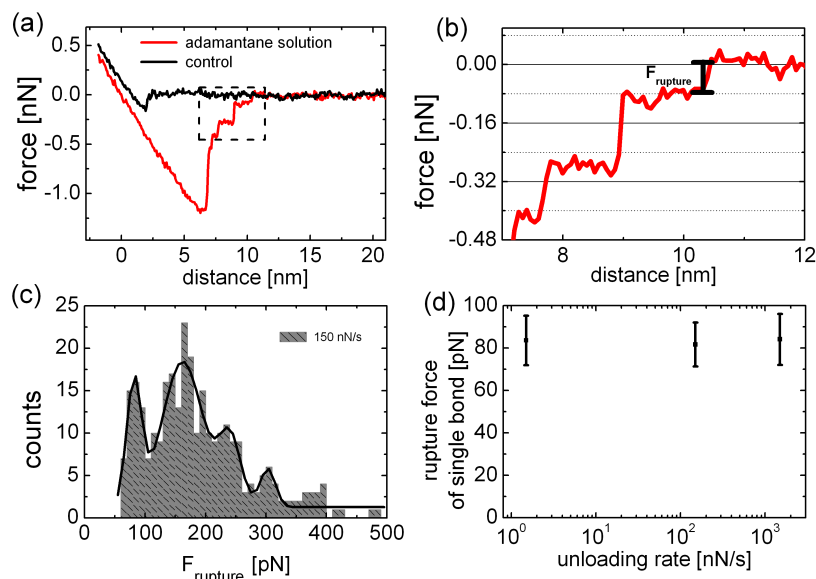


Figure 3.3: (a) Force curve recorded during retraction of a  $\beta$ -CD functionalized AFM-tip from the surface in solution of the ditopic connector **3** and in water (control); (b) zoom into the separation curve in adamantane connector solution, the last rupture event is marked which is included into histogram in (c); (c) histogram derived from the last rupture forces at an unloading rate of 150 nN/s, the solid line is the sum of Gaussian functions fitted to the peaks; (d) the single rupture force at different unloading rates, the error bars indicate the standard deviation of the Gaussian curve fitted to the first peaks, respectively.

functionality [21] were attached by forming a thiourea bond with the isocyanate groups at the surface [2]. The specific interaction between the  $\beta$ -CDs on the AFM tip and surface is mediated by ditopic connector molecules via the hydrophobic effect. The self-passivation of the surface by inclusion of both end groups into CDs at one surface is prevented by using a short tetraethylene glycol chain to connect the end groups of the connector molecule.

The effect of the connector molecules on adhesion was revealed in force distance curves as shown in Fig.3.3. The pull-off force between a  $\beta$ -CD covered AFM tip and surface increases significantly in the presence of connector molecules in comparison to the control experiments without connector molecules. During retraction of the AFM tip, a step wise rupture is observed in Fig.3.3(b) which reflects the subsequent rupture of single and multiple  $\beta$ -CD - adamantane complexes. For a statistical evaluation, the rupture forces of only the last rupture event (labeled  $F_{\text{rupture}}$  in Fig.3.3(b)) of 300 force curves were summarized in the histogram in Fig.3.3(c). By analyzing only the last event, we ensure that the cantilever is fully relaxed after the rupture. The periodic distribution in Fig.3.3(c) reveals the rupture

force for one or more bonds. The first maximum quantifies the rupture force of a single bond with  $82 \pm 10$  pN, the second a parallel rupture of two bonds etc. The experiment has been repeated for various unloading rates. No rate dependency is observed for the most probable single rupture force in the experimentally accessible range from 1.5 to 2500 nN/s (see Fig.3.3(d)).

In contrast, the maximum pull-off force and, interestingly, also the overall shape of the force curves are highly loading rate dependent when connector molecules are present (see Fig.3.4(a)). Without connector molecules, no rate dependency is observed. At low unloading rates, the force curve exhibits a plateau at adhesion forces of below 0.5 nN. With increasing unloading rate, a transition in shape occurs from the force plateau to a triangular shape with a high maximum pull-off force. After rupture at the maximum pull-off force, the curve turns into a plateau with forces similar to the plateau force observed for slow pulling. Note that all triangularly shaped adhesion curves last for several milliseconds, much longer than the response time of the cantilever of about 120  $\mu$ s. Fig.3.4(b) shows the unloading rate dependence of the maximum pull-off force.

A detail of the force curve recorded at a low unloading rate of 1.5 nN/s in Fig.3.4(c) shows that the plateau consists of several force drops with a similar spacing of about 0.15 nm. Between the force drops, the force curve develops a constant slope which reveals the effective stiffness of the contact which is close to the cantilever stiffness of 0.2 N/m. In Fig.3.4(d), a detail of the force curve at higher separation, the distance between force drops is about 1 nm, the peak force only around 80 pN, and the effective stiffness only  $k_{\text{eff}}^n = 0.02$  N/m.

The friction force is the force acting opposite to the direction of sliding when scanning across a surface. During sliding, adhesive bonds between the  $\beta$ -CDs on the AFM tip and surface cause a torsion of the cantilever. Scanning in forward and backward direction we can derive the friction force from the average torsion. The friction force caused by unspecific interactions between AFM tip and surface can be revealed from the control experiment without guest molecules in Fig.3.5. In order to minimize these contributions the normal force was kept below 0.5 nN so that friction was dominated by the specific host-guest interaction. When connector molecules are present, the friction force increased by up to a factor of five in comparison to the control experiment as shown in Fig.3.5(a). Contrary to adhesion, friction is not rate dependent. The sliding velocity has no significant impact on the measured friction force in the experimentally accessible range from 3 nm/s to 1000 nm/s. Representative friction loops recorded with a tip velocity of 100 nm/s are



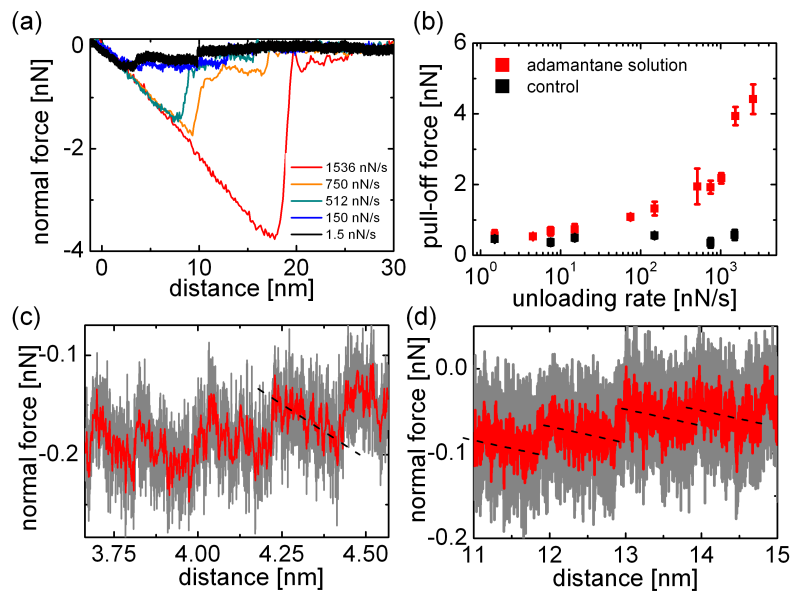


Figure 3.4: (a) Representative force vs. distance curves at different unloading rates in nN/s; (b) maximum adhesion force depending on the unloading rate in connector solution and control experiment, each data point represents the average of 300 force curves recorded at three independent surface positions. The error bars indicate the standard deviation of the three positions. (c) and (d) details of the force curve in (a) recorded with 1.5 nN/s, the dotted lines indicate the effective contact stiffness.

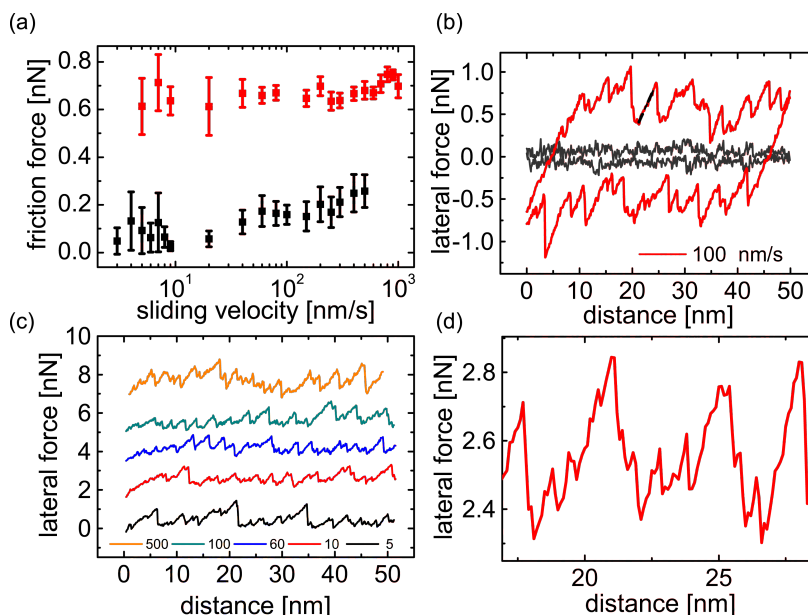


Figure 3.5: (a) Average friction force vs. scan velocity of a  $\beta$ -CD functionalized AFM-tip and surface in solution of the ditopic connector **3** and in water (control), the error bars represent the standard deviation of 50 friction loops; (b) representative friction loops recorded with 100 nm/s, the dashed line indicates the lateral contact stiffness; (c) forward scan of a friction loop recorded with different velocities, the unit of the velocity values in the legend is nm/s, force curves are offset for better readability, the average does not change with velocity; (d) detail of a forward scan of (c) recorded with a velocity of 10 nm/s.

shown for adamantane solution and the control experiment in Fig.3.5(b). The characteristic sawtooth shape reveals an irregular stick-slip motion of the tip apex which is observed for all sliding speeds Fig.3.5(c). In the control experiment no stick-slip motion is observed. The dotted line indicates the effective stiffness in lateral direction  $k_{\text{eff}}^l = 0.13 \pm 0.01$  N/m which is two orders of magnitude smaller than the torsional spring constant. A detail of the force curve recorded with a scan velocity of 10 nm/s in Fig.3.5(d) shows that the large triangular force drops consists of smaller drops with a distance of 0.5 nm to 1 nm.

## 3.4 Discussion

In the following we will discuss the dynamics of adhesion, normal and lateral, which are governed not only by rupture and rebinding of individual bonds, but also by the cooperative dynamics of multiple bonds at a given tip-sample distance.

The force required to rupture the bond between two  $\beta$ -CD guests established by the ditopic adamantane connector is revealed by the force drop measured when the last bond is ruptured in a pull-off experiment. The value for the most probable rupture force is  $82 \pm 10$  pN, comparable but significantly lower than the values of  $102 \pm 15$  pN [58] and  $97 \pm 19$  pN [17] reported for single adamantane hosts bound to  $\beta$ -CD guests. The most probable force to rupture one of the two complexes formed at the end of a ditopic connector molecule is expected to be lower than the most probable force to rupture a single complex. The probability distribution  $p(F)$  of rupture forces of one host-guest bond in Fig.3(d) of Ref. [58] can be approximated by a Gaussian normal distribution with a mean value of  $\mu=100$  pN and a standard deviation of  $\sigma = 15$  pN. The probability to rupture one of two such bonds in series at a force  $F$  is then given as

$$1 - (1 - p(F))^2 = 1 - \left[ 1 - \operatorname{erf} \left( \frac{F - \mu}{\sigma\sqrt{2}} \right) \right]^2 \quad (3.1)$$

For a standard deviation of  $\mu=15$  pN in the single bond rupture force, the most probable force for rupturing one of two bonds in series is 93 pN, for  $\mu=10$  pN the value is 95 pN and for  $\mu=20$  pN it is 90 pN. A small reduction of the most probable rupture force for two bonds in series by only a fraction of the width of the rupture force distribution is in agreement with a model by Williams and Evans [8] and recent experimental results [70]. In our experiment, the measured rupture force of 82 pN for the connection by the ditopic adamantane molecule is lower than expected from the probability argument. The lower value may be explained by interactions between the two  $\beta$ -CD hosts, whose distance is estimated to be less than 2 nm when the ditopic guest molecule is complexed. Furthermore, the ditopic connector used in this work carries one positive charge close to each adamantane end group, which is known to reduce the affinity for complexation in comparison to the uncharged adamantane derivatives [68]. The lower affinity is reflected in the lower binding free energy of -5.5 kcal/mol resulting from ITC measurements in comparison to that for single uncharged adamantane guest molecules of -6.5 kcal/mol [58]. The binding free energy and the rupture force for our connector molecule actually lie in between the respective values reported by Auletta et al. for ferrocene and (1,1-dimethylethyl)benzene guests, confirming that the lower rupture force of 82 pN is rather due to a lower affinity than to the effects of two bonds in series.

In the following we will discuss the dynamics of adhesion and start with the rupture of

a single bond. The loading rate was varied over more than three orders of magnitude (see Fig.3.3(d)) and in agreement with previous studies on adamantane- $\beta$ -CD interactions no loading rate dependence was observed for single bonds, indicating that the complexes are probed in thermodynamic equilibrium [17, 57, 58]. We determined the binding constant of ditopic guests with  $\beta$ -CD-hosts in solution by isothermal titration calorimetry as  $K = 1.1 \times 10^4 \text{ M}^{-1}$  which is slightly lower than value reported by Mulder et al. [61] for a similar system. The small difference is in line with the lower rupture force in our ditopic system. By assuming that  $k_{\text{on}}$  is diffusion limited and thus in the order of  $10^8 \text{ M}^{-1}\text{s}^{-1}$  [71], one concludes that  $k_{\text{off}}$  is  $8000 \text{ s}^{-1}$ . In surface bound cyclodextrin systems,  $k_{\text{off}}$  is expected to be the same, but the binding constants are even higher because the high concentration of guest molecules at the surface increases  $k_{\text{on}}$  [61]. We can draw the conclusion that we have very fast binding kinetics in the scale of the  $k_{\text{off}} = 8000 \text{ s}^{-1}$  and are certainly in equilibrium for our experimental pulling rates.

We turn now to the system with multiple bonds and discuss the strong loading rate dependence of the pull-off force and the overall shape of the force distance curves. We will start with the force curve recorded at slow pulling speeds and focus on the elasticity of the supramolecular assembly. The force curve exhibits a force plateau over which the bonds between tip and surface are successively ruptured. The length of the force plateau is unexpected large. The expected upper bound for the range of interaction between tip and surface is given by the thickness of the two  $\beta$ -CD monolayers, which are deformed upon contact formation plus the length of the ditopic connector molecule. Elastic deformation of silicon AFM tip and sample are of the order of tens of pm for the forces applied here and can be neglected. The thickness of the  $\beta$ -CD monolayer is estimated from the size of molecular constituents to be 3 nm, this thickness has been confirmed in AFM height measurements of areas where the monolayer was removed by scanning at higher load. The length of the ditopic connector is estimated to be 2 nm. Thus, the force plateau is longer than expected by up to 12 nm. We conclude that our supramolecular assembly offers more elastic flexibility than expected.

The shape of the force curves in Fig.3.4(a) are strikingly similar to those recorded by Pussak et al. [72] for the interaction between an soft elastic probe and a flat surface mediated by specific mannose-ConA interactions. In our system, such elastic flexibility can only be provided by the silane network layer binding the  $\beta$ -CD molecules to the oxidized silicon surface. This layer is known to be strongly cross-linked, but may provide flexibility

by ring formation and a limited number of covalent anchor points to the oxidized surface [73, 74]. Thus, the stiffness of the bonds is not only determined by the stiffness of the linker and CD molecules but additionally by the flexibility of the silane network.

The force plateau exhibit force drops in irregular distances, around 0.1 - 0.2 nm in the earlier part of the curve (Fig. 3.4(c)) and 1 nm in the later part (Fig. 3.4(d)). The height differences agree well with a bond density close to the maximum density of  $0.33 \text{ nm}^{-2}$  of  $\beta$ -CD molecules on a curved surface from which we can reveal the number of bonds of around sixty, a number highly dependent on the radius of the AFM tip. The slope of the force curve between the rupture events reflects the effective contact stiffness which is equal to the spring constant of the cantilever in the early part of the force curve because it is softer than the molecular springs in parallel. Due to the curvature of the AFM tip, the bonds are not equally distributed along the pulling distance but the height difference between the CD molecules increases closer to the tip apex. Thus, less bonds contribute to the force in the later part of the curve resulting in a significant lower contact stiffness and a larger distance between the rupture events. However, the low effective stiffness of only  $0.02 \text{ N/m}$  can only be explained by an elastic deformation of the silane network. The development of the effective contact stiffness is reflected by the noise of the force curve. The noise originates from thermal vibrations of the force probe which is damped in the early part of the force curve where the tip is bound by several parallel springs. In the later part of the force curve, the contact stiffness is low due to the lesser number of bonds stretched in parallel resulting in a weaker damping of the cantilever.

With increasing loading rate, the detachment process transforms from a zipper-like peeling of bonds, which resembles the macroscopic equilibrium situation described by Raman et al. [65], to a more parallel rupture of bonds with an increasing pull-off force indicating that the system moves out of equilibrium.

We will address three different aspects which can lead to a rate dependency of the curve shape and pull-off force and start with the dynamics of the cantilever. The force probe has a limited reaction time  $\tau = 1/4f$  caused by inertia and viscous damping which is in the order of  $120 \mu\text{s}$ . In contrast, typical force curves in the high unloading rate regime last at about  $3 \text{ ms}$  so that we can exclude inertia causing the rate dependency of the pull-off force. However, inertia does cause a delay in the cantilever movement whose possible role in the detachment kinetics is discussed below.

The second aspect leading to rate dependence of the pull-off force refers to the elasticity of the overall contact. For viscoelastic contacts, the pull-off force is determined by a crack

opening process. With increasing pulling speed, the viscoelastic losses at the edge of the contact increase, leading to an increase of the pull-off force [72]. For our system, scratch tests revealed a thickness of the organic layer composed of CD and silane of about 3 nm. The relaxation of the even thinner silane layer is presumably too fast on the time scale of the force curve measurement to explain an increase in energy dissipation by a factor of 10 during a force measurement by viscous effects. Nevertheless, the elasticity of the attachment allows a parallel stretching of several bonds which then leads to a cooperative rupture behavior.

In literature, multiple bond failure is described for either a parallel arrangement of bonds with equal load sharing or a zipper-like subsequent failure of independent bonds [8, 30, 29]. Due to its curvature, the situation is more complex for an asperity like the AFM tip. In the beginning of the force curve, the height difference between the bonds is less than the maximum stretching length of one bond. For this case, the overlap of bonds results in cooperative dynamics which can increase the life time of the ensemble of bonds by several orders of magnitudes [8]. This effect is referred to as multivalency, for example by Gomez-Casado et al. in the discussion of a rather weak increase of pull-off force with increasing loading rate for two and three parallel adamantane -  $\beta$ -CD bonds. [17] Because of the longer life time, and thus the lower off rate of the ensemble of bonds compared to a single bond, the bonds are probed out of equilibrium and a rate dependency of the pull-off force can be observed while the rupture force for a single bond is constant [17]. In our specific supramolecular system, the on rate is orders of magnitudes higher than the off rate so that the multivalency effect needs to be extremely effective to explain the significant loading rate dependence of the pull-off force. We suggest that, inertia of the cantilever enhances the multivalency effect. After one bond is ruptured, inertia causes a delay in the cantilever movement which is significant on the time scale of the on rate so that a rebinding of already broken bonds is favored. The higher the unloading rate, the higher the contribution of inertia to cooperative dynamic effects. Thus, the finite response time of the cantilever can lead to a higher pull-off force by a combined effect of multivalency and cantilever inertia. After the force drop at the pull-off force, the gap between subsequent bonds increases and a shape transition occurs from a parallel to a zipper-like peeling of bonds which reveals itself as a force plateau at a constant adhesion force.

In the following section we will discuss the dynamics resulting in the friction force with respect to the difference between friction and adhesion. The irregular saw-tooth

modulation of the lateral force, as observed in the friction loop, indicates that the repeated breaking of groups of irregularly distributed bonds determines the measured friction force. A stick-slip friction behavior caused by the cooperative rupture of subsystems of molecular bonds and subsequent rebinding was already predicted by the model introduced by Filippov et al. [33]. From the effective stiffness in lateral direction we can derive the force pulling rate which ranges from 0.4 nN/s to 130 nN/s, about one order of magnitude smaller than in our adhesion experiment. For intermediate pulling rates, adhesion and friction exhibit very similar rupture characteristics: multiple complexes are ruptured at the same time resulting in the triangular shape of the force curve in adhesion and in the characteristic stick-slip shape in friction, with comparable peak forces of about 1 nN. The slip events consist of a series of smaller force drops indicating that several bonds contribute to the peak force. Similar to the adhesion measurements, we can assume that the lateral distance between the host molecules is smaller than the maximum stretching length of bonds in lateral direction  $F_{\text{rup}}^l/k_{\text{eff}}^l = 1 \text{ nN} / 0.13 \text{ N/m} \approx 7.5 \text{ nm}$  due to the flexibility of the silane network and the overall length of the  $\beta$ -CD-adamantane- $\beta$ -CD complex.

However, a different development of the forces in lateral and normal direction is observed when varying the scanning speed and unloading rate, respectively. The friction force as well as the shape of the friction loop remain the same when varying the scan velocity over three orders of magnitude. To discuss the difference between adhesion and friction, we will address the same three aspects discussed above for the adhesion measurements. The first aspect is the response time  $\tau_l = 1/4f_l = 5 \mu\text{s}$  of the cantilever. Because of the high spring constant, the response time of the cantilever in lateral direction is two orders of magnitude smaller than in normal direction so that any direct contribution of inertia to the measured shape of the friction loop can be neglected. The second aspect is the viscoelasticity of the contact. As already discussed for the adhesion measurement, the relaxation of the molecular layer is presumably too fast compared to the time scale of the measurement to lead to a significant energy dissipation. Nevertheless, its elastic flexibility facilitates the simultaneous stretching of several bonds leading to the cooperative rupture behavior of the molecular ensemble. To discuss the contribution of multivalency in our friction measurements, we first focus on the kinetics of an individual bond and compare the reaction kinetics with the time scale of the experiment by considering the contact time for a single bond. With the fastest sliding velocity of 1000 nm/s and the stretching length of the bond of 7.5 nm, we arrive at a minimum contact time in the order of milliseconds, one order of magnitude higher

than the survival time of a single bond  $\tau = 1/k_{\text{off}} \approx 0.125$  ms. Because of the fast reaction kinetics the individual bonds are ruptured in thermodynamic equilibrium as observed for the single pull-off force. This interpretation of the data is supported by the observation of a saturation regime for friction as function of the connector molecule concentration (see Supplementary Information) for the respective Langmuir curve). The monotonous increase of friction with concentration and its saturation indicate that the connector molecules do not passivate the surface and that we probe the specific adamantane- $\beta$ -CD interaction. For a non-equilibrium situation with slow reaction kinetics, a high concentration of connector molecules would block the CDs on the surface resulting in a decrease of friction which is not observed for our system.

In contrast to adhesion experiments, the cantilever inertia does not contribute to multivalency effects in friction due to the fast response in lateral direction. Furthermore, broken bonds are permanently rebound across the contact in sliding friction experiments. As result, the fast reaction kinetics lead to an equilibrium situation in friction for the ensemble of bonds and the friction force remains constant for the range of sliding speeds investigated.

### 3.5 Conclusion

In summary, we quantified the dynamic effects in friction and adhesion caused by cooperative rupture of supramolecular bonds. For our system based on the inclusion of ditopic adamantane connectors in cyclodextrin hosts and probed by AFM, we discovered a remarkable difference in the dynamics of friction and adhesion. In force spectroscopy, the pull-off force for multiple bonds increased dramatically with loading rate although the rupture force for an individual complex remained constant indicating that a single bond is probed in thermodynamic equilibrium. We assign the loading rate dependence to a cooperative rupture of multiple bonds, where the multivalency effect is enhanced by the inertia of the cantilever, leading to a non-equilibrium situation. The friction force was found to be constant over three orders of magnitude in sliding velocity. In friction, equilibrium is maintained by the permanent fast rebinding of broken bonds and the fast response time of the force sensor in lateral direction. These results confirm the importance of microscopic time scales for macroscopic friction and adhesion results, as predicted in Ref. [33]. The molecular design of our approach provides the opportunity for studies of the microscopic dynamics underlying friction and adhesion because the wide range of possible connector molecules offers to tune the kinetics of the system. Connector molecules with different bind-



ing constants or different complexation kinetics open a pathway to systematically explore the influence of complexation strength and kinetics on friction.

## 3.6 Supplementary Information

### Connector concentration dependence of the friction and adhesion force

In order to investigate how the connector molecule concentration influences friction and adhesion, force measurements with varying connector concentration were performed (see Fig.3.6). For low concentrations a monotonous increase up to a concentration of about  $3 \mu\text{M}$  with a subsequent saturation regime are observed. From the Langmuir fit we can determine a binding constant of  $K_{\text{friction}} = (1.6 \pm 0.5)10^6 \text{ 1/M}$  for the friction force which is in good agreement with the Langmuir binding constant in adhesion  $K_{\text{adhesion}} = (1.0 \pm 0.28)10^6 \text{ 1/M}$ . The binding constants obtained for the  $\beta\text{-CD}$  SAMs are about two orders of magnitude higher than the binding constant obtained in solution from ITC measurements. The higher binding constant at surfaces in comparison to the binding in solution has been described before for monotopic guests [61] and can be explained by the higher concentration of guests at the surface and hosts in the confinement. For all AFM experiments in our study, a connector molecule concentration of  $10 \mu\text{M}$  was chosen in order to work in the saturation regime of the Langmuir curve.

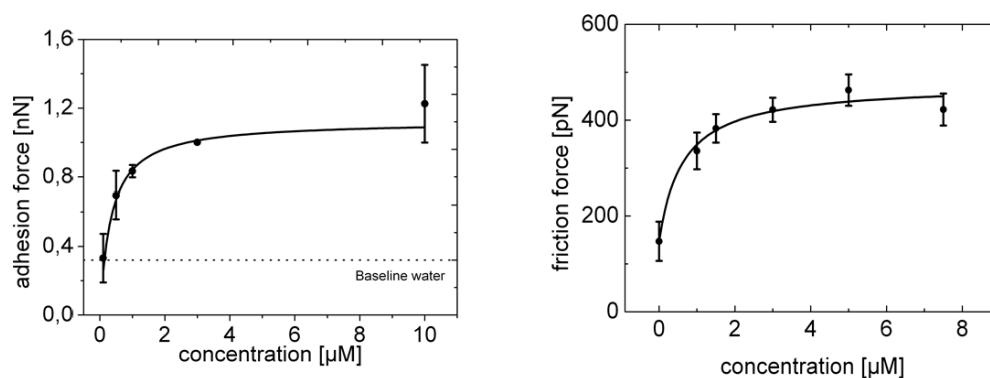


Figure 3.6: Mean adhesion (left) and friction (right) force as a function of connector molecule concentration recorded with a pulling velocity of  $250 \text{ nN/s}$  and a sliding velocity of  $100 \text{ nm/s}$ , the solid line represents a Langmuir fit to the data.

### Isothermal titration calorimetry (ITC) of ditopic connector **3**

1.00 mL of a 1.23 mM solution of  $\beta$ -CD in water at pH 6.40 was titrated with 25 injections of 10  $\mu$ g/L each of a 8.545 mM solution of ditopic connector **3**. The observed heat signals shown below were corrected with the corresponding heats of dilution of compound **3** were fitted with the program Launch NanoAnalyze version 3.1.2 for 1 independent binding site (see Fig.3.7). The stoichiometry ratio  $n \approx 0.5$  is due to the ditopic binding valency of the adamantane connector **3**.

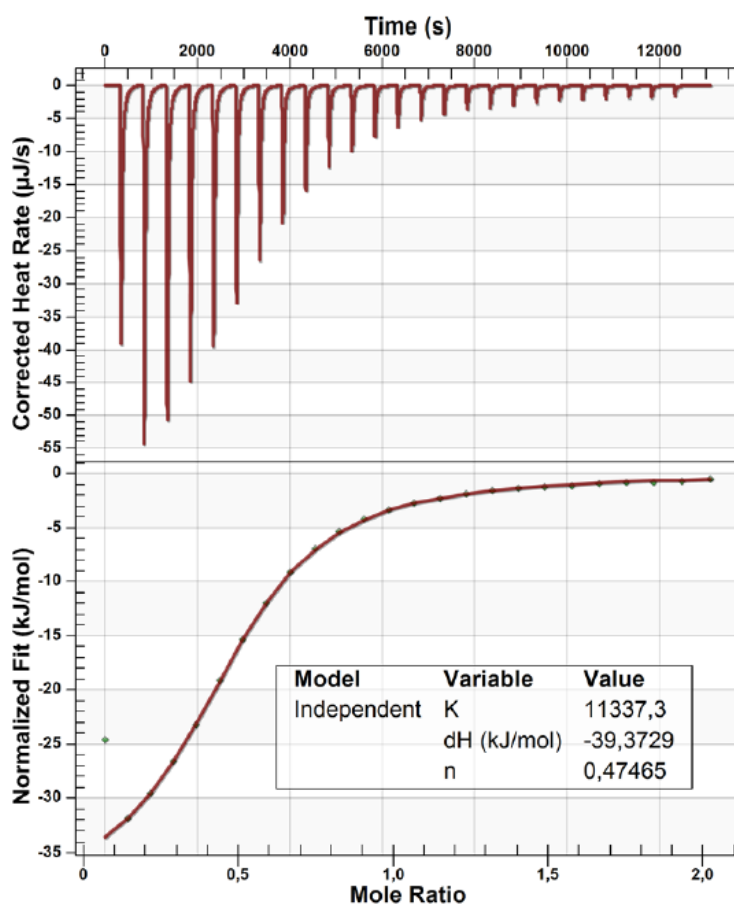


Figure 3.7: Heat changes for calorimetric titrations of **3** to a  $\beta$ -CD solution (top), normalized measured heats of injections and best-fit values (bottom).

# 4 Impact of attachment flexibility on dynamic effects of adhesive interactions

## 4.1 Introduction

Self assembled monolayers (SAM) are an effective tool in nanoscience for modifying surface functionalities which facilitate the investigation of molecular interaction by means of atomic force microscopy (AFM). In chemical force microscopy measurements, the AFM tip is functionalized by SAM in order to enable the attachment of the molecule of interest. High quality monolayers and good reproducibility are required in order to perform reliable force spectroscopy experiments. On oxide surfaces silanes with a specific head and tail group are used where the head group forms covalent bonds with the oxide and the tail group is exposed to the solution and determines the functionality of the silane.

The formation of silane SAM on oxide surfaces has been widely studied over the last decades [75, 76] and general agreement has emerged that the degree of order is highly dependent on several deposition parameters such as temperature [77], solution age [78] and water content in solution and on the surface [79, 77, 80]. The water content and the age of the solution determine the level of crosslinking of the silane molecules and the number of siloxane bonds formed with the surface. Explicit recipes were developed in order to achieve a well defined monolayer in terms of layer thickness, surface homogeneity and roughness [81].

In this chapter, we will demonstrate that the water content directly affects the stiffness of the silane layer. The effective stiffness of the attachment is a crucial parameter in chemical force microscopy measurements since the molecular stiffness predominantly determines the force ramp acting on the bonds. We modify the stiffness of the silane layer by using different preparation methods. There are two main options how to prepare a silane layer:

from liquid and from vapor phase. A scheme of both preparation methods is shown in Fig.4.1. In liquid phase, the silane molecules can oligomerize in solution forming a three dimensional network before coupling to the oxide surface [73, 79]. Prior to oligomerizing, a hydrolyzation of alkylsilanes is required [82]. Hence, water in the silane solution enhances the polymerization of silane molecules resulting in a loosely bound network attached via a limited number of silanol bonds with the surface [80, 83]. It is important to note that a formation of a fully crosslinked 2D network where all silane molecules are covalently attached to the surface is not possible due to the limited number of ethyl groups and the steric hindrance of the alkyl chain [79]. Nevertheless, it has been demonstrated that the self assembly of the monolayer is organized in a thin water film adsorbed on the surface [75]. Moisture is crucial for the formation of a homogeneous layer which was confirmed by a decrease of the root mean square (RMS) roughness for after silanization compared to the clean wafer [77]. The silanization from vapor phase prevents the molecules from polymerizing before binding to the oxide resulting in a 2D network that offers more anchor points [79]. Thus, we expect a system prepared by vapor phase deposition to exhibit a higher overall stiffness than one prepared by immersion in liquid phase.

A lower stiffness would have a remarkable effect on the measured friction and adhesion forces since several bonds could be pulled in parallel. In this way, the lower stiffness would enhance friction and adhesion. In order to test this hypothesis, we performed adhesion and friction force measurements on cyclodextrin functionalized surfaces on which the cyclodextrin molecules were attached to differently prepared silane layers. We also artificially aged the silane solution by exposing it to humid environment or adding water directly to the silane solution to investigate the effect of water on the layer formation. The humid conditions should accelerate the aging process of the silane molecules. Our molecular toolkit for the test of friction and adhesion based cyclodextrin functionalization and adamantane connector molecules is an appropriate model to study the effect of silane layer stiffness for two reasons. The first aspect is that the CD molecules are directly attached to the silane molecules so that no additional flexibility is added. The second aspect is that the inclusion complex is probed in thermodynamic equilibrium [2] so that no rate dependence of the single rupture force is expected.

We performed adhesion and friction measurements on CD surface with three differently prepared silane layers to investigate the effect of the presence of water in the silane deposition process on adhesion and friction. The first sample was prepared by the vapor deposition method (VPD) directly after receiving the silane molecules. Prior to preparing

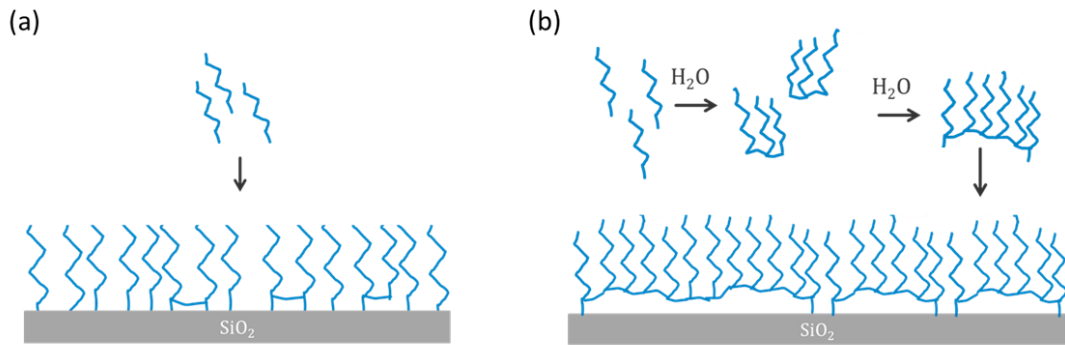


Figure 4.1: Scheme of the attachment of the silane molecules (blue) onto the silicon oxide surface from (a) vapor phase deposition and (b) liquid phase deposition.

the second sample, the silane was stored under humid conditions at room temperature for one week before it was deposited to an oxide surface by VPD. The third sample was prepared by immersing an silicon sample in silane solution. The silane was diluted in tetrahydrofuran (THF) which contained 0.1% water. The solution was stored at room temperature for one week before the oxide surface was exposed to it. The different methods were chosen in order to mimic the different aging processes in the laboratory. The THF used for liquid phase deposition (LPD), is hygroscopic and predominantly causes the water uptake of the silane solution so that the water was directly added to the THF. The silane used for VPD is not diluted prior to the deposition step so that the water uptake of the silane was mimic by storing it in humid conditions.

## 4.2 Experimental section

### Surface functionalization

Silicon Wafers were supplied by Si-Mat, Kaufering, Germany and cleaned with piranha, a mixture of sulfuric acid (95-98%) and hydrogen peroxide (30 wt.%) in the ratio 3:1, subsequently rinsed with water and dried with nitrogen. The silicon wafers were first silanized with 3-isothiocyanateisopropylsilan (the synthesis is described in ref.[2]) according to the three different protocols. The  $\beta$ -CDs were covalently attached to the functional groups of the silane. For the first protocol, the silicon was silanized by using a fresh silane solution which was deposited from vapor phase. The clean silicon sample and 75  $\mu$ L of the silane solution were placed into a desiccator. Before evacuation up to a pressure of 2 mbar

the chamber was floated with dry nitrogen in order to remove the remaining humidity inside the chamber. The sample was removed after 45 min, rinsed with tetrahydrofuran (THF) and water. For the second set of samples, the silane solution was stored in humid conditions for 7 days in a sealed chamber in order to mimic an aging of the silane solution when stored in laboratory conditions for a longer time scale. The samples were prepared in the same way as for the first samples. The third batch of samples was prepared by liquid phase deposition of an artificially aged silane solution. The silane was diluted in THF with a concentration of 0.1% and the same amount of water was added. The solution was stored for 7 days in a sealed beaker. After the storage period, a cleaned silicon wafer was incubated in the solution for 2 h, rinsed with water and dried with nitrogen. For attaching the  $\beta$ -CD molecules, the silanized samples were incubated in a 5 mM  $\beta$ -CD solution for a minimum of 12 h. The silicon cantilevers were functionalized in the same way as the surfaces. Both, the surface and cantilevers were stored in water and used within three days after preparation. For AFM measurements and data analysis see experimental section in chapter 3.

### 4.3 Results

The effect of the different silane preparation methods on adhesion and friction forces was studied by means of AFM. The adhesion force between a  $\beta$ -CD functionalized AFM tip and surface on differently prepared silane layers was determined in force spectroscopy measurements. The AFM tip and surface were prepared with the same functionalization method. In order to determine the unspecific interactions between AFM tip and surface, force measurements were performed in pure water without guest molecules prior to every experiment which serves as control experiment in this study. Subsequently, the connector molecules were added into the solution and the effect on the pull-off force was investigated. The maximum pull-off force was analyzed for 300 force-distance curves recorded at three different surface positions. For each surface position the most probable rupture force was obtained by fitting a Gaussian function to the histogram of pull-off forces. In Fig.4.2(a) the mean pull-off force is plotted as a function of unloading rate varied over three orders of magnitude. A remarkable difference in the mean pull-off force is observed when comparing the three surfaces. For the aged silane deposited from vapor and liquid phase, a dramatic increase in adhesion is observed when adding the connector molecules into the solution whereas an increase in adhesion on the fresh VPD silane is only observed for high

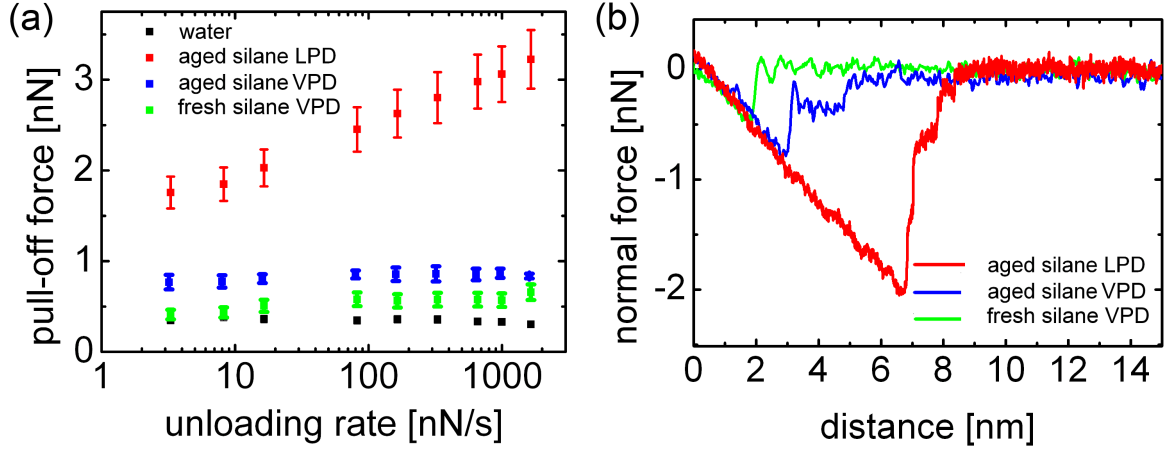


Figure 4.2: (a) Mean pull-off force between a  $\beta$ -CD functionalized AFM tip and surface with differently prepared silane layers in adamantane solution, the control experiment is performed in water. The error bars represent the standard deviation of the three mean force values of the different surface positions. (b) Representative force curves recorded on the different samples in adamantane solution with a pulling rate of 2  $\mu$ ms.

loading rates. In addition, the rate dependence varies dramatically for the different silane preparations. The pull-off force on the LPD silane increases by almost 1 nN for loading rates between 20 nN/s and 1500 nN/s and levels off for rates below 10 nN/s at a pull-off force below 1 nN. The pull-off forces recorded on the surface prepared with fresh silane by using VPD increases slightly with loading rate and does not surpass the level of the control experiment for pulling rates below 10 nN/s. In contrast, the pull-off force recorded on the aged VPD silane stays rather constant as function of pulling rate.

In Fig.4.2(b), representative force-distance curves are shown for the different surface preparations. The highest pull-off force and a step-wise detachment was observed on a sample containing a silane layer deposited from an aged solution (LPD). The high rupture force indicates that multiple bonds are ruptured in parallel. Due to the curvature of the AFM tip, the number of parallel bonds decreases during tip-sample retraction leading to the step-wise detachment with a decreasing plateau force as discussed in chapter 3. The separation length of about 10 nm on the LPD surface is a factor of two higher than expected for the molecular height of about 5 nm. In contrast, a smaller rupture force and a separation length comparable to or even below the height of the molecular attachment is observed for the samples prepared with a silane layer deposited by VPD. The force-distance curve recorded on the surface with a silane layer deposited from vapor phase of an aged

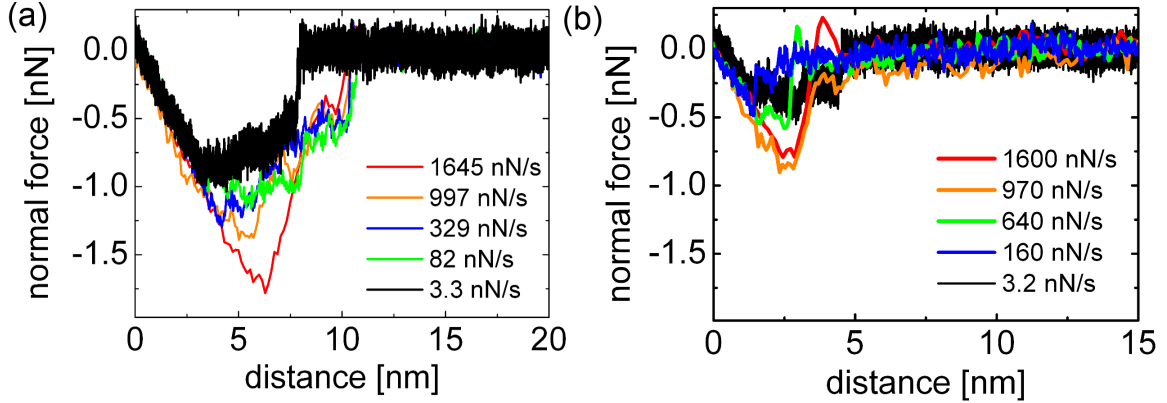


Figure 4.3: Representative force curves recorded in adamantane solution with different pulling rates on a surface functionalized with a silane layer (a) deposited from liquid phase (LPD) and (b) vapor phase (VPD).

solution exhibits a higher separation length than the surface with a silane layer deposited from fresh silane solution revealing a higher network flexibility for the surface deposited from aged solution.

The shape of the adhesion curve changes significantly with loading rate (see Fig.4.3). For slow pulling rates, the force exhibits a plateau and transfers into a triangular shape for high pulling rates as reported in chapter 3. The shape transfer is observed for all three surface preparations indicating that the underlying mechanism of rate dependence is the same for all samples.

The friction force between AFM tip and surfaces functionalized with  $\beta$ -CD molecules attached to differently prepared silane layers is studied in sliding experiments. When sliding across the surface, specific molecular bonds are formed between CD molecules at tip and surface. The adhesive interaction causes a torsion of the cantilever beam which is recorded in the lateral deflection signal. The hysteresis included in the friction loop reveals the dissipated energy during sliding across the surface. The average of the lateral force of forward  $\bar{f}_{\text{fwd}}$  and backward  $\bar{f}_{\text{bwd}}$  sliding equals the friction force  $\bar{f}_L = (\bar{f}_{\text{fwd}} - \bar{f}_{\text{bwd}})/2$ . In order to investigate the adhesive friction regime and exclude tip wear, the normal force was kept below 1 nN. In Fig.4.4(b)-(d) representative friction loops recorded on the three differently prepared surfaces with a scanning speed of 800 nm/s are presented. An erratic stick-slip characteristic of the AFM tip motion is observed on all surfaces independent of the sliding speed. The slope of the stick-slip events reveals the effective contact stiffness  $k_{\text{eff}}$  which is a combination of the cantilever stiffness  $k_c$  and molecular bond stiffness  $k_{\text{mol}}$  :  $1/k_{\text{eff}} = 1/k_{\text{mol}} + 1/k_c$ . Due to the high cantilever stiffness in lateral direction, the effective



contact stiffness is predominantly determined by the stiffness of the molecular attachment. The contact stiffness varies for the silane preparation methods. Surfaces prepared from silane solution exhibit the lowest stiffness with about 0.2 N/m compared to the silanes deposited from vapor phase which exhibit a similar contact stiffness of about 1 N/m.

The average friction force value as well as the rate dependence vary dramatically with the preparation method. In line with the pull-off force, the highest overall friction force was observed on the surface prepared by liquid phase deposition of the aged silane solution. Interestingly, the effect of the preparation method on the dynamic friction force is contrary to the effect observed in adhesion. No rate dependence was observed on the surface prepared from liquid phase. In contrast, a weak but significant increase of friction with the sliding speed is observed on the samples prepared from vapor phase deposition. For the silane layer deposited from vapor phase with aged silane solution, the friction force exhibits a similar value as the surface prepared with aged LPD silane whereas the friction force on the surfaces prepared with fresh silane matches with the friction force of the control experiment and exceeds this level only for sliding speeds above 100 nm/s.

## 4.4 Discussion

In this section we will discuss why the flexibility of the silane layer cause the opposite effect on the rate dependence of adhesion and friction. In the first part, the effect of preparation method on the contact stiffness and pull-off force is discussed and in the second part we address the different rate effects in adhesion and friction.

### 4.4.1 Contact stiffness of differently aged silane layers

The stiffness of the contact between the  $\beta$ -CD functionalized AFM tip and surface can be revealed in friction loops. The results demonstrate that the effective contact stiffness varies significantly with the preparation method of the silane layer below the  $\beta$ -CD layer. The liquid phase deposition method results in the lowest contact stiffness. We believe that the low contact stiffness originates in the compliance of a three-dimensional silane network, which is formed in LPD of aged silanes and which is bound to the surface with less anchoring points than a silane layer produced by VPD. In order to mimic an aging process, the silane solution was stored in THF which contained 0.1% water. The water leads to a hydrolyzation of the silane molecules which starts their polymerization already in solution [82]. A side product of the condensation reaction is water which again enhances the

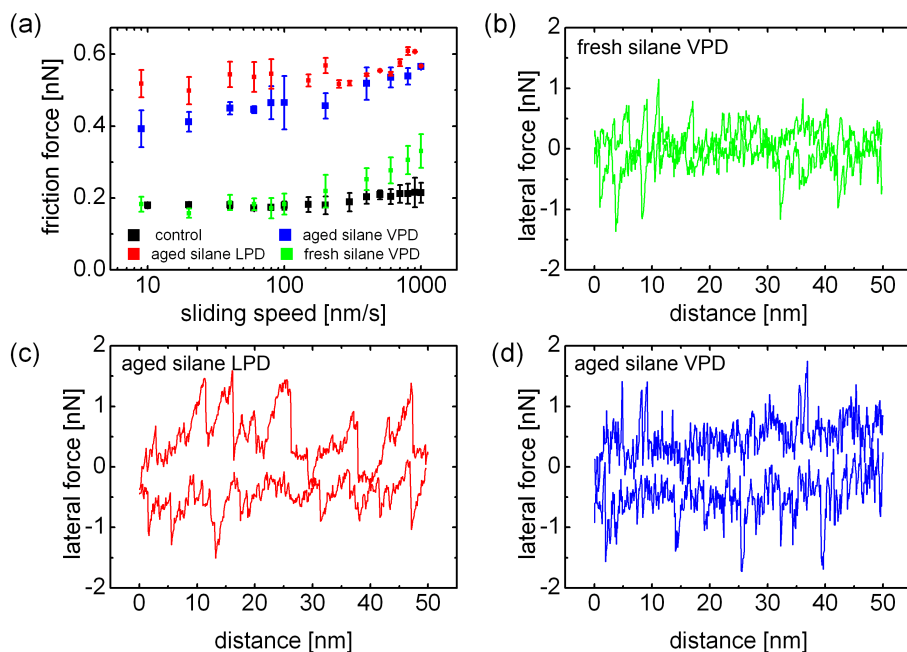


Figure 4.4: (a) Mean friction force between a  $\beta$ -CD functionalized AFM tip and surface for differently prepared silane layers in adamantane connector solution and the control experiment in water. The error bars are the standard deviation of the average friction force of 50 friction loops. Representative friction loops recorded in adamantane solution with a sliding speed of 800 nm/s on surfaces prepared with (b) fresh silane solution with VPD, (c) aged silane solution with LPD and (d) aged silane solution with VPD.

polymerization. When exposing the silicon oxide surface to the silane solution the already pre-polymerized or oligomerized patches attach to the surface by forming covalent bonds with the remaining free bonds. Hence, a loosely bound three dimensional network is formed whose compliance leads to a low contact stiffness in adhesion and friction measurements.

The higher contact stiffness of the samples prepared by VPD can be explained by two effects. The aged silane solution for the liquid phase deposition was prepared by adding the water not directly into the solution but storing the solution under humid conditions. We assume that the water content is lower than in the solution used for LPD resulting in a lower degree of polymerization. The second effect originates in the VPD process itself. During deposition, the silicon sample and the silane solution are located well apart from each other in the dessicator. At low pressure, the silane molecules enter the gas phase and eventually adsorb on the sample forming siloxane bonds with the silicon oxide surface. Individual molecules are more likely to evaporate than polymerized patches. The individually attached silane molecules form siloxane bonds with their neighboring molecules resulting in a stiff two dimensional network. Hence, the surface is covered most probably by individual molecules or small oligomerized silane patches resulting in an intermediate contact stiffness as revealed from friction measurements.

We assume that the fresh silane solution exhibits the lowest level of polymerization resulting in the highest contact stiffness. The effect is probably further enhanced by using the VPD method since individual molecules enter the gas phase more likely than polymerized silane molecules.

The effect of contact stiffness on the adhesion force is visualized through a simplified model in Fig.4.5(a). In our model, the molecules are attached at different heights with a constant distance of  $a = 0.2$  nm. This distance is motivated by the average density of bonds at the AFM tip to be  $0.33/\text{nm}^2$ . We considered the silane network to act as a Hookean spring with the stiffness  $k_{\text{bond}}$ :

$$F = \sum_{i=1}^N k_{\text{mol}}(x - x_i)\Omega_i \quad (4.1)$$

where  $N$  is the maximum number of contributing bonds and  $x_i$  the height of the attached bonds  $x_i = (i - 1) \cdot a$ . The step function  $\Omega_i = 1$  if  $(i - 1) \cdot a < x \leq (i - 1) \cdot a + f_{\text{single}}/k_{\text{bond}}$  and  $\Omega_i = 0$  otherwise. The parameter  $f_{\text{single}}$  is the most probable rupture force of one bond with about 80 pN. The maximum number of bonds was estimated with  $N = 20$  which is a reasonable number concerning a tip radius of 7 nm and a hexagonal arranged CD SAM

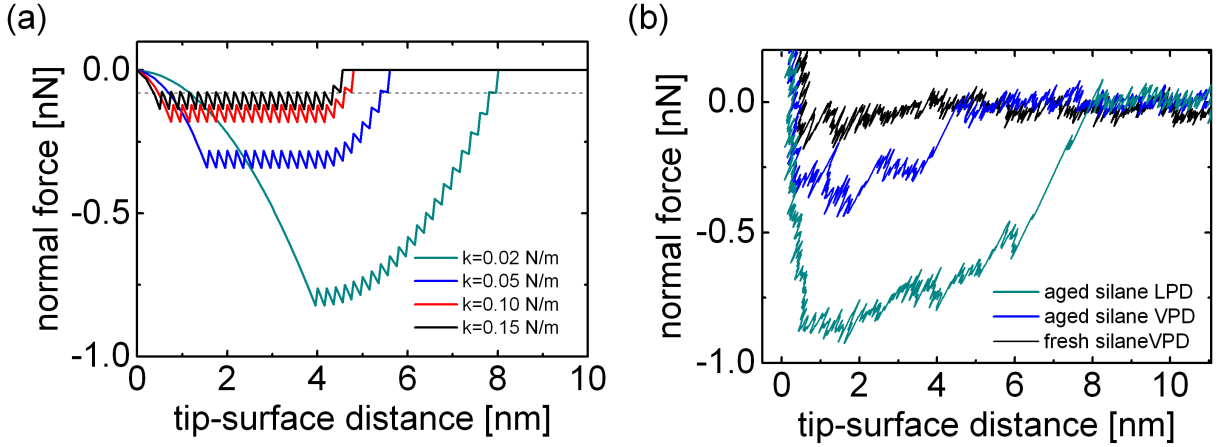


Figure 4.5: (a) Simulated force-distance curves with different molecular bond stiffnesses in the range of 0.02 N/m to 0.15 N/m. (b) Representative force-distance curves recorded with a velocity of 10 nm/s on the three surfaces in adamantane solution.

where a CD molecule has a diameter of 1.5 nm.

In Fig.4.5(a), the resulting force curves are presented. For stiff bonds, a plateau develops at a low normal force until the last rupture occurs at a distance of about 4.5 nm. In contrast, a triangular curve shape is observed for softer bonds with a larger maximum pull-off force of about 0.8 nN and maximum distance of 8 nm. It is important to note that the height of the last rupture event is not effected by the bond stiffness. This simple model is a crude approximation because in the experiment the bonds are rather attached to silane patches and not directly to the AFM tip. Nevertheless, the simulated data compares remarkable well to the experimental force curves shown in Fig.4.5(b). Due to the curvature of an AFM tip, the density of bonds is higher in the beginning of a force curve leading to a high adhesion force on small distance. This feature is not reflected in our model due to the constant separation distance. The good agreement between the simulation and experimental data confirms that the molecular bond stiffness has a significant impact on the pull-off force for assembles of molecular bonds. In the following, we will discuss how the contact stiffness affects the dynamic adhesion and friction force in respect to cooperativity effects.

### 4.4.2 Adhesion force on differently aged silane layers

The highest adhesion and friction forces are obtained for the lowest contact stiffness. Due to the high flexibility of the supporting silane layer, multiple bonds are formed and are pulled in parallel. The sharing of the applied force by parallel bonds lead to a dramatic change in the rate dependence of the overall adhesion. Load sharing leads to a cooperative interaction of parallel bonds which is described in literature as “multivalency effect” [17]. The kinetics of single bonds are fast since the bonds rupture and rebind more than a thousand times per second. In case of multiple bonds, the (un)binding kinetics are slowed down since the contact is stabilized by the remaining bonds when one bond unbinds. The probability to find all bonds simultaneously unbound describes the off-rate of the overall contact for parallel bonds which equals  $k_{\text{off}} = \frac{k_{\text{on}}}{K^n}$  where  $n$  is the number of parallel bonds and  $K$  is the binding constant of the inclusion reaction of single complexes [17]. For an attachment that offers a higher flexibility, more bonds are being pulled in parallel and, thus, the overall contact exhibits a much lower off-rate compared to a stiffer attachment where less bonds interact. The situation in this study is complex, since the bonds are attached at different heights due to the curvature of an AFM tip leading to a non-equal load sharing. The height distribution results in a change on the overall shape of the force curve when increasing the loading rate. In the low loading rate regime, the bonds are peeled subsequently, leading to a plateau shape of the force curve at a low force value. For high loading rates, the cooperative interaction stabilizes the contact which results in a triangular shape with a high maximum force value. A flexible network enhances this loading rate dependent change in rupture characteristic since more bonds can interact cooperatively than on a stiffer network. In a recently published theoretical study, the shape transformation of a force curve was simulated by R. Guerra et al. reproducing exactly the transfer of shape observed here [31]. Interestingly, changing the flexibility of the attachment leads to the opposite effect in friction. A constant friction force is obtained on the most flexible attachment and a rate dependence is observed when stiffer networks interact. In the following we will discuss the differences between adhesion and friction with respect to the contact time effects.

### 4.4.3 Dynamic effects in adhesion and friction on differently aged silane layers

In order to understand the difference between adhesion and friction we have to consider contact aging effects. Contact aging can be quantified by performing adhesion experiments as function of the time in contact before retracting the tip. Due to the fast bond kinetics, the supramolecular bonds are in thermodynamic equilibrium after about 10 ms which is the lower limit of the contact time in our friction experiments. However, a logarithmic increase of the pull-off force was observed on the contact time scale in the range of 10 ms to 10 s. The most probable pull-off force was fitted with the following equation

$$f_n = a \cdot \ln(t/t_0) + B(r) \quad (4.2)$$

where  $t$  is the contact time scaled to the time constant  $t_0 = 100$  ms,  $a$  the proportionality factor and  $B(r)$  a force constant which is dependent on the loading rate. The best fit to the data revealed a logarithmic increase of the pull-off force with the contact time with a slope of  $a = 0.19$  nN in connector solution (see supplementary information for more details). The increase in adhesion is probably due to a rearrangement of the CD molecules leading to a higher number of bonds formed between AFM tip and surface.

In adhesion experiments, the approach velocity is kept constant and a contact time of 5 s is applied for all loading rates. Only the retraction speed is varied leading to an overall contact time of 5.003 s for the highest pulling rate and 5.5 s for the slowest loading rate including a dwell time on the surface. Due to the logarithmic growth of adhesion force with contact time, the additional force contribution caused by the contact ageing is negligible.

In contrast to adhesion, the contact time changes remarkably with the sliding speed so that contact aging effects become significant in friction. For the flexible attachment (LPD), the stick-slip pattern exhibit a typical stretching length of about 5 nm leading to a contact time of 0.5 s for sliding speeds of 10 nm/s and to a contact time of 5 ms for speeds of 1000 nm/s. Due to the contact aging we would expect an increase in friction force of about 0.5 nN for 10 nm/s and 0.05 nN for 1000 nm/s. Hence, the contact aging effect presumably balances the rate effect resulting in a constant friction force. We believe that the contact aging effect on a stiffer attachment is smaller than on the flexible attachment because the bonds have less degrees of freedom to rearrange. In addition, the stretching length of the stiffer attachments is smaller by a factor of 5 so that the contact aging on the large scale does not contribute as much as it does on the flexible attachment.

In summary, the flexibility of the attachment provides the possibility to tune the strength and dynamics of the tip-surface contact. In adhesion, a flexible attachment enhances the loading rate dependence whereas the contact aging effect balances the rate effect in friction experiments. For a stiff attachment, a similar dynamic characteristic is observed in friction and adhesion which is in line with recent simulation [31]. Hence, well defined silane networks are crucial for investigating dynamic effects of adhesive interactions. A flexible silane network deposited by LPD provides high adhesion and friction forces and offers the possibility to study dynamic surface interactions on soft systems. The dynamics of ensembles of molecular bonds can be studied by stiffly attaching the silane layer to the surface by VPD in order to neglect additional contact time effects.

## 4.5 Conclusion

In conclusion, we demonstrated that the stiffness of the silane layer affects the friction and adhesion force between a cyclodextrin functionalized AFM tip and surface mediated by ditopic connector molecules. In particular, the water content in the silane solution used for surface functionalization was shown to be a crucial parameter for tuning the contact stiffness. We believe that the pre-polymerization of silane molecules in solution lead to this effect. The fresh silane showed a higher molecular stiffness and smaller adhesion and friction force indicating that a smaller number of bonds is stretched simultaneously. A lower contact stiffness was observed for the silane layer deposited from an aged solution caused by the higher level of polymerization resulting in a higher adhesion and friction force. Moreover, we observed a different rate dependence in adhesion and friction measurements. In adhesion, a more pronounced increase of the pull-off force was observed for a system with a low stiffness caused by the multivalency effect. In contrast, the friction force showed a significant rate dependence on the surfaces with lower stiffness which we attribute to a contact aging at low velocities which balances the rate effect. We suggest to prepare surfaces with a high stiffness for investigating the impact of bond kinetics on the overall dynamic friction and adhesion forces in order to neglect contact aging which can balance the rate effects.

## 4.6 Supplementary Information

In order to investigate the time scale of the bond forming process, we performed contact aging experiments. The AFM tip was approached to the surface and the contact time was varied between 0 s and 15 s before the tip was retracted. The experiment was repeated for different unloading rates and the maximum pull-off force was analyzed in a histogram by fitting a Gaussian function to the data. The most probable pull-off force at different loading rates is plotted versus the contact time in Fig.4.6. In particular for low unloading rates the actual contact time can differ from the instructed value. The “real” contact time was revealed from f-d curves after the measurement by determine the time span between the snap-in to the snap-off at the maximum pull-off force.

The equilibrium of the host-guest reaction is established within less than a microsecond which is not measurable with the help of an AFM due to experimental limitations. However, Fig. 4.6(a) shows the adhesion force increasing linearly with the logarithm of the contact time on a larger time scale. The aging phenomenon is probably due to strengthening of molecular bonds [34]. In order to determine the specific and unspecific contributions, the contact aging for different guest concentrations in solution was investigated. Fig. 4.6(b) shows that the slope increases with the concentration but is not zero in pure water. Hence, there is a contribution of unspecific bonds such as hydrogen and van der Waals bonds that are formed when the tip stays longer in contact with the surface. Additionally, specific bonds are strengthened probably due to a realignment of the guest molecules. Interestingly, the aging process seems to be independent of the unloading rate which indicates that the single bonds are in thermodynamic equilibrium.



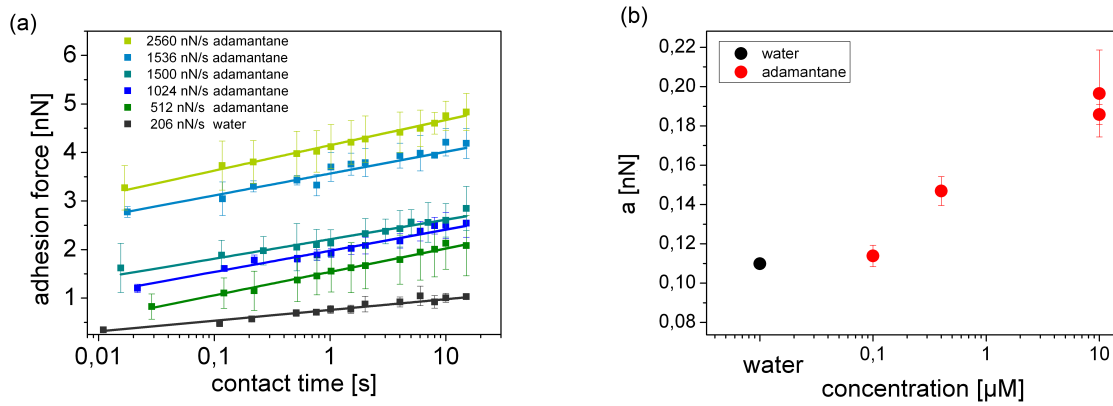


Figure 4.6: (a) Most probable pull-off force between the  $\beta$ -CD functionalized tip and surface at different contact times. The data is fitted according to equation (4.2). The most probable pull-off force is the average pull-off force of about 600 f-d curves recorded on three different surface positions, the error bar represents the standard deviation of the three surface positions. (b) The proportionality factor  $a$  in equation (4.2) of the contact aging experiment at different guest concentrations with a constant unloading rate of 260 nN/s.

# 5 Effect of system flexibility on single and multiple bond rupture force

## 5.1 Introduction

Atomic force microscopy is one of the key methods for analyzing single molecular interactions. Reversible molecular bonds can be probed under force using the dynamic force spectroscopy mode (DFS). Based on the theoretical framework of Bell [24] a model was derived by Evans et al. [8] which describes the kinetics of bonds under force. The so called Bell-Evans model reports a linear relationship between the rupture force of a single bond  $f$  and the logarithm of the unloading rate  $r$ :  $f \propto \ln(r)$  [8]. A large number of studies on different molecular systems reported this loading rate characteristic. In contrast, other studies reported divergent force spectra of single bonds which exhibit no rate dependency or regimes with different logarithmic constants such as the extensively studied streptavidin-biotin interaction. The different regimes were explained by inner energy barriers which dominate the rupture force for a certain range of loading rates [8]. No rate dependence was observed for the inclusion complexes of cyclodextrins when varying the loading rate over three orders of magnitude. This finding was attributed to the fast complexation kinetics of those supramolecular bonds [2, 58, 23].

The absolute rupture force for the same molecular system varied in reports from different research groups up to a factor of two indicating that the instrumentation has an impact on the measured rupture force [84]. The impact of force transducer stiffness was first theoretically predicted [85, 29, 86], and later experimental evidence was given by single molecular force experiments on the biotin-streptavidin bond [84]. The theoretical models are based on a superposition of the energy profile of the supramolecular bond and the harmonic potential of the cantilever. The harmonic potential of the AFM tip creates a second minimum in the energy landscape which allows for a continuous rebinding of thermally ruptured bonds (see Fig.1.3). The rebinding results in a monostable regime at low

pulling rates where the rupture force is not loading rate dependent. According to Friddle, the bond rupture occurs when the potential energy in the cantilever spring  $k_c$  equals the binding free energy of the molecular bond  $\Delta G$ . This equilibrium force  $f_{\text{eq}}$  is then given as [29]

$$f_{\text{eq}} = \sqrt{2k_c\Delta G}. \quad (5.1)$$

Unfortunately, detailed information about the transducer stiffness is missing in the most single molecular bond studies. In this study, we systematically vary the stiffness of the force probe and the molecular linker in order to determine the impact of both parameters on the single bond rupture force. We report on experiments with single host-guest interactions of cyclodextrin inclusion complexes in different molecular arrangements. The supramolecular bonds are in thermal equilibrium on the characteristic time scale of an AFM force probe. We found that the rupture forces indeed depend on the square root of the cantilever stiffness as proposed by Friddle et al. [29]. However, the value of  $\Delta G$  obtained with equation 5.1 is significantly lower than the binding energy obtained from Isothermal Calorimetry (ITC). As a molecular system we chose the inclusion reaction of cyclodextrin molecules as host and different guest molecules. Following a molecular toolkit approach introduced in Ref.[2], the same  $\beta$ -CD functionalization of the silicon surfaces was used in all experiments except for one system where the CD molecules are attached to polymer chains. In order to vary the flexibility and the dynamics of the interaction between AFM tip and surface we employed four different molecular systems (see Fig.5.1). In the first system, the AFM tip was functionalized by  $\beta$ -CD the same way as the silicon surface. Short ditopic adamantane connector molecules form a reversible bond between the  $\beta$ -CDs attached to the AFM tip and surface. The adamantane connector molecules consist of a tetraethylene glycole chain TEG which connects two hydrophobic adamantyl end groups TEG(Ad)<sub>2</sub>. A positively charged aminogroup is included into the TEG chain close to each of the two hydrophobic groups in order to enhance the solubility in water.

In the second system, the same tip and surface functionalization was used, but the ditopic connector molecule was modified by exchanging the TEG chain with a polyethylene glycole PEG for connecting the adamantyl end groups which increases the length and thus the flexibility of the connector molecules.

As a third system,  $\beta$ -CD-polymers were attached to the AFM tip and surface and the short ditopic adamantane connector molecules TEG(Ad)<sub>2</sub> were used as guest molecules. The results of the ditopic system were compared with a monotopic host-guest system (fourth system) where 6-(ferrocenyl)hexanthiol (Fc) was directly attached to a gold coated

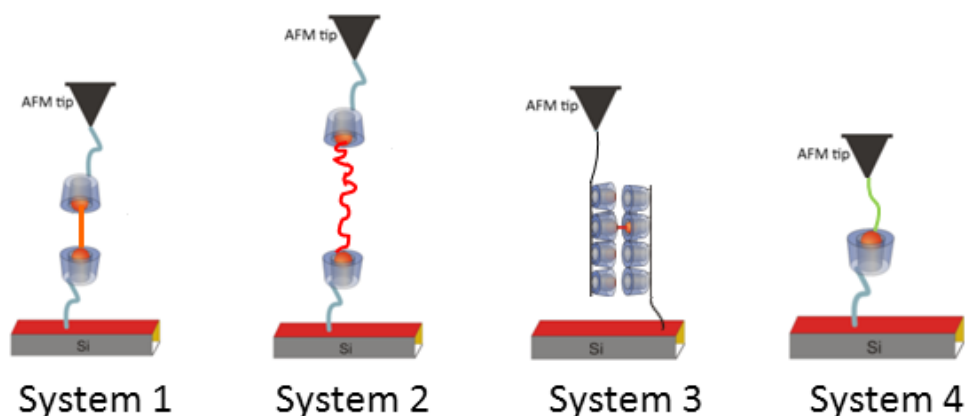


Figure 5.1: Scheme of the four different molecular systems which are used in this study; System 1: CD-TEG(Ad)<sub>2</sub>-CD, System 2: CD-PEG(Ad)<sub>2</sub>-CD, System 3: CD-polymer-TEG(Ad)<sub>2</sub>-CD-polymer and System 4: Fc-CD.

cantilever via a thiol bond. The ferrocenyl end group forms a weaker inclusion complex with the CD cavity than adamantane. Our functionalization approach provides the opportunity to analyze single and multiple bond interactions in the same data set. In the first section we will discuss the impact of cantilever stiffness on the single bond rupture force and later we will turn to a multiple bond system.

## 5.2 Experimental section

For details of the surface functionalization and the chemical modification of the silicon AFM tips (Nanosensors PPP-Cont AFM Probes, NanoandMore, Wetzlar, Germany) in system 1 and 2 see the experimental section of chapter 3.

The attachment of the polymer in system 3 is done similar to the functionalization of the CD molecules. The AFM tips were silanized by vapor phase deposition at a pressure of 2 mbar for 45 min and subsequently rinsed with tetrahydrofuran and water. The silanized AFM tips were incubated in a 5 mM CD-polymer solution where the amino groups of the polymers react with the isothiocyanate head group of the silane molecules forming covalent bonds.

In system 4, a gold coated AFM tip (Bruker AXS GmbH, Karlsruhe, Germany) was functionalized by incubation in 0.5% 6-(Ferrocenyl)hexanthiol diluted in an ethanol solution containing 1% 6-mercaptoethanol. All three substances were used as supplied by Sigma Aldrich, Munich, Germany.

## 5.3 Results and Discussion

The impact of cantilever stiffness on the adhesion force curves was studied by means of AFM. In dynamic force spectroscopy measurements force-distance curves were recorded in aqueous solution. A minimum of 300 force curves recorded on three different surface positions were analyzed for each molecular system. We investigated single bond rupture forces with compliant force probes with a stiffnesses ranging from 0.09 N/m to 0.34 N/m. For the multiple bond system we additionally used a non-contact cantilever with a stiffness of 20 N/m. We will first discuss the overall shape of the force-distance curves and then the influence of the cantilever stiffness on measured single and multiple bond rupture forces.

### 5.3.1 Shape of the force-distance curves

Representative force-distance curves are shown in Fig.5.2. For systems 1 to 3 a control experiment is performed in water without guest connector molecules, result are plotted in gray. The adhesion in the control experiment is caused by nonspecific CD-CD interactions such as hydrogen bonds of the hydroxyl planes. The force increases significantly when the connector molecules are added into the solution (black) indicating a successful inclusion of the connector molecules into the CD cavities. For system 4 in Fig.5.2(d) no direct control measurement is available because the ferrocene guest molecules are directly attached to the AFM tip. In case of ferrocene, a full force-distance cycle is shown, where the high pull-off force reflects the attractive interaction between the ferrocene end groups and the CD cavity. The shape of the force curves differs significantly for the particular molecular system. However, stepwise rupture is observed for all systems during retraction, demonstrating that multiple bonds contribute to the adhesion between tip and surface. At small tip-surface separation, the maximum adhesion force is observed. When tip and surface are close, a parallel rupture of several bonds occurs due to the large contact area resulting in the maximum pull-off force. Due to the curvature of the AFM tip, the contact area decreases during retraction leading finally to the rupture of the single bond before the tip snaps back into its equilibrium position. The last rupture event for the CD-polymers and the PEG(Ad)<sub>2</sub> connector molecules occurs at a separation of 20 nm (PEG(Ad)<sub>2</sub>) and 160 nm (polymers) which corresponds to the respective molecular length. System 1 and 4 exhibit an unexpected large separation length compared to the molecular height of about 3 nm (system 4) to 5 nm (system 1). The higher flexibility was provided by a differently prepared silane layer underneath the CD molecules. The silane molecules were deposited

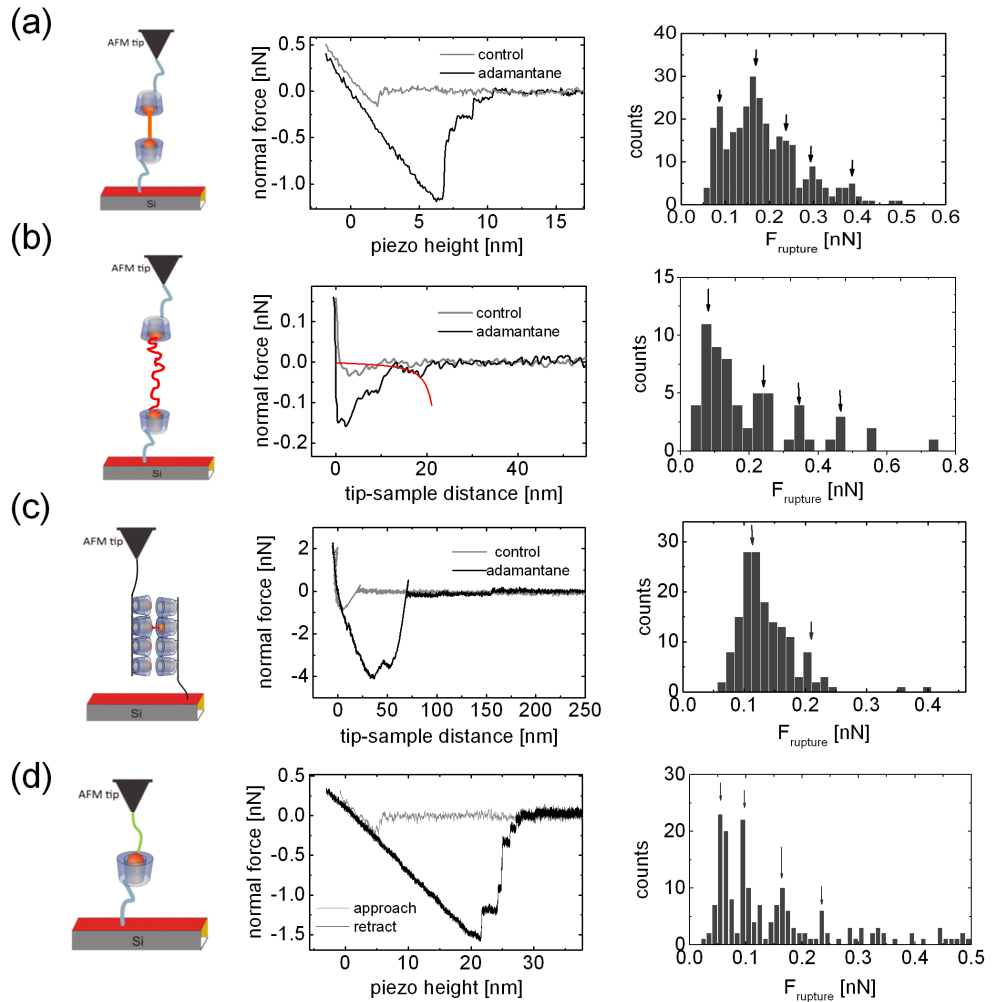


Figure 5.2: Representative force-distance curve recorded in aqueous solution with (black) and without connector molecules (grey) for the four systems: (a) CD-TEG(Ad)<sub>2</sub>-CD, (b) CD-PEG(Ad)<sub>2</sub>-CD, (c) CD-polymer-TEG(Ad)<sub>2</sub>-CD-polymer and (d) Fc-CD. The red line in (b) represents a WLC fit to the data. Histograms of the last rupture forces for the four systems, the arrows indicate most probable single and multiple ruptures forces.

from liquid phase in a humid environment instead of vapor phase deposition at low pressure as in system 3 and 4. The water starts an oligomerization of the silane molecules in solution prior to the covalent attachment to the oxide surface. The oligomerized silane patches form fewer anchor points with the surface resulting in a flexible 3D silane network. The CDs are subsequently attached to the silane network. When pulling on the  $\beta$ -CD molecules, the silane network is stretched leading to a higher separation length and a lower effective stiffness than expected for the molecular stiffness of single silane molecules (for more details see chapter 4). For small separation length, the lower silane flexibility promotes a parallel bond rupture of multiple molecules resulting in a high maximum pull-off force compared to systems 2 and 3. However, single bond rupture events with the same force were also observed on stiffly bound cyclodextrin layers (data not shown). The last step in the retraction curve reveals the rupture force for a single complex, while the maximum force is relevant for the study of a multiple bond contact. In the following section, we will discuss the impact of cantilever stiffness on the rupture force of a single complex.

### 5.3.2 Effect of cantilever stiffness on single bond rupture force

The rupture force for a single complex was determined from the last step in force-distance curves recorded in the guest solution for the (Ad)<sub>2</sub>- $\beta$ -CD systems and in water for the Fc- $\beta$ -CD system. The fd-curves were fitted by a step function around the rupture event to determine the force at rupture. The f-d curves for system 2 exhibit a nonlinear force increase due to the PEG stretching, and were fitted with a worm-like chain (WLC) model as indicated by the red line in Fig.5.2(b). The contour length was a fitting parameter and the persistence length was fixed at 3.5 Å which is half of the Kuhn length of a PEG chain. Events with a contour length of  $25 \pm 5$  nm were included in the analysis. The rupture forces were summarized in a histogram for further evaluation. A typical histogram for each molecular system is shown in Fig.5.2. The first peak in the histogram represents the most probable rupture force of a single complex, the second for two parallel ruptured bonds, etc.

The single complex rupture forces  $f_{eq}$  for ditopic adamantane and monotopic ferrocene were included in Fig.5.3 where the rupture force is plotted as a function of the square root of the cantilever stiffness. A linear correlation between rupture force and square root of the cantilever stiffness is observed. The result confirms the significant impact of cantilever stiffness on the rupture force. The fact that the rupture forces of all ditopic adamantane systems fall onto the same line indicates that the molecular attachment has a

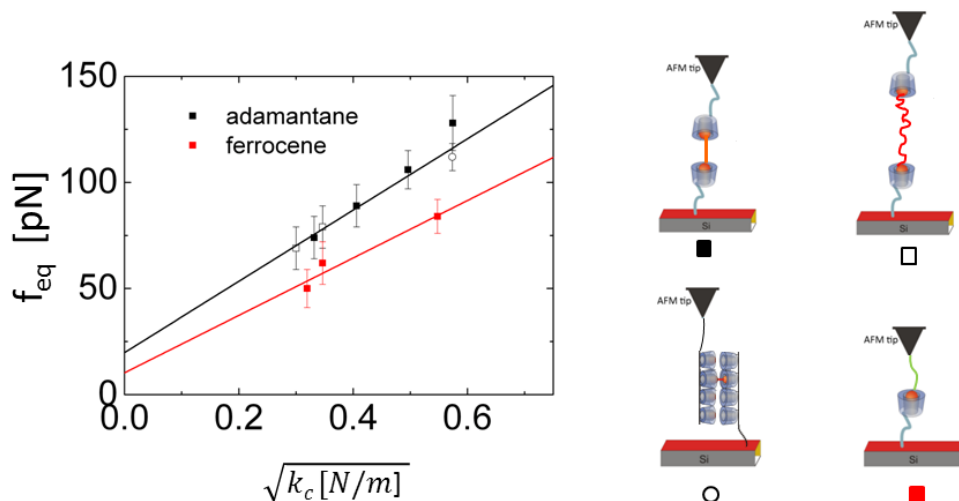


Figure 5.3: Most probable single rupture force as a function of cantilever stiffness for the four different systems. The solid lines represent best linear fit to the data. The error bar is the deviation of the mean single bond rupture force obtained on at least three different surface positions. As a legend the schemes of the molecular systems are shown.

minor impact on the rupture force of the  $(Ad)_2$ - $\beta$ -CD complexes. The single rupture force for the same system (system 1 and 2) exhibits different rupture forces depending on the force probe stiffness. Vice versa, a similar rupture force is obtained for system 1 and 3 when using the same cantilever stiffness although the systems differ remarkably in the molecular attachment. This result demonstrates that the molecular linker stiffness does not effect the measured rupture force of supramolecular bonds in thermal equilibrium. The dependence of the single bond rupture forces on only the cantilever stiffness surprises, given that the linker is a spring in series and, as the softer spring should dominate the overall stiffness. We believe that this is due to the different time scales of the molecular components and cantilever spring. The kinetics of the inclusion reaction and the relaxation time scale of the molecular linker are fast compared to the characteristic time scale of the cantilever so that the cantilever stiffness has a dominating effect on the single rupture force.

The single rupture forces were also analyzed for monotopic ferrocene directly tethered to a gold coated AFM tip. The rupture forces of ferrocene are smaller than for adamantane indicating a weaker interaction with the cyclodextrin cavity. We will discuss the result for adamantane and ferrocene below with respect to the different time scales of the molecular components and cantilever spring.

In order to understand the data, we have to consider the energy landscape probed by



the AFM tip. The pulling experiments can be modeled as a molecule which is tethered to the AFM tip by a soft linker (see Fig.5.4). Hence, we have to consider three energy potentials during pulling:

$$\begin{aligned} V_m(x_m) &= D_e(1 - e^{-ax_m})^2 \\ V_c(x_c) &= \frac{1}{2}k_c(x_c - x_{c,0})^2 \\ V_l(x_l) &= \frac{1}{2}k_l(x_l - x_{l,0})^2 \end{aligned}$$

The bond potential can be described as a single potential well which is simulated by a Morse potential  $V_m(x_m)$  where  $D_e$  is the well depth which is in the order of several  $k_B T$  and  $a$  the stiffness of the potential. The force probe behaves like a Hookean spring whose energy profile follows the potential  $V_c(x_c)$ . At the rupture distance, the potential  $V_c(f_{\text{rup}}/k_c)$  is also in the order of several  $k_B T$ . For sake of simplicity, the potential of the linker  $V_l(x_l)$  is described by a harmonic potential which is fair for small forces below to 100 pN where the PEG is in the elastic regime [87]. Due to its low stiffness  $k \leq 0.03$  Nm, the linker potential exceeds the energy of the bond and cantilever by one order of magnitude at the rupture distance. During one experiment, the distance  $z$  of the piezo stage is increased which is the sum of the elongations  $z = x_1 + x_m + x_c$ . The bonds investigated in this study are in thermodynamic equilibrium meaning that the bonds un- and rebind continuously during the pulling experiment. In the following we will discuss the time scales of rebinding in comparison to the relaxation time of the molecular linker and the AFM tip.

The lifetime of the adamantane cyclodextrin inclusion complex is  $\tau_m^{\text{off}} = 125 \mu\text{s}$  meaning the bond thermally detaches 8000 times per second. The on-rate is diffusion limited and depends on the concentration of the guest molecules  $k_{\text{on}} = 10^{-9} \text{ M}^{-1}\text{s}^{-1}$ . For the short TEG connector molecules in system 1 and 3 the concentration close to the surface  $C_{\text{eff}} \approx 0.22 \text{ M}$  is high resulting in a fast rebinding constant  $\tau_m^{\text{on}} = 1/(k_{\text{on}}C_{\text{eff}}) = 5 \text{ ns}$  (see chapter 7). In system 2, the hydrophobic end groups are connected via a flexible polymer chain which has its own intrinsic relaxation time scale described by the Zimm time [88]

$$\tau_l = \nu N^2 a^3 / (k_B T) \approx 100 \text{ ns} \quad (5.2)$$

where  $\nu$  is the viscosity of water,  $a$  is the Kuhn length and  $N$  the number of monomers. In contrast to the complete polymer chain, the relaxation of a monomer is fast:  $\tau_1^0 \approx 0.1 \text{ ns}$  which is faster than the complexation kinetics. We conclude that the thermally induced

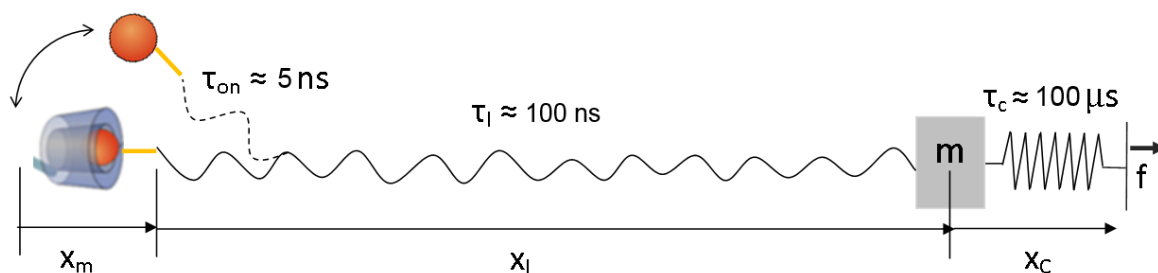


Figure 5.4: Scheme of the experimental arrangement with the time scales of the inclusion reaction  $\tau_{\text{on}}=1/k_{\text{on}}$ , relaxation time of the molecular linker  $\tau_l$  and the reaction time of the cantilever  $\tau_c$ .

un- and rebinding of the molecular bonds is possible due to the fast movement of the monomers. The whole PEG chain is not able to relax and withdraw within the short “off” period of the bond so that the bond rebinds continuously during a pulling experiment leading to a quasi-static equilibrium even for a mildly stretched PEG chain. The response time of the cantilever  $50 \mu\text{s} \leq \tau_c \leq 200 \mu\text{s}$  is much larger than the characteristic rebinding time. Due to its slow response time, the AFM tip is acting as a low-pass filter facilitating the constant rebinding. The TEG and PEG chains are built of the same monomers leading to fast binding kinetics compared to the characteristic time scale resulting. Due to the fast complexation kinetics in comparison to the reaction time of the AFM, the bonds are probed in thermodynamic equilibrium so that the rupture force is predominantly determined by the cantilever stiffness and binding energy.

Experimental evidence that rebinding matters in our study is provided in Fig.5.5 which presents a detail of the force curve between a ferrocenyl functionalized AFM tip and a  $\beta$ -CD covered surface (system 4) shown in Fig.5.2(d). Starting from a distance of 28 nm the force trace is rather smooth indicating that the potential of the AFM tip and the potential well of the bond overlap. For distances between 28.3 nm and 28.8 nm, the force trace becomes instable which can be interpreted as the fluctuations between two potential wells. The force jump at a distance of 28.8 nm marks the rupture of the bond. Auletta et al. demonstrated in Ref.[89] for this molecular system that a transition from the bound to the ruptured state occurs within 4 Å in which the bond thermally un- and rebinds. They proposed that rebinding events should be observed within this distance. Beyond their experiment, we applied a sufficient high sampling rate of 50 kHz at a low pulling velocity so that we can detect the thermal un- and rebinding. For adamantane no rebinding events were observed. The off-rate of ferrocene is higher than the off-rate of adamantane leading

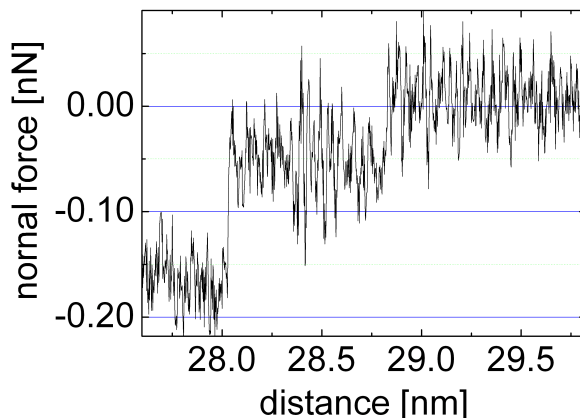


Figure 5.5: Detail of the force curve in Fig.5.2(d) between a ferrocenyl functionalized AFM tip and a  $\beta$ -CD coated surface.

to a larger “off”-period which apparently exceeds the reaction time of the cantilever so that the AFM tip can fluctuate into its equilibrium position until the bond rebinds again.

We will now discuss why the rupture force is affected by the cantilever stiffness. Upon pulling, the stretching of the molecular linker is observed as a non-linear increase of the normal force until a sudden rupture occurs. The height of this jump is considered the rupture force of the molecular bond. Due to the high on rate and slow relaxation rate of the whole polymer, thermally broken bonds continuously rebind so that the energy stored in the molecular linker has no impact on the rupture force of a single bond. In the following we will discuss three models that propose different reconstructions of the bond potential from the single rupture force. The first model describes the “snap-off” effect and relates the stiffness of the bond potential to the stiffness of the force probe. In a quasi-static approach, the force acting in the system is the universal parameter. The force in the cantilever spring equals the force acting on the bond. At a certain force, the force gradient in the Morse potential equals the cantilever stiffness  $d^2V_m(x_m)/dx_m^2 = d^2V_c(x_c)/dx_c^2$ . Beyond this point, the stiffness of the bond potential decreases further so that the bond will be ruptured. In this model, the rupture force decreases with increasing cantilever stiffness. Figure 5.3 demonstrates that for our system the rupture force increases with cantilever stiffness. Hence, the classical “snap-off” effect does not dominate the rupture force.

The second model, developed by Evstigneev and Reimann, is based on to the energy landscape of bond and cantilever. It states that the cantilever potential creates a second minimum which is separated by an energy barrier from the initial bond potential well [90]. The bond rupture occurs as soon as the bond is transferred from one minimum to the

other. For the transition, two assumptions are made: (i) the transition from one minimum to the other is thermally activated and (ii) the transition occurs close to the inflection point of the bond potential [90]. Evstigneev and Reimann proposed that the rupture occurs at the force  $f_{\text{rup}} = f_0 - k_{\text{eff}}^2 / (2V_m'''(x_m))$  where  $f_0$  is the force at the inflection point and  $V_m'''(x_m)$  the third derivative of the bond potential at the inflection point [90]. From this equation, two cases can be derived. For stiff molecular linkers, the effective stiffness is determined by the stiffness of the force probe leading to a decreasing rupture force with increasing cantilever stiffness. For compliant molecular linkers, the effective stiffness is predominantly determined by the linker resulting in a rupture force that is independent of the force probe stiffness. Both cases do not agree with our experimental results.

The first and second model describe the bond rupture as a quasi-static process, meaning that the bond is locked constantly until the rupture occurs. In contrast to covalent bonds, supramolecular bonds are characterized by an equilibrium at the on- and off-rates that is determined by the energy barrier of the bond potential. In case of cyclodextrin inclusion complexes, the binding kinetics are fast compared to the time scale of an AFM experiment. We can assume a quasi-static situation where the bond is in thermal equilibrium during the pulling experiment.

The third model proposed by Friddle et al. takes the continuous un- and rebinding into account and considers only the potential energies of bond and force probe. When tip and surface are in contact, the minima of the potential of the bond and the harmonic potential of the force probe fall together. Upon pulling, the free probe potential creates a second minimum with a low energy barrier in the direction of the bond potential minimum leading to a fast rebinding of a thermally dissociated bond. Pulling further, the bond potential minimum is lifted and the energy barrier between the two minima increases. The tip induced rebinding becomes less probable leading finally to the rupture event. According to Friddle et al. the most probable rupture occurs at a distance where the energy difference between bound and unbound state equals zero such that  $\Delta G - 1/2k_c(\Delta x_c)^2 = 0$  [29] so that  $f_{\text{rup}} = \sqrt{2k_c\Delta G}$ . The rupture occurs always at the same energy, so that a stiffer cantilever leads to a higher rupture force which is in line with our experiment. The slope of the rupture force vs. the square root of cantilever stiffness reveals the binding energy of the molecular bond.

The best linear fit to the data results in a higher binding energy for adamantane  $\Delta G = 8.2$  kJ/mol compared to ferrocene  $\Delta G = 5.4$  kJ/mol (see Fig.5.3. Forcing the interception point to be equal to zero as suggested by Friddle's model, slightly higher binding

energies are obtained for both guest molecules (see tab.5.1). The trend of the binding energy for the different guest molecules is in agreement with ITC measurements. However, the absolute values obtained from the Friddle plot are a factor of three to four smaller than those reported from ITC measurements [91, 89] and in chapter 3. Moreover, the best linear fits exhibit a significant interception with the y-axes of 18.8 pN for adamantane and 10.3 pN for ferrocene, larger than the estimated errors. The interception indicates that a force is required to break the bond even for cantilevers of vanishing stiffness. The finite force at the interception point could reflect thermally induced detachment of the bond if no external force is applied. Evans introduced this force as the force scale  $f_\beta$  [8] which is directly related to the barrier width of the molecular potential  $f_\beta = k_B T / x_\beta$ . The energy barrier width  $x_\beta$  for adamantane is then  $x_\beta = k_B T / 18.8 \text{ pN} = 2.3 \text{ \AA}$  which is in good agreement with the barrier width obtained in force spectroscopy experiments of monotopic adamantane-cyclodextrin inclusion complexes performed by Gomez-Casado et al.[17]. For ferrocene a wider energy barrier width is obtained with  $x_\beta = 4.1 \text{ \AA}$ . In the following we will discuss the difference in binding energy obtained from force spectroscopy and ITC experiments with respect to the relevant time scales.

Table 5.1: Parameters describing the molecular kinetics of the host-guest interaction between cyclodextrins and connector molecules. The results for ditopic ferrocene and azobenzene are obtained from chapter 2 and chapter 7. (\* for monotopic guest, \*\* estimated as double of monotopic ferrocene)

connector molecule	$\Delta G$ [kJ/mol] ITC	$\Delta G$ [kJ/mol] Friddle	$\Delta G$ [kJ/mol] Friddle, best fit	$x_\beta$ [ $\text{\AA}$ ]
adamantane (ditopic)	23.0	9.2	8.2	2.3
azobenzene (ditopic)	22.3*[63]	4.2	XX	XX
ferrocene (ditopic)	21.5 [91]	4.5	XX	6.0**
ferrocene (monotopic)	22.5[61]	5.9	5.4	3.0

The trend of the binding energy for adamantane, ferrocene and azobenzene is in good agreement with the binding energies obtained from ITC or SPR [89], but the absolute dissociation energy derived in this study is three to four times lower. This difference could arise from the different experimental methods. In ITC experiments, the heat change

is integrated over time so that solely the difference between unbound and bound state matters. ITC measurements reveal a similar well depth of the potential for all host-guest bonds. In DFS experiments, the shape of energy landscape might also play a role. The results of the DFS experiments reveal a different energy barrier width  $x_\beta$  for each guest and, thus, a different shape of the energy landscape. A larger energy barrier width leads to a smoother energy potential compared to a smaller energy barrier width when considering the same well depth. A ligand probing the smooth potential will experience a lower attractive force than a ligand which explores the steep energy landscape caused by a small energy barrier width. Hence, a smaller energy barrier as is the case for adamantane would lead to a higher rupture force than a larger barrier width as obtained for ferrocene.

A further reason for the different energy values could be caused by additional solvation effects in ITC experiments. In the ITC experiments, the guest solution is titrated into a  $\beta$ -CD solution and the temperature change caused by each droplet is recorded over about  $10^3$  s until the system reaches equilibrium again. The integration of the heat yields the free binding energy of the inclusion reaction which is the sum of the reaction enthalpy and the entropy change  $\Delta G = \Delta H - T\Delta S$ . Two effects dominate the free energy change of the inclusion reaction: the loss of the hydration shell which surrounds the hydrophobic guest in water and the inclusion of the guest molecules into the CD cavity [19]. The dehydration of the guest molecule and the CD cavity contribute to the entropy change. The enthalpy change is due to the penetration of the guest into the CD cavity leading to the displacement of 6 to 7 water molecules [92] and the attractive interaction between the inner cavity of the CD and the guest molecule. The enthalpy change dominates the Gibbs free energy of the cyclodextrin complexes investigated in this study due to a strong van der Waals interaction between host and guest [93]. The entropy contribution to the adamantane- $\beta$ -CD complex reaction is close to zero whereas the reaction of the ferrocene- $\beta$ -CD complex exhibit a small but significant entropy change. ITC results not only include the free energy of the complexation reaction but also the solvation process of the titrated substance and an eventual rearrangement of molecules. The ditopic guest TEG(Ad)<sub>2</sub> contains an iodide counter ion which is dissolved in water during titration leading to an additional heat change in ITC measurements. In contrast, force spectroscopy measurements focus on the rupture event of single complexes. Only local, fast processes such as the penetration of the CD cavity which is diffusion limited and in the order of  $10^{-8}$ s and the (de)hydration of the guest molecule in the order of femtoseconds [94] contribute to the rupture force in equilibrium resulting in a more specific and lower  $\Delta G$  value than ITC. The direct

access to single complexes and the fast measurement provide a more accurate measure of the inclusion thermodynamics by force spectroscopy experiments compared to ITC. This argument also explains the larger relative difference of  $\Delta G$  for different guests obtained by force spectroscopy measurements as compared to ITC. ITC measurements report a similar Gibbs free energy for all guest molecules whereas force spectroscopy measurements show a larger difference which is in line with the significant difference in rupture force reported here and other reports [89]. Moreover, the substituents of the CDs are different in DFS and ITC measurements. In ITC experiments, the native CD is used whereas in DFS experiments the CDs are attached to a surface by forming a thiourea bond with the isocyanate group of the silane molecule. There is evidence that an amino substituent attached to the  $\beta$ -CD lowers the binding affinity in the order of  $k_B T$  [21]. The contribution of the substituent is probable to additionally lower the binding affinity obtained by DFS experiments.

### 5.3.3 Impact of cantilever stiffness on adhesion of multiple bonds

In order to study the impact of cantilever stiffness on the force spectrum of a multiple bond contact, the maximum pull-off force was analyzed for different unloading rates. The maximum pull-off force is a measure for the adhesion force and was revealed in force distance curves recorded between a monoamino- $\beta$ -CD functionalized AFM tip and surface in TEG(Ad)<sub>2</sub> solution (system 1). We chose three different cantilever stiffnesses which span a wide range from soft contact ( $k_c = 0.15$  N/m) to stiff non-contact force probes ( $k_c = 20.17$  N/m). With each type of force probe, 300 curves were recorded on three independent surface positions and the maximum pull-off force was analyzed for each curve. The data points in Fig.5.6(a) represent the mean pull-off force and the error bars reflect the standard deviation of the positions. For all three force probes, a characteristic equilibrium value develops at low pulling speeds, respectively, that is shifted to higher values when a stiffer cantilever is used. After the pulling rate exceeds a certain value, the pull-off force increases with the loading rate indicating that the contact is probed out of equilibrium. The force spectra for the different cantilevers overlap but do not merge into a continuous force spectrum. In the following we will discuss the shape of the force spectra with respect to cantilever stiffness and multivalency effect.

Multiple bonds contribute to the pull-off force changing the rupture dynamics dramatically compared to the kinetics of a single bond. The contact is established by several individual bonds with fast complexation kinetics which dissociate and rebind independently. If one bond unbinds, the AFM tip is held in place by the remaining bonds stabilizing the contact

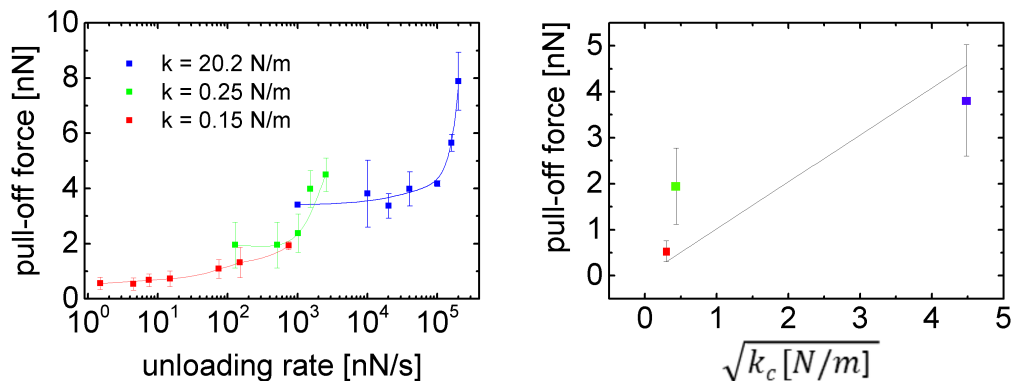


Figure 5.6: (a) The maximum pull-off force as a function of unloading rate for the three different force probes, the solid line serves as a guide to the eye. The data points represent the mean value of 300 force curves recorded on three different surface positions. The error bars reflect the standard deviation of the surface position. (b) The equilibrium force of the three different force probes vs. the square root of the cantilever stiffness. The line is a linear fit of the data points with an y-intercept equal to zero according to the model of Friddle et al. [29].

between AFM tip and surface. This cooperative interaction of multiple bonds results in a lower off-rate of the overall contact as reported in previous multiple bond studies [8, 17] and in chapter 3 of this thesis. The decrease of the off-rate for multiple bonds is described as multivalency effect in literature [17, 11]. The lower off-rate result in a rate dependent force spectrum.

For slow pulling speeds, the complexation kinetics of the established bonds are fast compared to the time scale of the experiment so that a plateau force develops where the bonds are subsequently peeled in equilibrium. The plateau force increases with increasing cantilever stiffness which is in line with the observations for single bonds. However, in contrast to single bonds, the plateau force is not proportional to the square root of the cantilever stiffness (see Fig.5.6(b)). Moreover, the three force spectra do not merge into one continuous force spectrum as proposed in Ref.[29].

The fact that the three curves do not collapse into one spectrum is probably the result of the varying number of bonds involved in the contact. The more bonds interact cooperatively, the lower the off-rate of the contact resulting in a more prominent increase of force [8, 29]. A varying number of bonds could be caused by the functionalization process. We demonstrated in chapter 4 that the water content in the silane solution effects the adhesion force. Water in the silane solution enhances the level of crosslinked silane molecules



resulting in a more flexible network. A more flexible network leads to a higher number of bonds stretched in parallel resulting in a higher adhesion force.

## 5.4 Conclusion

In conclusion, the rupture force for supramolecular bonds in thermal equilibrium increases proportional to the square root of the force probe stiffness. Surprisingly, the single bond rupture force was found to be independent of the molecular linker stiffness. We attribute the negligible effect of the molecular linker stiffness to the different time scales of our system. The relaxation rate of the molecular linker is approximately 200 times larger than the reaction rate of the force probe resulting in a continuously rebinding of thermally unbound bonds. Due to the slow reaction rate of the force probe, the system is in a quasi static situation and the potential energy of the cantilever predominantly determines the rupture force. The effect of force probe stiffness was also observed for the pull-off force of a multiple bond system. Moreover, we found that the single bond rupture force is related to the free energy of the inclusion reaction as proposed by Friddle et al. The trend of the dissociation energies are in good agreement with the binding energy obtained by ITC and SPR experiments in previous studies. However, the absolute values are lower by a factor of three to four which we attribute to the different measurement techniques. In force spectroscopy measurements, the supramolecular bonds are directly probed whereas in ITC experiments additional solvation processes can cause an additional the heat exchange.

# 6 Friction and adhesion of CD-functionalized Polymers

In this chapter, the impact of geometry and flexibility on the adhesive interactions of polymer-functionalized surfaces mediated by supramolecular bonds is studied. In the first section, the adhesive interaction of different functionalization configurations will be discussed with respect to the single bond rupture force. In the second section the contact forming process of polymer chains is investigated with time resolution by means of continuous wavelet transform which is a new approach in this field.

## 6.1 Impact of geometry and flexibility on friction and adhesion of CD-functionalized Polymers

### 6.1.1 Introduction

The specific interaction of two or more components is an important concept in nature in order to tune adhesive interactions [11, 95]. Inspired by nature, artificial systems were developed for controlling chemical and physical surface properties [96] based on supramolecular assemblies. Supramolecular interactions such as hydrogen bonding,  $\pi$ - $\pi$ -interactions or hydrophobic host-guest interactions are a promising approach for developing adaptable systems due to their reversible and specific nature. Specific interaction between opposing surfaces was achieved by implementing supramolecular bonds into polymers [95, 15, 59] and molecular printboards [97, 58]. Based on the cooperative interaction of multiple supramolecular bonds, the strength and dynamics of the system can be adjusted [17, 72].

The strength of the adhesive interaction can be quantified by two main parameters: the maximum adhesion force and the work of separation. Both have to be overcome in order to separate the involved components and can be quantified by means of atomic force microscopy (AFM). The work of separation depends on the number of supramolecular

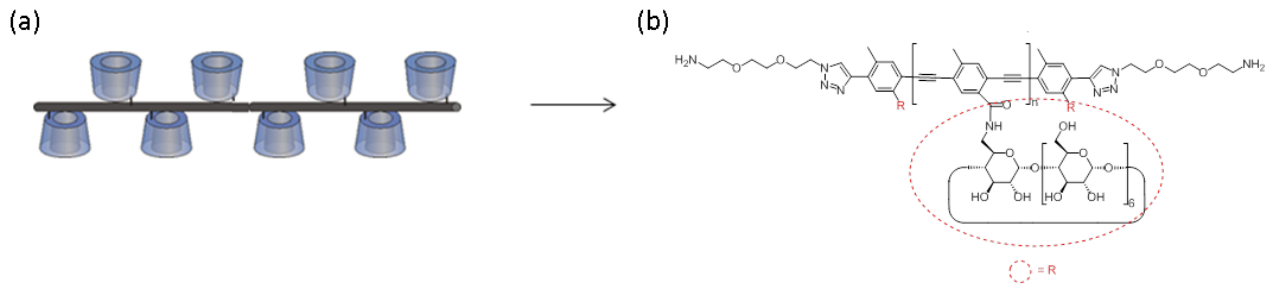


Figure 6.1: (a) Scheme of the cyclodextrin functionalized polymers (CD-polymers), (b) chemical structure of CD-polymer.

bonds formed between the opposing surfaces and can be determined by integrating the forces along the separation path.

In this chapter, we introduce an innovative polymer system based on host-guest interaction of cyclodextrin inclusion complexes (see Fig.6.1). Cyclodextrins (CD) form inclusion complexes with a variety of hydrophobic guest molecules. The inclusion complexes are characterized by a high binding affinity [19] and fast complexation kinetics compared to the time scale of our experiments [89], (see chapter 3). The CD molecules are attached to stiff polymer chains (CD-polymer) and the adhesive interaction is established by short ditopic connector molecules introduced in chapter 3. Systems based on stiff polymer fibers are ideal candidates for investigating multivalent interactions since they do not exhibit additional unfolding events as observed in flexible polymer chains or proteins [98].

Our ditopic approach offers the possibility to vary the kinetics of the individual bonds (chapter 7) or introduce switchability (chapter 2) by solely exchanging the connector solution. The same surface functionalization can be used, which is a great advantage compared to monotopic systems where the guests or ligands are attached to one surface as it was done in previous studies [15, 17, 59]. Friction and adhesion forces will be investigated on the molecular scale by means of AFM. CD-polymers are either covalently attached to the AFM tip or the surface in four different combinations (see Fig.6.2): CD-polymers attached to the AFM tip and surface coated with CD SAM (*polymer-CD*), CD-polymers attached to AFM tip and surface (*polymer-polymer*), AFM tip covered with CD SAM and CD-polymers attached to the surface (*CD-polymer*) and CD SAM at AFM tip and surface (*CD-CD*). We will show that geometrically induced peeling and shearing concepts offer the possibility to tune the work of separation.

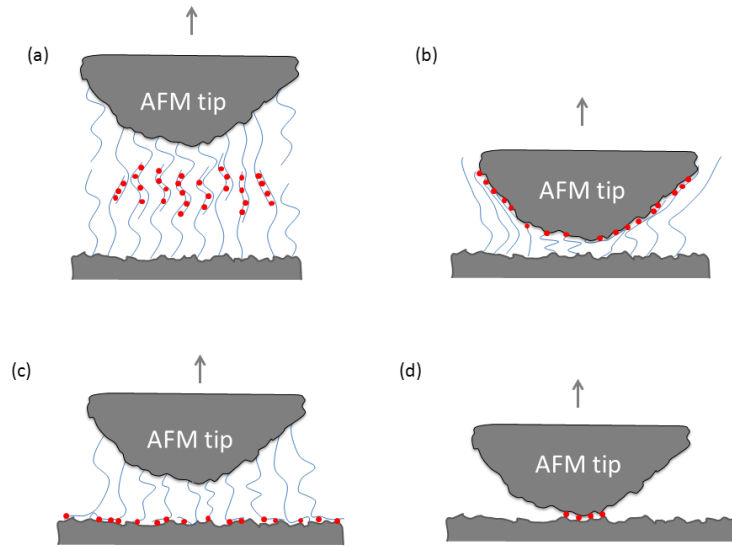


Figure 6.2: Scheme of the four different molecular systems (a) *polymer-polymer*, (b) *CD-polymer*, (c) *polymer-CD* and (d) *CD-CD*. The polymers are sketched as blue lines and supramolecular bonds are indicated in red.

## 6.1.2 Experimental section

### Surface preparation

Commercial available Si(111) wafers were used as substrates (Si-Mat, Kaufering, Germany). The surfaces were cleaned with piranha solution (3:2 mixture of sulfuric acid and hydrogen peroxide) prior to surface functionalization to remove organic contamination. Subsequently the samples were rinsed with ultrapure water and dried with N<sub>2</sub>. The silane monolayer was attached by vapor phase deposition of 3-isothiocyanatopropyltriethoxysilane at a pressure of 2 mbar for 45 minutes. The silane 3-isothiocyanatopropyltriethoxysilane was synthesized according to Ref.[67]. After a washing procedure with tetrahydrofuran (THF) and water the wafer remained either in 1 mM solution of mono(6-deoxy- 6-amino)-CD diluted in water or in 5 mM CD-Polymer solution over night at room temperature. All samples were freshly prepared for the AFM measurements and stored in water for not more than three days. The silicon AFM tips (Nanosensors(TM) PPP-Cont AFM Probes, NanoandMore, Wetzlar, Germany) were functionalized in the same way as the surfaces.

## AFM measurements

The adhesive interaction between the different surface functionalizations was investigated by force spectroscopy measurements performed with a Nanowizard 3 setup (JPK Instruments, Berlin, Germany) in water or connector solution at room temperature. A connector molecule concentration of  $10\ \mu\text{M}$  was chosen in order to work in the saturation regime of the Langmuir curve (see chapter 7 for more details). Silicon cantilevers with nominal normal spring constant of  $0.3\ \text{N/m}$  have been calibrated using the thermal noise analysis. To avoid surface damage and unspecific contributions to the adhesion force the maximum normal force was kept below  $2\ \text{nN}$ . The force-distance curves were analyzed with the implemented Data Processing software (JPK instruments, Berlin, Germany). Each force curve was examined for the maximum pull-off force and the corresponding rupture length. The results were plotted in a histogram and the most probable pull-off force was obtained by a Gaussian curve fitted to the data. The shown adhesion forces represent average values of the pull-off forces obtained on at least three different surface positions, more than 200 force-distance curves each. The error bars reveal the standard deviation of the three surface positions. The rupture force of a single complex was obtained from the height of the last rupture event in force-distance curves. The height of the last rupture event was included in a histogram where the first peak reveals the most probable rupture force.

### 6.1.3 Results

The interaction between cyclodextrin functionalized CD-polymers was studied on the molecular level by means of AFM. Polymers bearing cyclodextrin molecules were either immobilized on the AFM tip or a flat surface. Prior to the CD-polymer attachment, the surface was coated with a silane SAM containing an isothiocyanat group which forms a stable thiourea bond with the amino species included in the end of a polymer chain. The adhesive interaction was established by the host-guest interactions between the cyclodextrins (host) on tip and surface connected by ditopic guest molecules containing two adamantane (guest) moieties at either end. A scheme of the configuration is provided in Fig.6.2. Four different combinations of AFM tip and surface functionalizations were prepared in order to study the impact of geometry and flexibility on the adhesive interaction. The interaction was quantified in force-distance curves recorded in aqueous solution with and without adamanatane connector molecules.

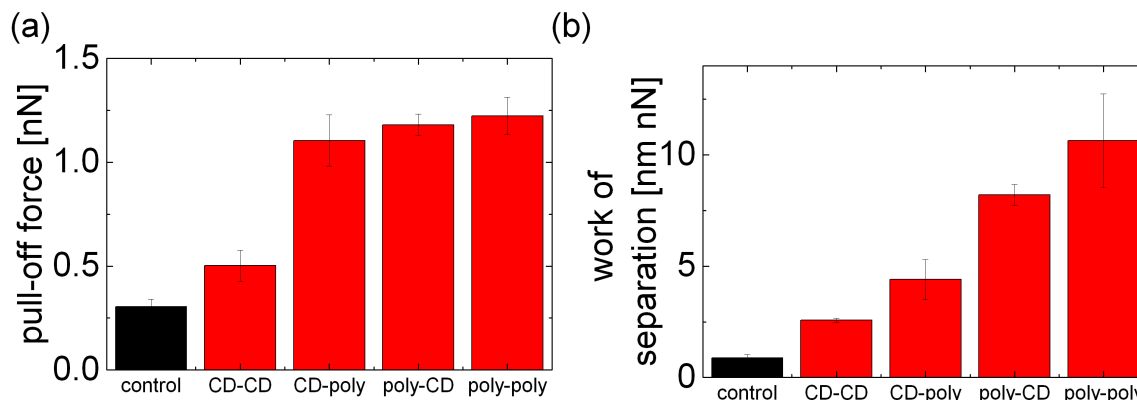


Figure 6.3: (a) Average pull-off force and (b) work of separation of the four different configurations performed in guest solution (red). The control experiment is performed in water without guest molecules (black). The mean value represents the average over 600 force curves recorded on three different surface positions, the error bar represents the standard deviation of the surface positions.

### Adhesion of CD-polymers

The maximum pull-off force and the work of separation were revealed from 600 force-distance curves recorded on three different surface positions with a constant retraction speed of  $1 \mu\text{m/s}$ . For each position the most probable rupture force was determined by a Gaussian fit. As a control experiment, the adhesion force was determined in pure water without connector molecules prior to every measurement in order to investigate the unspecific interactions.

In Fig.6.3(a) the adhesion force of the four different configurations is presented. The control experiment reveals a force contribution of unspecific bonds of 250 pN in all system. The adhesion force increases significantly when connector molecules are present indicating that the hydrophobic end groups are included into the CD cavity. All force curve exhibit the maximum pull-off force at a tip-surface distance close to zero. The three polymer systems exhibit a similar maximum pull-off force of about 1 nN which is double of that of the *CD-CD* system. The pull-off force of the *polymer-polymer* system is slightly higher than for the *polymer-CD* and *CD-polymer* configuration.

In contrast to the similar pull-off force the appearance of the force-distance curves is different for the three polymer configuration. In Fig.6.4 representative force curves in adamantane connector solution and for the control experiment are presented. After the maximum pull-off occurred, different rupture characteristics are observed for the respective configuration. In the *CD-CD* (Fig.6.4(a)) configuration, a the smallest adhesion force of

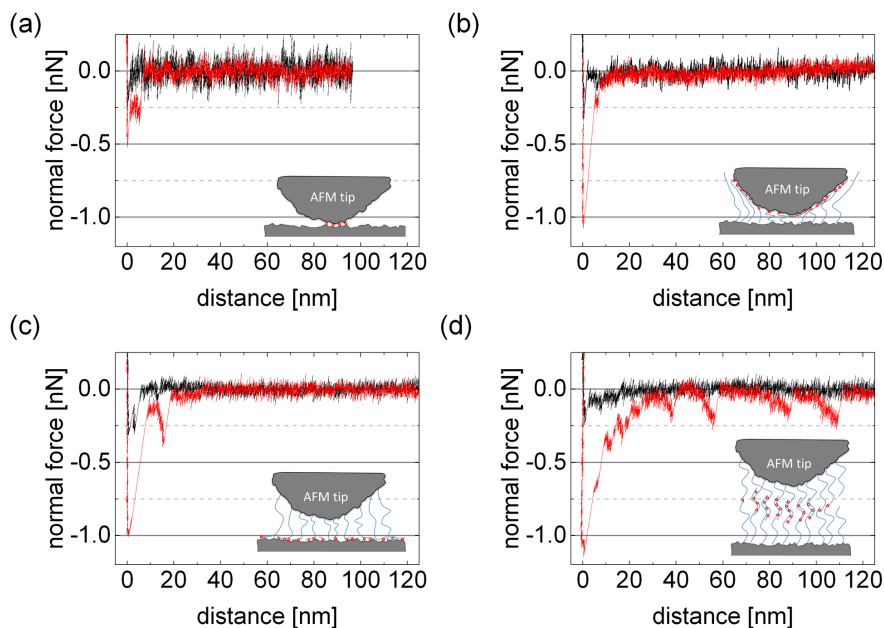


Figure 6.4: Representative force-distance curves recorded on the (a) *CD-CD*, (b) *CD-polymer*, (c) *polymer-CD* and (d) *polymer-polymer* configuration in adamantane solution (red) and control (black). A sketch of the respective configuration is shown in the inset.

0.5 nN and the lowest separation length of about 10 nm is observed. The force of the *CD-polymer* system (Fig.6.4(b)) exhibit a maximum force peak followed by a sudden force drop and a small last rupture event at about 10 nm. The sudden force drop indicates that the contact is rather stiff and the majority of bonds is ruptured when the AFM tip is close to the surface. In contrast, the force of the *polymer-CD* system (Fig.6.4(c)) exhibit an additional force peak at about 15 nm and a subsequent plateau at a low force until the last rupture event occurs at a separation length of about 30 nm. The plateau at low force is characteristic for the *polymer-CD* configuration and indicates that polymers are peeled from the surface. The force of the *polymer-polymer* system (Fig.6.4(d)) exhibits several force peaks during separation indicating that the adhesive force is the result of many host-guest bonds between different polymers which are subsequently stretched. The last rupture is observed at a tip-surface distance of of about 110 nm so that we can estimate the length of the longest polymers with 55 nm.

The difference in the shape of the force-distance curves is reflected in the work of separation in Fig.6.3(b). The connector molecules have a higher effect on the work of separation

than on the pull-off force indicating the short range of non-specific contributions. The *polymer-polymer* system exhibits the highest work of separation in line with the additional stretching events observed in the force curves. Interestingly, the pull-off force of the *polymer-CD* and *CD-polymer* configuration are alike whereas the work of separation is significantly higher for the *polymer-CD* system indicating that the surface geometry plays a crucial role. For the *CD-polymer* configuration, a simultaneous rupture of almost all bonds close to the surface is observed resulting a lower work of separation than obtained from the *polymer-CD* system. Polymers attached to the AFM tip exhibit a combination of peeling and shearing effects leading to a higher work of separation in comparison to the *CD-polymer* system.

The height of the last rupture provides information about the rupture force of a single inclusion complex. The last step during retraction of the *polymer-polymer* system was fitted by a step function and the height of the last rupture was included in a histogram in Fig.6.5(b). The most probable rupture force for a single host-guest interaction can be obtained from the highest peak in the histogram with a force of 112 pN. The smaller second peak is the double of that of the force of the first peak indicating the rupture of two parallel bonds. The single bond rupture force is higher than the single bond rupture force obtained for the *CD-CD* configuration in chapter 3. Friddle et al. demonstrated that the single rupture force of supramolecular bonds in thermodynamic equilibrium depends on the cantilever stiffness. The expected rupture force from the Friddle analysis obtained with a cantilever stiffness of 0.34 N/m is  $f_{rup} = \sqrt{0.34/0.2} \cdot 82 \text{ pN} = 107 \text{ nN}$  where the single rupture force of the *CD-CD* system is 82 pN obtained with a cantilever stiffness of 0.2 N/m.

### Friction of CD-polymer

The friction force between a CD-polymer functionalized AFM tip and CD functionalized surface (*polymer-CD*) was studied when sliding across the surface. The friction force is the force acting against the movement of the AFM tip and was studied in force loops when sliding back and forth across the surface. The hysteresis of the force loop equals the dissipated energy and is directly related to the friction force. The distance of a friction loop was chosen with 500 nm which is well above the polymer length and the tip radius and small enough to study molecular interactions. The normal force was kept below 1 nN in order to operate in the adhesive friction regime and keep the unspecific interactions as small as possible.

Representative friction loops in water and adamantane solution recorded with a sliding



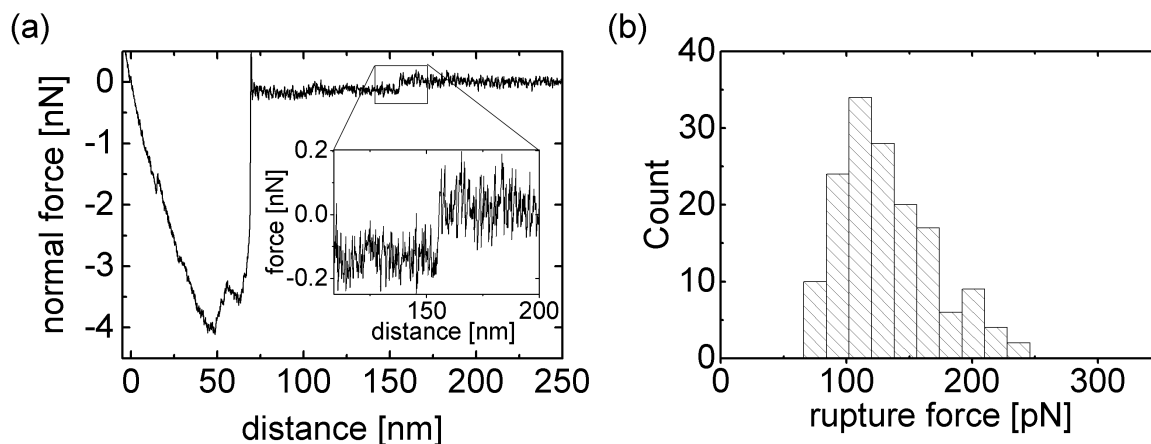


Figure 6.5: (a) Representative force-distance curve recorded with the *polymer-polymer* system in adamantane solution, the inset shows the last rupture event which provides information about the rupture force of a single complex. (b) Histogram of the height of the last rupture event with a maximum on 112 pN. *This Figure is adapted from the Master thesis of Franziska Emmerich.*

velocity of 45 nm/s are given in Fig.6.6(a). In water, a smaller hysteresis and small erratic stick-slip events are observed. In adamantane solution, a larger hysteresis and higher peaks indicate that the polymers at the AFM tip form supramolecular bonds with the CD molecules at the surface mediated by the guest connector molecules leading to a higher friction force. A similar rupture characteristic was observed for the *CD-CD* system where the stick-slip events exhibit smaller peak forces in chapter 3. The average friction force was studied as a function of velocity from 40 nm/s to 5000 nm/s in adamantane guest solution Fig.6.6(b). The control experiment in water was performed prior to the measurement. After adding the adamantane guest molecules, the friction force increases significantly by a factor of 2.5 compared to the control experiment. No velocity dependence was observed indicating that the bonds are probed in thermodynamic equilibrium as reported for the *CD-CD* system in chapter 3. In line, no loading rate dependence was observed for the maximum pull-off force for all tip-surface configurations (data not shown).

#### 6.1.4 Discussion

In the following we will discuss the adhesive interaction in normal and lateral force measurements of the different tip-surface configurations with respect to the flexibility of the attachment and geometrical effects.

The successful attachment of cyclodextrin molecules onto the polymer chains and the

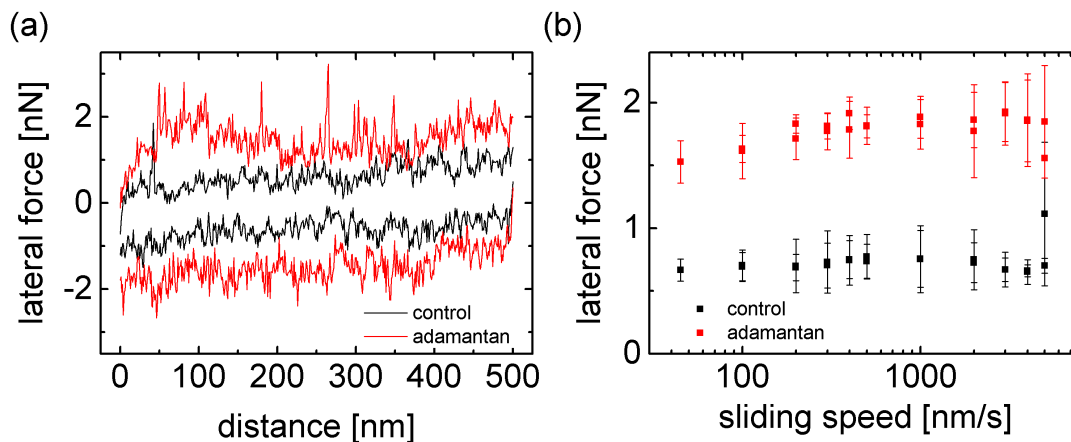


Figure 6.6: (a) Representative friction force loops of the *polymer-CD* system recorded with a sliding speed of 45 nm/s. In adamantane solution prominent peaks are observed which are missing in the control. (b) Average friction force of 50 force loops as a function of sliding speed increased in adamantane solution by a factor of two. *This Figure is adapted from the Master thesis of Franziska Emmerich.*

attachment of the polymer chains onto an AFM tip and a flat surface was verified by the increase in adhesion and friction forces when adamantane connector molecules are present in comparison to the control experiment in water where the adhesion is caused by unspecific interactions.

Force spectroscopy measurements reveal the length of the CD-polymer chains. The last rupture event in force-distance curves for the *polymer-CD* system is about 30 nm. In order to obtain the correct polymer length we have to consider the underlying SAM. The surface is coated with a CD monolayer attached to a silane network assembled on the silicon surface. The stretching length of this SAM can be estimated from f-d curves for the *CD-CD* configuration to be 10 nm leading to an estimated maximum polymer length of 20 nm. This value matches the result of MALDI-TOF experiments which reveal a maximum of 38 repetition units. One repetition unit has a length of about 0.52 nm leading to a maximum polymer length of 20.6 nm including one tetraethylene glycol molecule at the end of each polymer chain.

We expect a distribution of the polymer length as result of the synthesis. The longest polymers were observed in the *polymer-polymer* system rupture events at a larger distance of about 110 nm to 160 nm (see Fig.6.5) are observed indicating that there are polymers with about 45 nm to 70 nm when considering the compliance of the silane network. The most probable polymer length obtained from MALDI-TOF measurements is much shorter

with below six repetition units leading to a maximum adhesion peak close to the surface.

The value of the pull-off force is mostly determined by the number of initially broken bonds. The rather stiff attachment of the *CD-CD* configuration leads to the lowest number of bonds between tip and surface, and thus the lowest pull-off force. The higher pull-off force for the polymer configurations indicates that a system with a higher flexibility offers the possibility that more CD-connector-CD bonds are formed. A pull-off force of 1 nN is caused by a minimum of 9 bonds. The actual number might be significantly higher since we do not expect that all bonds are loaded to their maximum rupture force.

In contrast to the pull-off force, the work of separation varies significantly with the functionalization configurations. Particularly interesting is the difference in the work of separation of the *polymer-CD* and *CD-polymer* system. In the *CD-polymer* configuration, the polymers attached to the surface adhere to the sloped facets of the tip apex (see Fig.6.2). Upon separation, the bonds have to be ruptured simultaneously leading to the high rupture force and the sudden force drop. The short peak leads to the small work of separation. In contrast, polymer attached to the tip can be both, sheared and peeled leading to a significant force at larger separation distance and, thus, to a higher work of separation. Hence, the work of separation is determined by the attachment angle of the polymer chains. At small separation distance, the shearing dominates also in the *polymer-CD* system leading to a similar pull-off force as observed for the *CD-polymer* system.

In case of the *polymer-polymer* configuration, several stretching events in the force-distance curve indicate that a shearing of bonds dominates. Due to the well defined distance of the CD molecules attached to the polymer chains, we expect that the polymer chains are connected by several supramolecular bonds. During separation, the polymers are stretched with a normal force so that they protrude either perpendicular from the surface or in a small angle. The bonds between the CD molecules attached to the polymer chains have to be ruptured simultaneously in order to separate the polymers. The rupture force of these stretching events is about 0.2 nN which is low if we assume that a polymer has a length of several tens of nanometer bearing several tens of CD molecules. The rather low rupture force of 0.2 nN indicates that not all CD pairs but a minimum number of two attached to two different polymer chains are connected by a ditopic connector molecule.

The friction force is quantitatively in good agreement with the adhesion force. In line with the pull-off force, the friction force increases by a factor of 2.5 after adding the connector molecules in comparison to the control experiment. The remarkable compliance of friction and adhesion measurements reflects that the friction force is predominantly

caused by adhesive interactions. The AFM tip exhibits an erratic stick-slip movement when guest molecules are present reflecting that the sliding process is dominated by a shearing the polymer chains against the surface. During the “stick” phase, the adhesive interaction between the polymers and the surface cause a torsion of the AFM tip until a certain force is reached and a “slip” occurs. During the “slip” event, the polymers are sheared from the surface by breaking all bonds in parallel resulting in a high friction force. A force peak of 2 nN reveals a minimum number of 18 supramolecular bonds formed between tip and surface.

Due to the fast complexation kinetics of the single host-guest bonds, the polymers are instantaneously bound to the surface as soon as a CD pair is close enough to be connected by an adamantane connector molecule. A single host-guest bond is in thermodynamic equilibrium on the time scale of an AFM measurement (see chapter 3) so that the friction force is not affected by the sliding velocity.

### 6.1.5 Conclusion

In conclusion, we presented a novel surface functionalization based on CD-functionalized polymers and quantified the effect of attachment flexibility and geometry on the adhesive interaction between supramolecular assemblies. Four different tip-surface combinations were tested where the CD molecules are either attached to polymer chains or stiffly bound to the surface. The polymer functionalized surfaces offer a higher flexibility resulting in a four times higher adhesion force and work of separation compared to stiffly attached CD molecules. The higher flexibility of the polymers leads to a higher number of bonds formed between the AFM tip and surface. Interestingly, the CD-polymers exhibit a remarkable contrast between peeling and shearing mechanisms depending on the different surface geometries. The effect is particularly large in the work of separation where the different attachment angle of the *polymer-CD* configuration introduces an additional peeling characteristic leading to a significantly higher work of separation than for the shearing dominated *CD-polymer* system. In contrast, the maximum pull-off force is determined by the simultaneous rupture of several bonds close to the surface leading to a similar pull-off force for all configurations.

The rupture force for a single complex of 112 pN is in good agreement with the single rupture force on the *CD-CD* system in chapter 3 indicating that the molecular linker stiffness does not affect the rupture force of single supramolecular bonds in thermal equilibrium. Experimental evidence that the bonds are probed in thermal equilibrium was

provided by a constant friction force over three orders of sliding velocity.

## 6.2 Time resolved thermal noise analysis of reversible polymer binding

### 6.2.1 Introduction

The control of adhesive contacts plays a key role in nature [7] as well as in fabrication of small systems [3] or medical devices [5]. In surface science, the strength of adhesive interactions is mainly quantified by the separation energy or maximum pull-off force. In order to control adhesive interactions, the understanding of the contact formation process is as well as important. In AFM studies, the contact formation can be investigated in force-distance curves when approaching a surface with an AFM tip. In case of an attractive force, the cantilever bends towards the surface and the adhesive force can be quantified by the normal cantilever deflection. It was recently demonstrated that the contact formation process in biological systems is mediated by the stochastic binding of cell wall proteins [99]. In particular for small forces and slow processes, the information obtained from the vertical deflection is limited by cantilever noise and instrumental drift. Moreover, the vertical deflection does not reveal any information about the contact stiffness.

In this section, we report on a novel approach for studying the initial contact formation process by monitoring the thermal fluctuations of an AFM cantilever while approaching a surface. Thermally induced AFM cantilever fluctuations provide information about the cantilever stiffness [41] but also about the contact stiffness [100] and the molecular details of tip-surface interaction [101, 102]. Marshall et al. demonstrated that even single molecules affect the resonance frequency [103] and that the elasticity of single molecules can be reconstructed from the thermal fluctuations of an AFM cantilever by means of Fourier Transform (FT)[103].

Dynamic modulations of the cantilever resonance frequency can be studied by Continuous Wavelet Transform (CWT) [101] of force-distance curves. Simultaneous resolution in time and frequency makes CWT to a powerful tool for analyzing tip-surface interaction during dynamic force spectroscopy experiments. In this section, the attachment of CD-polymers to a CD coated silicon surface is investigated. The CD-polymers are attached to an AFM tip and the adhesive interaction is mediated by ditopic connector molecules in solution (see *polymer-CD* configuration in section 6.1). In slow approach experiments the

AFM tip is slowly moved towards the surface and the frequency spectrum of the AFM cantilever is monitored with high temporal resolution. In the following, a basic introduction to the frequency spectrum of a force probe and the CWT of the normal deflection signal of a force probe is provided.

The basic concept arises from the *equipartition theorem* which states that the thermal energy  $k_B T$  is sheared equally among the degrees of freedom in thermal equilibrium. In case of an ideal spring, the mean square amplitude  $\langle x^2 \rangle$  of the thermal vibrations is directly related to the spring constant  $k_C$

$$\frac{1}{2}k_B T = \frac{1}{2}k_C \langle x^2 \rangle \quad (6.1)$$

where  $k_B$  is the Boltzmann factor and  $T$  the temperature of the environment. Due to the mass distribution along the cantilever beam, AFM cantilevers cannot be treated as an ideal spring and several corrections are required to determine the spring constant [39]. However, changes in the resonance frequency and vibration amplitude provide information about the contact stiffness. The resonance frequency  $\omega_0$  of the spring can be derived from the power spectrum density (PSD) of the time series of the normal force signal fitted with the Lorentz function

$$PSD(\omega) = \frac{F_0}{(\omega_0^2 - \omega^2)^2 + \omega^2 \gamma^2}. \quad (6.2)$$

In case of a free cantilever,  $\omega_0$  equals the resonance frequency and the vibration amplitude at resonance is given by equation (6.1). If the AFM tip is in contact with a hard surface, the vibration frequency increases due to a stiffer contact [100] and the amplitude of the thermal noise decreases but does not fully vanish [104]. The quality factor equals the resonance width of the frequency compared to the center frequency  $Q = \omega_0/\Delta\omega$  where  $\Delta\omega$  is the full width at half maximum.

The frequency spectrum of thermal fluctuations can be followed by Fourier analysis which supplies the average frequency information over a certain time period [103, 100]. In this study, time resolution will be provided by analyzing the cantilever deflection by means of CWT. Prior to the CWT analysis a complex wavelet function has to be defined, the “mother wavelet” whose translated and dilated “daughter wavelets” are later convoluted with a time series with equidistant time steps  $dt$ . A wavelet function has a zero mean and is localized in frequency and time space [105]. In this study, the Morlet function  $W_0$  is used which is a special case of the commonly used Garbor wavelet and is modulated by a Gaussian function with the non-dimensional parameter  $\alpha_0$  representing the frequency and

the time parameter  $\eta$  [106]

$$W_0(\eta) = \pi^{-\frac{1}{4}} e^{i\alpha_0 \eta} e^{-\eta^2/2}. \quad (6.3)$$

The mother wavelet is translated by the parameter  $n$  and dilated by the scale  $s$  and convoluted with the discrete signal  $x_n$  [101, 105]

$$Wf(n, s) = \sum_{n'=0}^{N-1} x_{n'} \hat{W}_0^* \left( \frac{(n' - n)dt}{s} \right) \quad (6.4)$$

where  $W_0^*$  is the complex conjugate of the wavelet function. Similar to the Heisenberg uncertainty, time and frequency resolution cannot be improved simultaneously [107]. More oscillations under the wavelet lead to a higher frequency resolution which goes along with a lower time resolution. The wavelet power spectrum density can be expressed as  $|Wf(s)|^2$  which is included into the wavelet maps as a function of time, called *scalogram*.

The computation of the Continuous Wavelet Transform was done by a python script adapted from Ref.[108]. In order to increase the time efficiency, the calculation of the wavelet transform is done in Fourier space using discrete Fourier transform [106]

$$\hat{x}_k = \frac{1}{N} \sum_{n=0}^{N-1} x_n e^{-2\pi kn/N} \quad (6.5)$$

where  $k$  is the frequency index. The wavelet transform in Fourier space is [106]

$$Wf(n, s) = \sum_{k=0}^{N-1} \hat{x}_k \hat{W}_0^*(s, \alpha_k) e^{i\alpha_k n dt} \quad (6.6)$$

where  $\hat{W}(s, \alpha) = \pi^{-\frac{1}{4}} H(\alpha) e^{-(s\alpha - \alpha_0)^2/2}$  is the Fourier transform of  $Wf(n, s)$  in the continuous limit and  $H(\alpha)$  is the Heaviside step function with  $H(\alpha)=1$  if  $\alpha \geq 0$ ,  $H(\alpha) = 0$  otherwise [106]. The scales obtained from the Fourier Transformation are converted into frequency information by the Fourier wavelength  $\lambda$ :

$$\lambda = \frac{4\pi s}{\alpha_0 + \sqrt{2.0 + \alpha_0^2}}. \quad (6.7)$$

### Exemplary CWT of approach in air

In order to demonstrate the concept of CWT, an exemplary approach curve in air is shown in Fig.6.7. The vertical deflection (Fig.6.7(a)) of a silicon cantilever during approach towards

a silicon surface is analyzed by means of FT (Fig.6.7(b)) and CWT (Fig.6.7(c)). The power spectrum density of the frequency spectrum exhibits a peak at the resonance frequency of the cantilever at 10.4 kHz. Since FT is time invariant, the PSD shows the average over the whole time span. In contrast, the CWT provides frequency and time resolution so that the frequency modulation with time can be observed in the *scalogram*. The color code in the *scalogram* reflects the square modulus of the wavelet coefficient  $|Wf(s, d)|^2$  which is proportional to the local energy density of the signal [101]. The resonance frequency at 10.4 kHz is clearly observed in the *scalogram* for the free cantilever. Its discontinuous appearance is due to the thermal activation of the cantilever [101]. The thermal activation exhibits a white frequency spectrum that cause small displacements of the cantilever beam. The loose end of the cantilever beam bends and relax with a frequency close to resonance frequency.

A snap-in is observed at about 95 ms. Just before the snap-in occurs, the resonance frequency of the cantilever shifts to smaller frequencies. The frequency shift reflects the force gradient caused by the attractive interaction between tip and sample. At a certain distance, the force gradient of the tip-surface interaction exceeds the cantilever stiffness leading to a sudden bending of the cantilever towards the surface, the snap-in. The snap-in is followed by a repulsive tip-surface contact where the resonance frequency of the free cantilever is fully damped.

## 6.2.2 Results and Discussion

In the following section, the frequency spectrum of an AFM cantilever in dynamic force spectroscopy measurements is investigated in three consecutive steps. In the first part of this section, a full force-distance cycle recorded in liquid with CD coated tip and surface (*CD-CD* configuration) is studied with respect to the vibration frequencies in vertical and lateral direction. In the second part, the AFM tip is functionalized with CD-polymers (*polymer-CD* configuration) and the frequency shift according to the number of attached polymers is quantified. In the last section, the contact formation process of CD-polymers with a CD coated surface is monitored with temporal resolution in slow approach measurements by means of CWT.



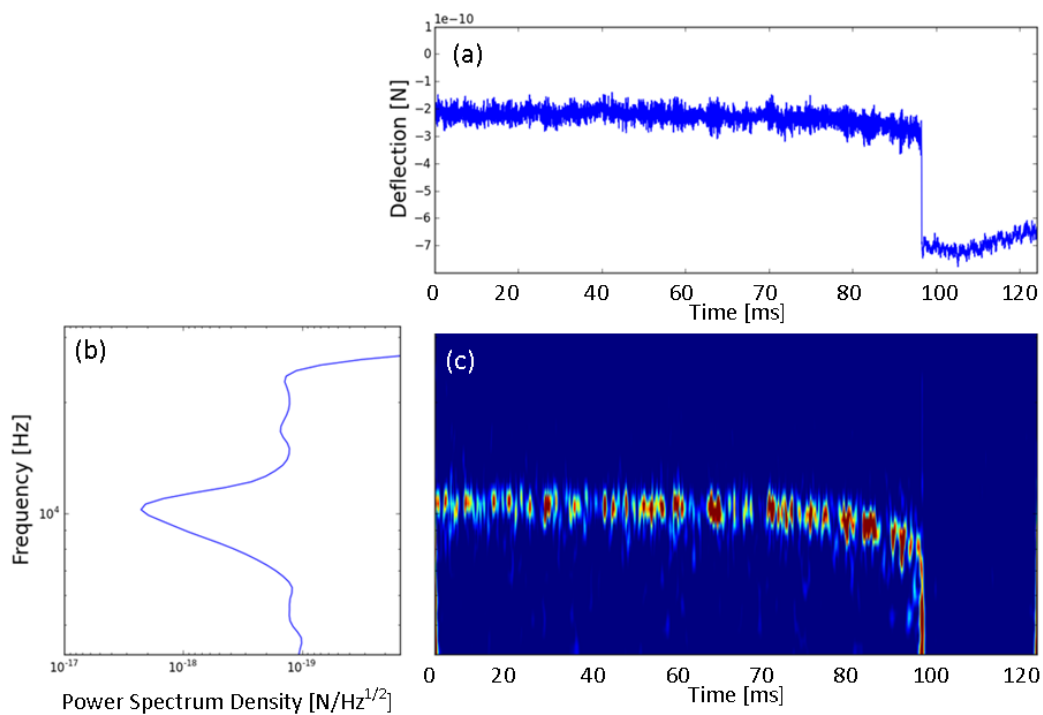


Figure 6.7: Wavelet transform of the normal deflection signal during approach of a bare silicon AFM tip and surface in ambient conditions. (a) Normal deflection (blue) as a function of time, (b) PSD averaged over hole time span, (c) *scalogram*: time resolved PSD. The bending of the resonance frequency in the *scalogram* is caused by the force gradient of the attractive tip-sample interaction.

### CWT of force-distance curve in liquid

In Fig.6.8, a force-distance curve in adamantane guest solution is presented versus time. The AFM tip and surface are functionalized with rigidly attached CD molecules in order to keep the system simple so that the basic appearance of a CWT and the emerging frequencies can be discussed. In Fig.6.8(a) the vertical deflection during approach and retraction is shown in the top image as a time series. On the left the PSD averaged over the whole time is presented which exhibits four prominent peaks (see tab.6.1). The broad peak with the lowest frequency represents the resonance frequency of the cantilever in water of  $f_0 = 4.2$  kHz where most of the energy of the thermally activated cantilever is concentrated. The patchy appearance of the frequencies around the resonance frequency reflects the discontinuous fluctuations of the cantilever caused by random thermal activation [101]. Due to the damping in liquid the quality factor is low ( $Q=2$ ) leading to the broad frequency band around the resonance frequency. Due to the low quality factor in aqueous solution, no frequency shift prior to the snap-in is observed. The resonance frequency vanishes when tip and surface are in repulsive contact.

Additional frequencies  $f_i$  are observed in the *scalogram* and average PSD which are higher harmonics of the resonance frequency  $f_i = \beta_i f_0$  (see Tab.6.1). The parameter  $\beta_i$  is characteristic for each frequency and was obtained from Ref.[104]. A second frequency peak  $f_2 = 20.6$  kHz is observed for the free cantilever which corresponds to the second harmonic oscillation ( $f_2 = 4.69 \cdot f_0 = 19.7$  kHz [104]). The second harmonic is also damped during contact. When tip and surface are in repulsive contact, a third frequency with an intermediate frequency of about  $f_1^s = 15.1$  kHz appears which is close to the first harmonic for a supported cantilever  $f_1^s = 3.92 \cdot f_0 = 16.4$  kHz [104]. This frequency arises from the change in boundary conditions of the AFM tip. During contact, the AFM tip is pinned to the surface leading to a change in the oscillation mode (see Tab.6.1).

The lateral deflection signal of the same f-d curve is shown in Fig.6.8(b). Due to cross talk, the lateral deflection changes during the force curve. From the ratio between the maximum deflection in lateral and normal direction we can estimate the proportion of cross talk with about  $V_{\text{pull-off}}^{\text{lateral}} / V_{\text{pull-off}}^{\text{normal}} = 10 \text{ mV} / 48 \text{ mV} \approx 5\%$  where the deflection in volts is obtained from the original data.

Two prominent frequencies are observed in the *scalogram* of the lateral deflection. The higher frequency  $f_0^l = 109$  kHz corresponds to the lateral resonance frequency. The Q-factor ( $Q=5$ ) is higher than the Q-factor of the normal resonance frequency resulting in a more narrow frequency peak. In contact, the intensity of the resonance in the *scalogram* is

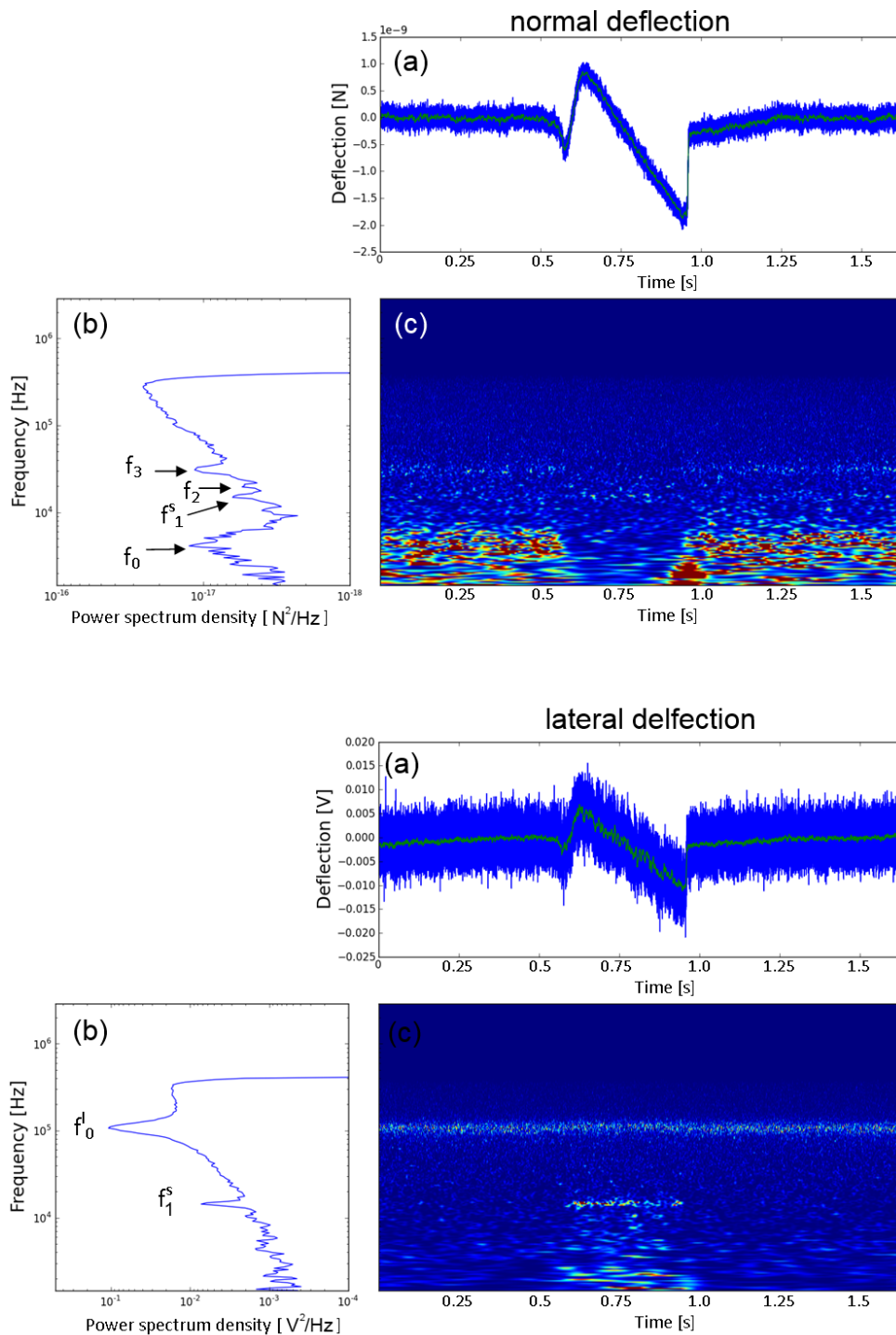






Figure 6.8: CWT of the normal (up) and lateral (down) deflection signal (a) of a f-d curve between a  $\beta$ -CD functionalized AFM tip and surface in adamantane connector solution. The pronounced frequencies in PSD (b) and *scalogram* (c) are discussed in the text. The green line in (a) represents a moving average over 500 data points of the original deflection data.

slightly lowered. At the same time, a lower frequency peak at 15.1 kHz appears which corresponds to the frequency  $f_1^s$  of the supported cantilever in the normal deflection signal. This frequency arises when the AFM tip is in repulsive contact with the hard substrate. From the crosstalk in repulsive contact we know that it is likely that the movement of the cantilever has a torsional component which is visible in the *scalogram* of the lateral deflection. Additional frequencies below 0.1 kHz appear in repulsive contact which are probably caused by instrumental noise.

Table 6.1: Vibration modes of free and supported cantilever in vertical and lateral deflection.

vibration mode	vertical deflection [kHz]	pictogram	lateral deflection [kHz]
$f_0$ free	4.2		109.1
$f_1$ supported	15.1		15.1
$f_2$ free	20.6		-
$f_3$ free	31.4		-

### PSD of CD-polymer detachment

Force-distance curves of a CD-polymer functionalized AFM tip vs. a CD covered flat surface were recorded in aqueous solution. The adhesive interaction is established between the CD molecules attached to the AFM tip and the CDs at the surface. The effective contact stiffness is determined by the number of stretched polymers and can be derived from the changes in the resonance frequency of the cantilever beam. In order to study the correlation between resonance frequency and effective contact stiffness we will analyze the PSD of the thermal fluctuations when the AFM tip is retracted from the surface. The effective contact stiffness can be derived from a simple model (see Fig.6.9(a)). The effective spring constant is the sum of the stiffness of the cantilever beam  $k_c=0.12$  N/m and the attached polymers  $k_p$ :  $k_{\text{eff}} = k_c + n \cdot k_p$  where  $n$  is the number of attached polymers. The

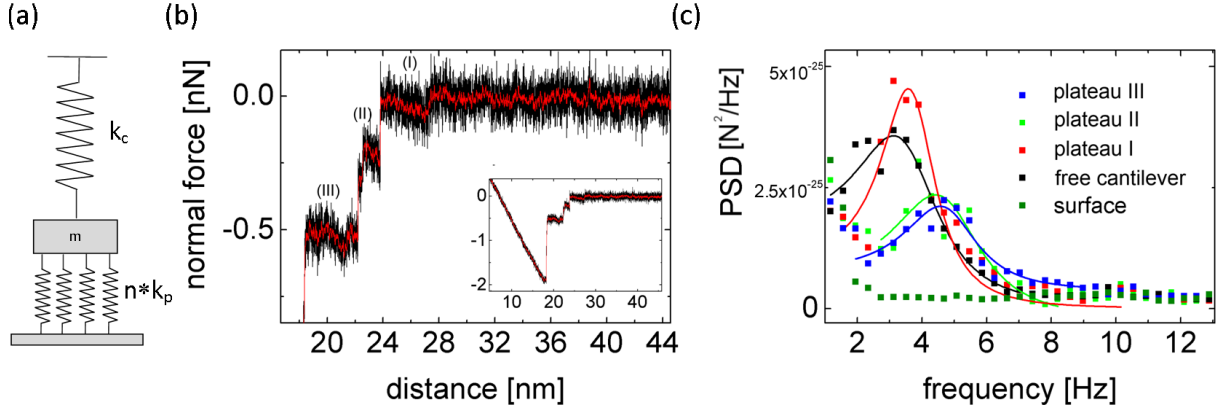


Figure 6.9: (a) Simplified model for determine the effective contact stiffness of an AFM tip bind to a surface via several polymer chains. (b) Normal force vs. distance during separation of a CD-polymer functionalized AFM tip from a CD functionalized surface, the inset shows the full retraction path of the f-d cycle. (c) PSD of the normal deflection data of the three plateaus of (b), free cantilever and in repulsive contact (surface) fitted with equation (6.2).

resonance frequency of this system is

$$f_0 = \frac{1}{2\pi} \sqrt{\frac{k_{\text{eff}}}{m_{\text{eff}}}}. \quad (6.8)$$

The effective mass  $m_{\text{eff}} = 3.12 \times 10^{-10}$  kg was obtained from the resonance frequency of the cantilever where the effective stiffness is determined by the spring constant of the cantilever  $k_c = 0.12$  N/m.

The effective contact stiffness is different than the one which determined the force ramp on the contact in pulling experiments. During pulling, the effective spring constant is determined by the springs connected in series  $k_{\text{eff}} = k_c \cdot n \cdot k_p / (k_c + n \cdot k_p)$ . A stiffer contact leads to a higher resonance frequency than obtained for the free cantilever so that we expect a shift towards higher frequencies when CD-polymers are attached.

Upon separation, several force drops in the normal force signal indicate that CD-polymers are detached from the surface resulting in an step-wise movement of the AFM tip (see Fig.6.9(b)). The resonance frequency for the different force plateaus was obtained from the Power Spectrum Density (PSD) of the vertical deflection signal. In order to obtain a smooth PSD with a well defined resonance peak, the normal deflection for each plateau was divided into packages of 128 data points. The PSD was calculated for each package and the PSD spectra were averaged. The averaged PSD was fitted with the Lorentz function,

equation (6.2) (see Fig.6.9(c)).

The resonance frequency shifts from 3.1 kHz for the free cantilever to 3.6 kHz for the first plateau (I) indicating a stiffer contact. The effective stiffness derived from equation (6.8) increases to  $k_{\text{eff}}=0.241$  N/m so that we can obtain the stiffness of the CD-polymers to be  $k_p=0.04$  N/m. The height of the last step of 105 pN corresponds to the rupture force of a single host-guest complex (see section 6.1) indicating that a single CD-polymer is stretched before the force drop occurs. We can conclude that the frequency shift is caused by stretching a single polymer chain which is linked to the surface by a single molecular bond.

For plateau (II), the resonance frequency increases further to 4.4 kHz indicating that more CD-polymers are attached revealing an additional stiffness of  $n \cdot k_p=0.12$  N/m. This value is a factor of three higher than the stiffness of a single CD-polymer indicating that three polymers are stretched in parallel which is confirmed by the normal force which is a factor of two to three larger than the force of a single host-guest bond.

The resonance frequency of the plateau (III) shifts slightly to 4.6 kHz leading to an additional stiffness of  $n \cdot k_l=0.14$  N/m indicating that about four polymers are stretched. The higher number of parallel stretched bonds is confirmed by the normal force of about 500 pN indicating that about five host-guest bonds contribute. When tip and surface are in repulsive contact, no frequency peak is observed. We assume that the thermal variations are damped by the extended contact.

The similarity of the resonance frequency for plateau (II) and (III) indicates the limit of the frequency analysis which is caused by the low quality factor of the resonance frequency in liquid. In order to give evidence for the number of attached polymers, the normal force and frequency analysis has to be performed complementary. In the following we will discuss slow approach experiments in order to investigate the time resolved binding of CD-polymers attached to an AFM tip.

### **CWT of slow approach experiments**

Slow approach experiments were performed in order to investigate the time resolved binding process of polymers when drawing closer to a surface. The AFM tip slowly approached the surface for 3 s, starting from a height of about 60 nm. The gains in the feedback-loop were kept low during the dwell time so that the AFM tip slowly approached the sample whereby the height was measured by means of the capacitive sensor. In Fig.6.10 the CWT of the a representative approach measurements recorded in connector solution and water

are presented, respectively. We start with the discussion of the f-d curve recorded in connector solution with focus on the modulation of the resonance frequency of 4.2 kHz.

In the beginning of the approach, when tip and surface are well apart from each other, the frequency band around the resonance frequency appears with a constant intensity. Significant variations in the frequency spectrum are observed around arrow 1 until the resonance frequency completely disappears for  $z \leq 1$  nm which is indicated by arrow 2. The intensity variations between arrow 1 and 2 in the *scalogram* can be correlated with jumps in the vertical deflection signal indicating that polymer chains form reversible bonds with the surface. Hence, the intensity variations in the *scalogram* can be interpreted as changes in the overall contact stiffness, and thus in the number of bonds between tip and surface.

Stretching experiments discussed above have shown that stretched polymers cause a shift of the resonance to higher frequencies. These frequency shifts are small and a sufficient number of data points is required in order to quantify them. Due to the low Q-factor in liquid, no quantitative information can be obtained from the *scalogram*. However, the intensity variations in the *scalogram* around the resonance frequency visualize the multiplicity of bonds since this is in clear contrast to a single bond which can either be in the “on”- or “off”-state. Moreover, the time scale of the polymer binding can be estimated from the intensity variations around the resonance frequency. The variations of the resonance frequency in the *scalogram* appear in the order of tens of milliseconds indicating slower kinetics of the overall contact compared to the single bonds. Previous studies demonstrated that the single CD-(Ad)<sub>2</sub>-CD bonds attach and detach several thousand times per second [2]. In our multiple bond system, the contact is established by several single polymer chains which contain several CD molecules. The formation of one ditopic bond enlarges the probability that either the neighboring CD molecules or CD molecules attached to another polymer chain also bind to the surface. Just as well leads the detachment of one bond not to the detachment of the whole AFM tip because the overall polymer attachment is stabilized by several of supramolecular bonds. The phenomenon of slower kinetics of an assembly of bonds compared to a single bond is referred to as multivalency effect [17, 12].

As a control, the same experiment was performed in water without guest molecules (see Fig.6.10(b)). No pronounced events are observed in the *scalogram* and normal force signal until the cantilever bends by 200 pN towards the surface at a z-height of 0.5 nm (arrow 1). Arrow 2 marks the point of repulsive tip-surface contact  $z \leq 0$  nm where the resonance frequency is fully damped. Pull-off force measurements in section 6.1 revealed a

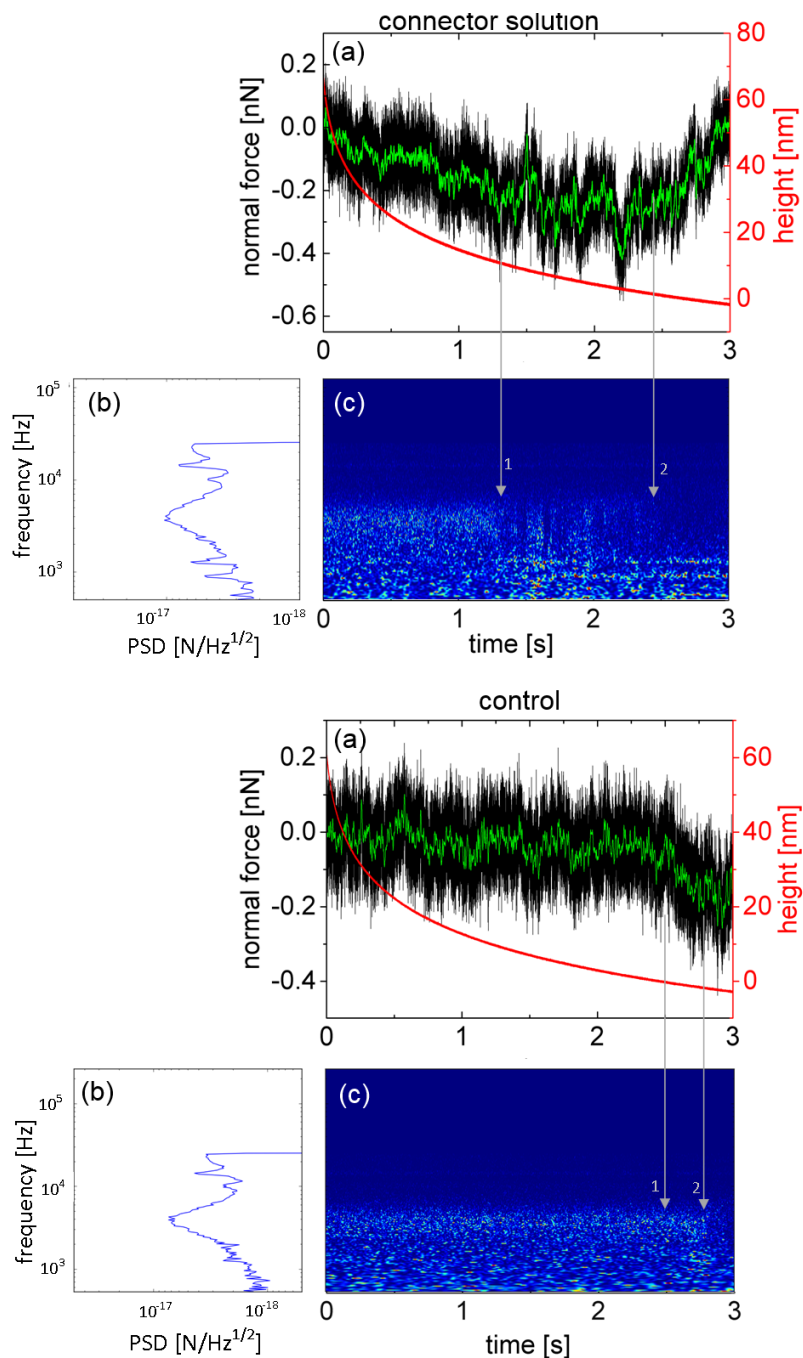


Figure 6.10: CWT of a slow approach experiment in adamantane connector solution (up) and the control experiment (down) without connector molecules. In (b) the time averaged PSD with the resonance frequency of the cantilever of 4.2 kHz is shown. The arrows mark prominent points which are discussed in the text. In connector solution, pronounced variations in the normal force (a) and scalogram (c) are observed which are missing in the control experiment. The green line in (a) represents a moving average of 500 data points of the original deflection data. *The slow approach experiments were performed by Franziska Emmerich.*



low adhesive interaction between tip and surface in pure water. Due to the low adhesive force a tip-surface contact is not established until the AFM tip is close ( $z \leq 0.5$  nm). The absence of the formation of an adhesive contact on larger distances in water provide evidence for the specific attachment of polymer chains due to the high binding affinity of the CD-(Ad)<sub>2</sub>-CD inclusion complex in adamantane connector solution. Moreover, we conclude that polymers protrude from the surface of the AFM tip forming the initial contact at a distance of  $z=15$  nm which is comparable to the estimated polymer length (see section 6.1 in this chapter).

The detection of the time resolved contact formation process by CWT is particularly interesting when considering a recent AFM study on the attachment of cells [99]. Thewes et al. reported that the initial cell-surface contact formation is mediated by cell wall proteins starting from a distance of about 50 nm above the surface. Further insights into the initial contact formation process in biological systems could be provided by means of CWT which could yield time resolved information about the contact stiffness and thus about the number of attached molecules, while approaching the surface.

### 6.2.3 Conclusion

In conclusion, we presented a new method for investigating the contact formation process of polymer chains with high temporal resolution. The time resolved frequency analysis provides information about the reversible attachment of several CD-polymer chains during slowly approaching a CD coated surface. The comparison with the control experiment confirms the specificity of the interaction. The reversible binding occurs on a time scale of milliseconds which is three orders of magnitude slower than a single host-guest interaction due to the multiplicity of bonds. The potential of a quantitative analysis was shown by means of Fourier transform where a correlation between frequency shift and number of attached polymers was achieved. A quantitative analysis of the reversible binding of polymers was not possible by means of CWT analysis due to the damping effects in liquid. In future experiments the Q-factor of the resonance frequency should be increased in order to enhance the frequency resolution.

# 7 Dynamic study of adhesive friction mediated by supramolecular bonds with different molecular kinetics

## 7.1 Introduction

Understanding the molecular origins of friction is one of the main challenges in the field of nanotribology. Recently adhesive friction has been investigated as rupture of molecular bonds [33, 31, 2, 35]. Dynamic friction studies provide evidence that the sliding speed dependence of friction forces is determined by the thermally activated rupture and reformation of molecular bonds which can be tuned by temperature [35]. Different regimes were reported that dependent on the ratio between sliding speed and bond kinetics and include stick-slip behavior caused by the cooperative interaction of multiple bonds [33, 31].

The relation between adhesion and friction force is not yet fully understood. Several studies investigate the adhesion-kinetics of a multiple-bond contact based on the single bond kinetics [17, 10, 2, 109]. The binding kinetics of multiple bonds differ dramatically from the binding kinetics of each single bond. The slower binding kinetics of a multiple bond system were attributed to the multivalency effect which describes the cooperative interaction of individual bonds [11]. In contrast, most dynamic friction experiments were based on nonspecific interactions between bare silicon tips and for example a NaCl surface [35] or self assembled monolayers [110], where the attractive interaction between tip and surface arises from van der Waals forces so that the number, exact nature, and kinetics of the involved molecular bonds remains unclear. Recently, a model was developed that predicts adhesion and friction forces caused by multiple supramolecular bonds arranged on an AFM tip [31]. The situation on an AFM tip is more complex than for a system with perfectly parallel surfaces since the molecular bonds are attached on different heights.

In this section, we describe dynamic friction and adhesion measurements which were

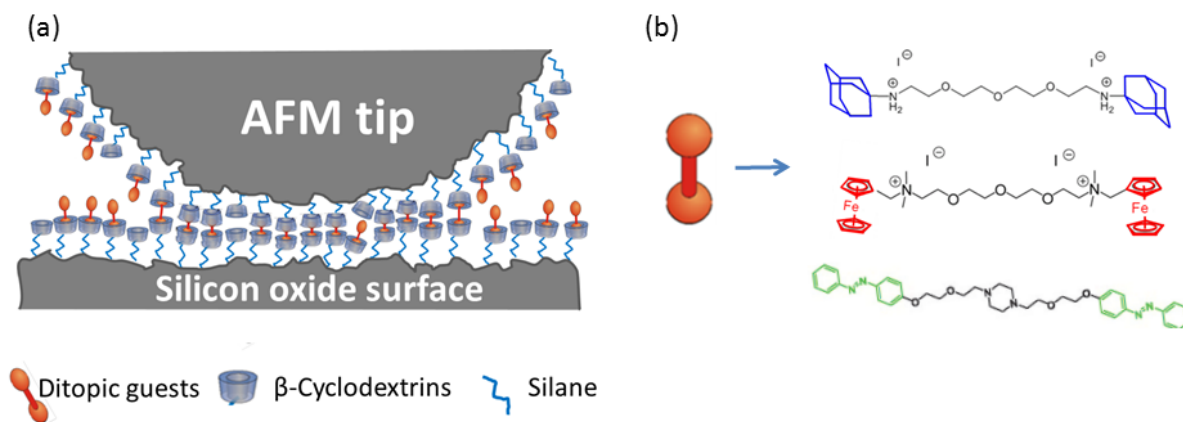


Figure 7.1: (a) Scheme of the molecular arrangement of the experiment. (b) Chemical structure of the connector molecules from top to bottom: adamantane, ferrocene and azobenzene.

performed to investigate the relation between adhesion and friction for multiple bonds and the binding kinetics of single bonds. The attractive interactions between AFM tip and surface arise from the cyclodextrin inclusion reaction. AFM tip and surface are decorated with a cyclodextrin monolayer. Ditolipic connector molecules added to the aqueous solution bind the gap between the AFM tip and surface by including one end into a CD attached the surface and one into the CD on the tip (see Fig.7.1). In order to tune the binding kinetics on the single bond level, we will follow a molecular toolkit approach where the surface functionalization remains the same and the bond kinetics are modified by varying the guest molecules in solution. By using the same surface functionalization, the bond kinetics are solely determined by the complexation kinetics of CD molecules and their guests. Our experimental results will be discussed in terms of the model recently developed by R. Guerra et al. [31] describing dynamic friction caused by supramolecular bonds.

## 7.2 Experimental section

### Preparation of cyclodextrin monolayers

The solid substrates were commercially available Si(111) wafers (Si-Mat, Kaufering, Germany). Prior to the chemical functionalization, the wafers were cleaned with piranha solution (3:2 mixture of sulfuric acid and hydrogen peroxide), rinsed with ultrapure water and dried under a stream of  $N_2$ . In a first functionalization step, the cleaned oxide surface

was kept together with a vial of 3-isothiocyanatpropyl-triethoxysilane solution in a desiccator under low pressure (2 mbar) for 45 min. Subsequently, loosely bound silane molecules were removed by rinsing the surface with THF and ultrapure water. In order to attach the  $\beta$ -CD molecules, the silanized surface was kept in 1 mM mono(6-deoxy-6-amino)- $\beta$ -CD diluted in water at room temperature for more than 12 h. All samples were freshly prepared prior to each measurement and stored in ultrapure water for not more than three days. Cantilevers were functionalized in the same way.

## AFM measurements and data analysis

For all friction and adhesion measurements we used a Nanowizard 3 AFM (JPK Instruments, Berlin, Germany). The measurements were performed in aqueous solution, either in ultrapure water or connector molecule solution, at room temperature. Soft cantilevers (PPP-Cont, NanoandMore, Wetzlar, Germany) were used with a normal spring constant of  $k_c = 0.3 \pm 0.03$  N/m and lateral spring constant of  $k_l = 110 \pm 10$  N/m. The normal spring constant of each cantilever was calibrated by thermal noise analysis as suggested by Sader et al. [39]. A calibration wedge was scanned in air in order to confirm the calibration of the lateral spring constant. The correction factor which was introduced by Tocha et al. [43] was applied for calibration of the data obtained in liquid. Friction force experiments were performed by sliding perpendicular to the cantilever axis with the lowest possible loads of 1 nN in order to prevent surface damage. The mean friction force was obtained as the average of trace and retrace recorded in a friction loop. Concentration-dependent friction measurements were performed in a droplet of ultrapure water with a volume of 250  $\mu$ L. To increase the concentration, 5  $\mu$ L to 20  $\mu$ L droplets of connector solution with a concentration of 30  $\mu$ M were subsequently added. For all other friction and adhesion data shown in this section, a standard concentration of 10  $\mu$ M was used for the connector solution in order to perform the AFM measurements in the saturation regime of the Langmuir curve.

Force spectroscopy results were analyzed with the data processing software provided by JPK Instruments, Berlin, Germany. Force curves were obtained on different surface positions and the maximum pull-off force, the work of separation or the height of the last rupture were analyzed and included in histograms for statistical evaluation. The most probable pull-off force and work of separation values are presented in the data plots. The standard deviation for the three surface positions is represented as error bars.

## 7.3 Results

In the adhesive regime, friction is dominated by adhesive bonds between the AFM tip and the surface. In order to gain insights into the molecular mechanisms underlying friction and adhesion, the forces while sliding across a surface and during tip-surface separation were studied independently. We performed friction and adhesion measurements with three different connector molecules which differ in their end groups: adamantane, ferrocene and azobenzene. In order to investigate unspecific contributions to the forces, the adhesive interaction was studied in pure water before each measurement.

### 7.3.1 Loading rate dependence of adhesion

The pull-off force and the work of separation are a measure for adhesion which were both derived from force-distance curves between CD-covered AFM tips and surfaces. A minimum of 300 force distance cycles recorded on three different surface positions were included in the analysis. The pull-off force is plotted versus the unloading rate in Fig.7.2(a) for the three connector molecules and the control experiment. The pull-off force of the control experiment is low with a value of about 0.4 nN and increases only slightly for higher loading rates. After adding the connector molecules, the pull-off force increases for all three connector molecules. The strongest effect is observed for adamantane for which the pull-off force is almost the double of that of the control experiment. The pull-off force for adamantane increases only weakly with loading rate. A clear loading rate dependence is observed for azobenzene which shows an increase of about 200 pN within the investigated range of loading rates. Ferrocene exhibits the lowest pull-off force of the three connector molecules which slightly exceeds the control level for pulling rates above 400 nN/s. In addition to the rate dependence of the pull-off force, the shape of the force-distance curve is also rate dependent for all connector molecules (see Fig.7.2(c)-(e)). For low loading rates, the force curve exhibits a force plateau with several force drops. With increasing pulling rate, the maximum adhesion force increases and the shape changes into a triangular shape. The change of shape was reported before for the adamantane connector in chapter 3 and was attributed to a combination of multivalency effect and cantilever inertia. Observation of the shape change also for azobenzene and ferrocene indicates that the same mechanism leads to the loading rate dependence for all three connector molecules.

A combined quantification of the pull-off force and the curve shape can be derived from the area under the force curve. The work of separation follows a similar overall trend as the

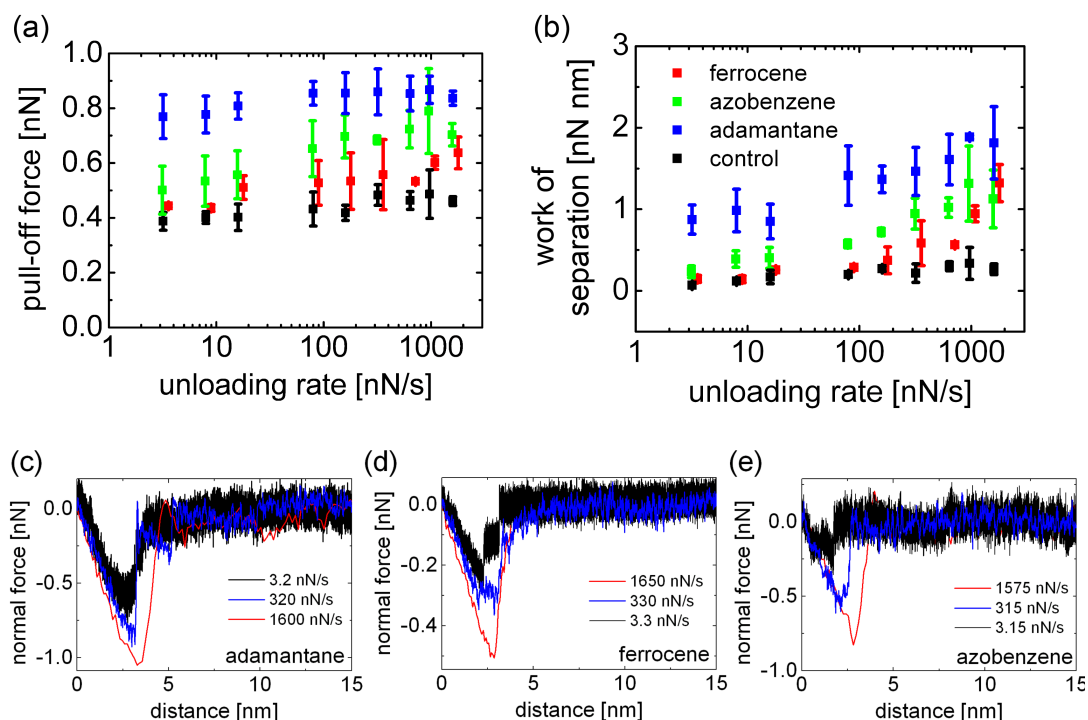


Figure 7.2: (a) Mean of maximum pull-off force recorded in three different connector solutions and control experiment as a function of unloading rate. (b) Work of separation of the same force curves recorded in (a) as a function of unloading rate. The mean value represents the average of 300 force curves recorded on three different surface positions with the standard deviation as error bars. Representative f-d curves recorded with different velocities in (c) adamantane, (d) ferrocene and (e) azobenzene connector solution.

pull-off force, but the variation for different connector molecules is stronger (see Fig.7.2(b)). For high loading rates, the work of separation increases by an order of magnitude for all guest molecules. Adamantane leads to the highest work of separation which shows a more pronounced rate dependence than observed for the pull-off force. The higher rate dependence of the work of separation compared to the pull-off force is probably due to the large separation length of 7 nm to 10 nm. In case of ferrocene and azobenzene, the rate dependence of the work of separation is in good agreement with the development of the pull-off force. For both connectors, a smaller separation length of up to 5 nm is observed.

From the last rupture event in a force-distance curve, the rupture force for a single bond can be determined (see Fig.7.3(a)). In order to obtain a sufficient force resolution, a softer cantilever with a stiffness of 0.11 N/m was used. The height of the last step

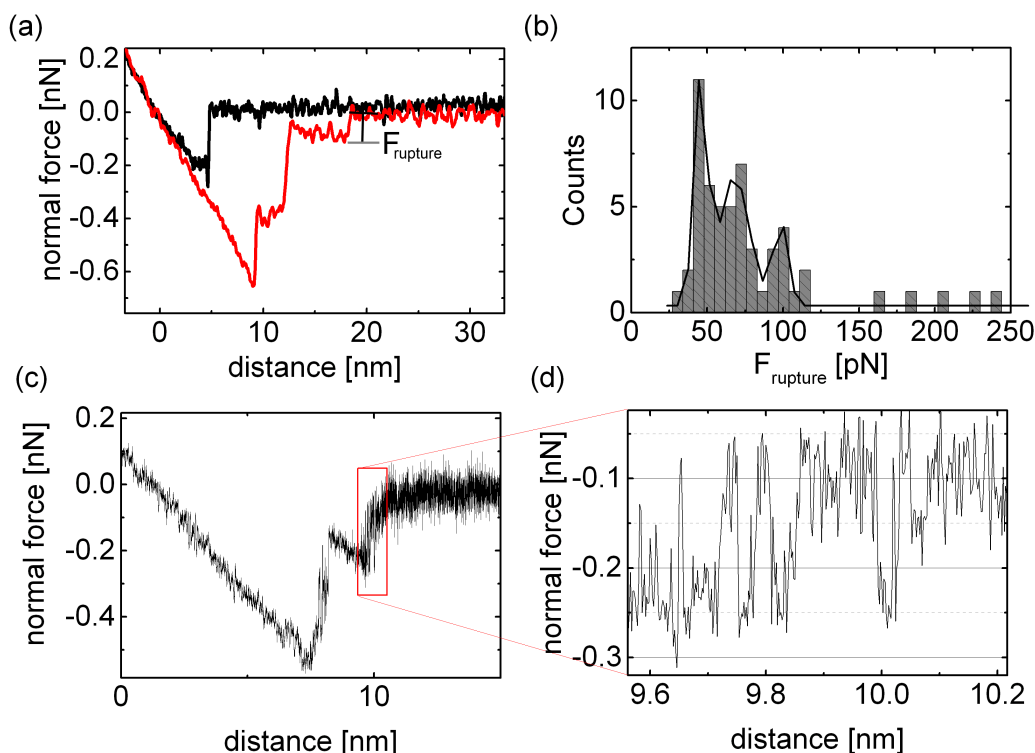


Figure 7.3: (a) Force-distance cycle recorded in ferrocene solution with a pulling rate of 110 nN/s (approach in black, retraction in red). The height of the last rupture step was included in the histogram in (b). The solid line represents a Gaussian fit to the data included in the Histogram and serves as a guide to the eye. The first peak indicates the rupture force of a single bond. (c) Separation curve recorded with a sampling rate of 50 kHz in ferrocene connector solution with a pulling speed of 10 nN/s, the rectangle indicates the position of the detail presented in (d) where multiple force jumps between two force plateaus indicate rebinding events of several parallel bonds.

was plotted into a histogram that exhibit several maxima (see Fig.7.3(b)). The force corresponding to the first maximum reveals the rupture force of a single bond, the second of two parallel bonds, etc. For ferrocene, the single bond rupture force is  $f_{\text{rup}} = 40 \pm 10$  pN leading to a binding energy of  $\Delta G = f_{\text{rup}}^2 / (2k_c) = 4.4$  kJ/mol [29]. The binding energy of ferrocene is in good agreement with the binding energy of azobenzene  $\Delta G = 4.3$  kJ/mol ( $f_{\text{rup}} = 61 \pm 10$  pN,  $k_c = 0.26$  N/m, see chapter 2) and is significantly lower than that for adamantane with a binding energy of  $\Delta G = 10.1$  kJ/mol ( $f_{\text{rup}} = 80 \pm 10$  pN,  $k_c = 0.2$  N/m, see chapter 3). In Fig.7.3(c) a force-distance curve recorded with high bandwidth and low pulling velocity in ferrocene solution is shown. After a linear force increase, several rupture occur until the AFM tip reached its equilibrium position. The steps are characteristic for

rupturing a multiple bond contact. Interestingly, several force jumps are observed at the transition between two force plateaus in Fig.7.3(d) indicating that the bonds rebind during the rupture process. The height of the force jumps is about 150 pN. This value is more than three times the single rupture force of  $40 \pm 10$  pN indicating that a minimum of three bonds detach and rebind in parallel. A few smaller force jumps with a force of about 50 pN are also observed which correspond presumably to single events. The rebinding feature was not observed for adamantane and azobenzene.

### 7.3.2 Velocity dependence of friction

The friction force is the force acting against the movement of sliding. In our system, the friction force is mainly caused by the rupture of supramolecular bonds formed by ditopic connector molecules between the CD molecules on tip and surface. While sliding, the bonds lead to a lateral torsion of the cantilever which is measured as lateral deflection. The hysteresis between forward and backward scan reveals the dissipated energy which is proportional to the friction force. In order to investigate the adhesive friction regime, the applied load were kept below 1 nN. A minimum of 100 force loops was averaged for obtaining the mean friction force. The design of our molecular system allows to determine the unspecific contributions by control experiments in water prior to every measurement. After adding the connector molecules into the solution, a significant increase in friction was observed for all three connector molecules (see Fig.7.4). The sliding speed dependence of friction varies between the three connector molecules. For adamantane, the friction force shows a weak sliding speed dependence but the highest overall friction force. The friction increases logarithmically with sliding speed indicating that the bond rupture is irreversible and thermally activated [111]. In contrast, azobenzene and ferrocene lead to a strong rate dependence while the overall friction force is lower than for adamantane. Azobenzene connector molecules exhibit a linear increase starting from 150 nm/s. In case of ferrocene, a friction plateau is observed for velocities of about 100 nm/s which changes into a linear increase for sliding speeds above 400 nm/s. In the linear regime, the friction force of ferrocene overlaps with the data for azobenzene.

In Fig.7.5 characteristic friction loops are presented. The shape of the loops depends strongly on the connector molecules. For adamantane, erratic stick-slip events with a peak height of up to 2 nN are observed indicating a collective rupture of multiple parallel bonds. The stretching length is about 1 nm which corresponds to the length of the tetraethylene glycole (TEG) chain connecting the end groups of the connector molecules. The friction



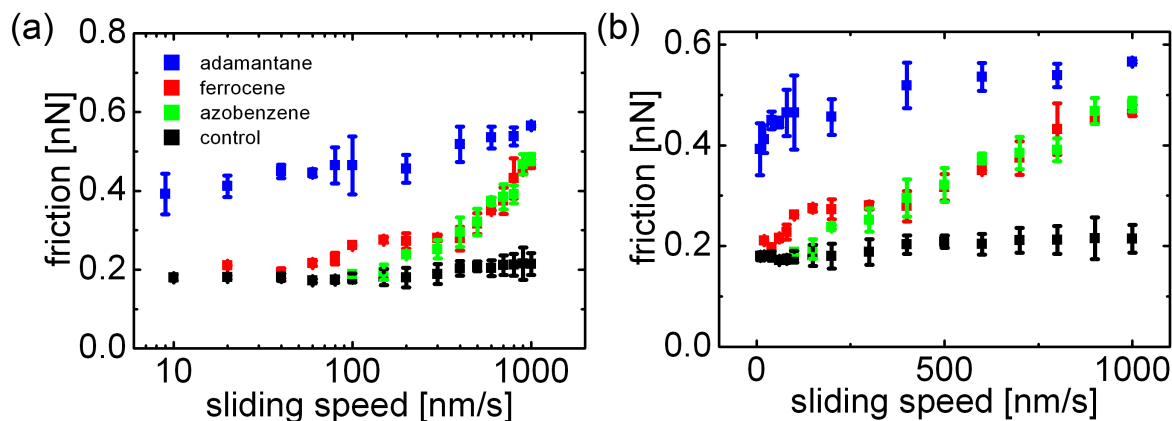


Figure 7.4: (a) Mean friction force vs. scanning speed at a concentration of  $10 \mu\text{M}$  in aqueous solution for the three connector molecules and control experiment. The data points represent the mean value of 100 lines, the error bars represent the standard deviation of the lines. (b) same data as in (a) with a linear x-axis to demonstrate the linear increase of the friction force for ferrocene and azobenzene.

loop of ferrocene and azobenzene exhibits less pronounced stick-slip events. A more regular stick-slip with a smaller peak height and smaller stretching length of about  $0.6 \text{ nm}$  is observed.

The influence of the sliding speed on the shape of the friction loop can be observed in Fig.7.5(d)-(f). Three exemplary force traces are shown for the respective connector molecule. For adamantane, no change in the shape of the overall friction loop is observed when increasing the sliding speed. For all investigated sliding speeds, stick-slip events are observed. The shape of the stick-slip events vary slightly with the sliding speed. For high velocities, the stick-slip event exhibit a triangular shape with a sudden force drop in the direction of sliding. In contrast, for low velocities, the stick-slip event exhibits several peaks and no prominent force drop.

The force trace of ferrocene shows a smooth sliding for low sliding velocities. At an intermediate sliding velocity of  $100 \text{ nm/s}$ , a more noisy force trace is observed which probably indicates a beginning stick-slip movement. At this sliding velocity the friction force exceeds the value of the control experiment (see Fig.7.4). The third force trace is recorded with a sliding speed of  $800 \text{ nm/s}$  and shows rare but clear stick-slip events.

For azobenzene, a similar change in the force trace is observed. For slow sliding speeds, the force trace exhibits a smooth sliding. For the intermediate sliding velocity of  $400 \text{ nm/s}$ ,

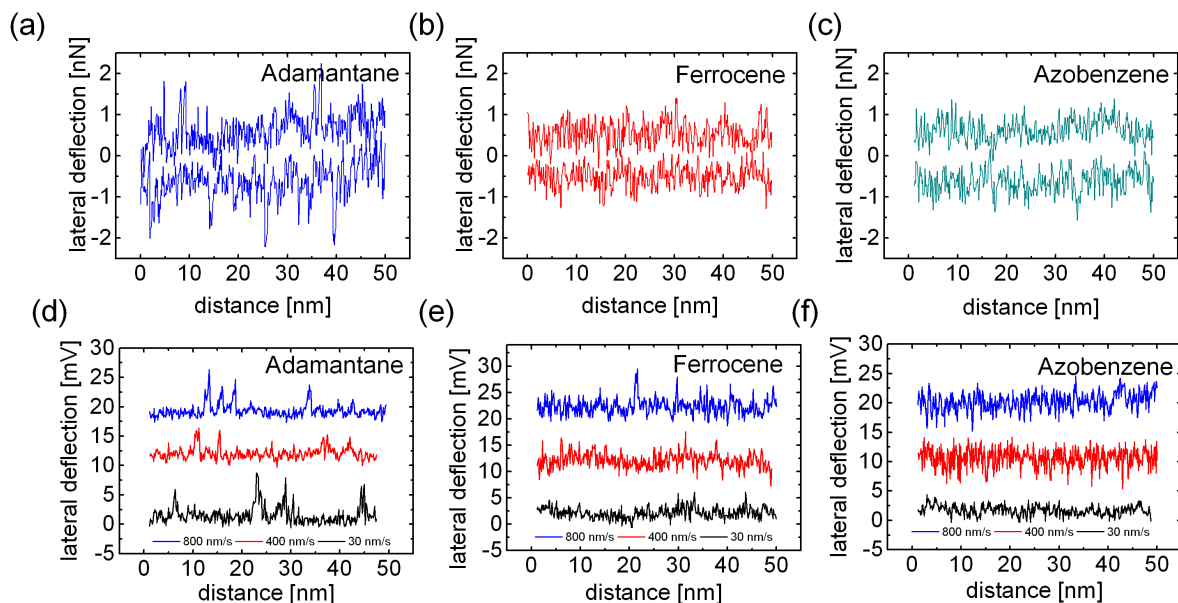


Figure 7.5: Representative friction loops recorded at 800 nm/s for (a) adamantane, (b) ferrocene and (c) azobenzene. Representative friction traces recorded at 30 nm/s, 400 nm/s and 800 nm/s for (d) adamantane, (e) ferrocene and (f) azobenzene.

the force trace becomes more noisy indicating an erratic rupture of specific bonds. For the high sliding velocity of 800 nm/s, the force trace becomes again smoother and a few peaks are observed. The peak forces arise from a stick-slip movement of the AFM tip indicating a beginning correlation of bond rupture.

### 7.3.3 Friction force and connector concentration

The adhesive friction in our system is caused by connector molecules that bridge the CD molecules attached to the opposing surfaces. One can assume that the concentration of the connector molecules in solution will affect the adhesive forces. The effect of connector concentration on the adhesive force was investigated in friction force measurements. As a control experiment, the first friction measurement was recorded in pure water. Subsequently, small droplets with a volume of 5  $\mu\text{L}$  to 30  $\mu\text{L}$  of the respective connector solution with a concentration of 30  $\mu\text{M}$  were added into the solution. In order to allow the system to adjust the surface coverage of connector molecules to the new concentration in solution, the AFM tip was retracted from the surface when a droplet was added. After waiting for 10 min, the AFM tip was approached again and 100 friction loops at five different velocities were recorded. The mean friction force at a sliding speed of 800 nm/s is shown as a func-

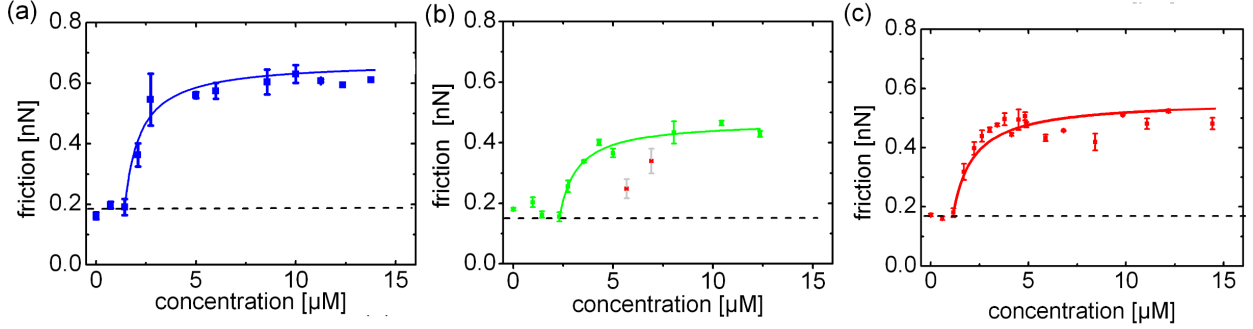


Figure 7.6: Friction force recorded with a velocity of 800 nm/s as a function of (a) adamantane, (b) azobenzene, and (c) ferrocene connector molecule concentration. The dotted line indicates the force of the unspecific interactions and marks the baseline for the Langmuir fit (solid line). The red data points in the graph of ferrocene were not included in the Langmuir fit.

tion of connector concentration in Fig.7.6(a)-(c). For low concentrations, a friction force of 0.2 nN is observed which is the typical value of the control experiment in pure water and arises from the unspecific bonds between AFM tip and surface. The unspecific bonds, e.g. hydrogen bonds between the hydroxyl plane of opposing CD molecules, prevent the friction force from falling below a threshold value. Above the threshold, the concentration dependence of all three connector molecules exhibits a Langmuir characteristic with a saturation value for connector concentrations above 5  $\mu\text{M}$ . Interestingly, the friction force enters the saturation regime directly after the monotonous increase. The absence of a maximum friction force at intermediate concentration indicates that the connector molecules do not passivate the surface at high concentrations. For slow complexation kinetics, the CD molecules would be blocked at high connector concentrations leading to a decrease of friction which was not observed for our system. We conclude that the reaction kinetics are fast compared to the time scale of our measurement. The similarity with the Langmuir isotherm indicates that the friction force is related to the surface coverage of connector molecules. A higher surface coverage leads to a higher number of connector molecules in the gap between AFM tip and surface and, thus, to a higher friction force. According to the Langmuir model, the surface coverage  $B$  depends on the binding affinity of the adsorbates  $K^L$  and the concentration  $c$

$$B = B_{\infty} \frac{K^L \cdot c}{K^L \cdot c + 1} \quad (7.1)$$

where the parameter  $B_{\infty}$  is the maximum surface coverage. The data above the threshold was fitted with the Langmuir model (equation (7.1)). In case of azobenzene, a drop in

the friction force at a concentration of 5  $\mu\text{M}$  is attributed to a slightly different solution. Due to the poor solubility of azobenzene in water, 1% DMSO was added to the solution which is known to lower the binding affinity of azobenzene and cyclodextrin [112]. These data points were not included into the Langmuir analysis. From equation (7.1) the binding constant at the surface can be obtained for adamantane  $K_{\text{Ad}}^{\text{L}} = 12.8 \times 10^5 \text{ M}^{-1}$ , azobenzene  $K_{\text{AzO}}^{\text{L}} = 11.2 \times 10^5 \text{ M}^{-1}$  and ferrocene of  $K_{\text{Fc}}^{\text{L}} = 8.77 \times 10^5 \text{ M}^{-1}$ . The trend of the values is in agreement with the binding constants obtained in solution by Isothermal Calorimeters measurements (ITC) included in Tab.7.1. However, the binding constant on the surface is two orders of magnitude larger than the constant obtained in solution. A larger binding constant at the surface was reported recently for a similar system investigated by surface plasmon resonance experiments [61]. The reason for the higher binding constant at the surface will be discussed in the following section.

Table 7.1: Parameters describing the molecular kinetics of the host-guest interaction between cyclodextrins and connector molecules (\* for monotopic guest)

connector molecule	$K^{\text{L}}$ [ $\text{M}^{-1}$ ] Langmuir	$K^{\text{ITC}}$ [ $\text{M}^{-1}$ ] ITC	$\Delta\text{G}$ [ $\text{kJ/mol}$ ] ITC	$k_{\text{off}}$ [ $\text{kHz}$ ] ITC
ferrocene	$8.77 \times 10^5$	$6.3 \times 10^3$ [91]	21.6 [91]	16
azobenzene	$11.2 \times 10^5$	$8.4 \times 10^3$ * [63]	22.4*[19]	12
adamantane	$12.8 \times 10^5$	$11.3 \times 10^3$	23.1	8

## 7.4 Discussion

The rate dependence of adhesion and friction force of the three connector molecules are in good agreement. The similar force values for adhesion and friction and the similar rate dependence provides evidence that the friction experiments were performed in the adhesive regime and the friction force is predominantly caused by multiple adhesive bonds formed between the AFM tip and surface. In the following we will discuss the dynamics of adhesive friction caused by supramolecular bonds between the AFM tip and surface. We observed that the mean friction force and the stick-slip characteristic of adhesive friction are rate dependent. We believe that this rate dependence is correlated to the unbinding dynamics of the supramolecular bonds and is due to a cooperative interaction of individual bonds. The effect of cooperativity on adhesive friction was predicted by Filippov et al. based on

simulations [33]. We will discuss the rate dependence with respect to the binding kinetics at the surface in relation to the driving velocity in our experiments.

### 7.4.1 Binding kinetics at the surface

We will first discuss the concentration dependence of the friction force in order to obtain insights into the binding kinetics at the surface. A delayed onset of the increase in friction as a function of connector concentration was observed indicating that a minimum concentration is required to achieve a significant increase of the friction force. The guest solution was added drop wise into the solution. The first droplet increases the concentration in the solution to  $0.6 \mu\text{M}$ . By considering the binding affinity of adamantane of  $K^{\text{ITC}} = 11,300 \text{ M}^{-1}$ , the surface coverage of the CDs occupied by connector molecules can be estimated by  $B = 0.6\%$ . The friction force is determined by the number of bonds between tip and surface. At a surface coverage of  $0.6\%$  it is likely that no connector molecules enter the gap between AFM tip and surface. When the connector concentration exceeds  $2 \mu\text{M}$ , a sudden increase in friction indicates that a significant number of connector molecules contributes to the friction force. The rapid increase in friction indicates a high binding affinity for the complexation between the CD cavity and all three connector molecules.

The binding constant obtained by the Langmuir model is two orders of magnitude higher than the binding constant obtained from ITC experiments. The higher binding affinity at the surface was reported before for surface plasmon resonance experiments and can be understood by the higher connector concentration at the surface compared to the concentration in solution. Due to the complex formation with the CD molecules, the residence time of the connector molecules is increased leading to a higher concentration at the surface compared to the concentration in solution. In the saturation regime, above a concentration of  $5 \mu\text{M}$ , we assume that all cavities of the CDs are occupied by connector molecules so that for the effective concentration  $C_{\text{eff}}$  in the tip-surface contact follows [113]

$$C_{\text{eff}} = \frac{3}{2} \frac{1}{A_{\text{host}} N_A r_{\text{con}}} \approx 0.22 \text{ M} \quad (7.2)$$

where  $A_{\text{host}}$  is the surface area occupied by the host cavity,  $r_{\text{con}} \approx 2 \text{ nm}$  the radius of the connector molecule and  $N_A$  the Avogadro constant. The on-rate at the surface is then  $k_{\text{on}}^{\text{eff}} = k_{\text{on}} C_{\text{eff}} = 2.2 \times 10^7 \text{ Hz}$  which is a factor of  $10^3$  higher than the on-rate in solution. The on-rate at the surface is three order of magnitude larger than the off-rate leading to

an effective rebinding of broken bonds.

The different connector molecules exhibit different off-rates leading to a different rate dependence. In the following, the impact of bond kinetics on the rate dependence of friction and adhesion will be discussed.

### 7.4.2 Loading rate dependence of adhesion

Adhesion and friction forces increase with increasing driving velocity. The velocity dependence varies for the different guest molecules. In order to understand this variation we have to consider the relation between bond kinetics and driving velocity. In pulling experiments, the shape of the force curves is rate dependent as observed earlier in chapter 3. Fast pulling rates lead to a parallel stretching of bonds resulting in a high contact stiffness which exceeds the cantilever stiffness so that the slope in the force curve is determined by the cantilever stiffness. Recent simulations revealed that a constant number of bonds contributes to the linear increase at high loading rates [31]. Due to the curvature of the AFM tip, the rupture starts at the periphery and propagates towards the tip apex [31]. The number of molecules stretched in parallel in the outer ring of the contact can be determined by the tip radius of  $r_{\text{tip}}=7$  nm. Considering the outer ring with a distance of the diameter of one CD molecule of  $r_{\text{CD}}=0.75$  nm and a maximum packing fraction with 0.74, the maximum number of molecules within the outer ring of the contact can be roughly estimated to be  $N_{\text{max}} = 0.74 \frac{r_{\text{tip}}^2 - (r_{\text{tip}} - 2r_{\text{CD}})^2}{r_{\text{CD}}^2} \approx 25$  CDs. At high pulling rates, these bonds are stretched in parallel so that the number  $N$  of bonds can be estimated from the single rupture force  $f_{\text{rup}}$  to be  $N \geq f_{\text{pull-off}}/f_{\text{rup}} \approx 0.8$  nN/82 pN  $\approx 10$  which is lower than the number of estimated bonds so that we conclude that not all CD molecules on tip and surface are connected by a ditopic guest molecule. The number of contributing bonds is determined by the binding affinity and can be obtained from the Langmuir model (equation 7.1). Azobenzene and ferrocene exhibit higher off-rates so that the number of contributing bonds is lower than for adamantane leading to lower pull-off forces.

The force-distance curve for ferrocene recorded with high bandwidth exhibits several rebinding events which were not observed for adamantane and azobenzene (see Fig.7.3(d)). In order to observe rebinding events, two conditions have to be fulfilled. The first requirement is that the duration of the “off”-state exceeds the response time of the cantilever. If the duration of the “off” state is shorter the cantilever cannot relax within this time gap and the unbinding cannot be observed. Ferrocene exhibits the highest off-rate compared to adamantane and azobenzene leading to a larger duration of the “off” state than for the

other two connectors. The second aspect refers to the reformation of the bond. In the moment of unbinding, the molecular linker is stretched to a certain extend and relaxes right after the unbinding event. In order to rebind the bond, the linker has to be stretched again. This stretching is activated by thermal energy  $k_B T$ . For a bond with a higher rupture force, the molecular linker bond has to be stretched to a higher extend leading to higher energy costs than for a weaker bond with a lower rupture force. Ferrocene exhibits the lowest rupture force of the investigated connector molecules leading to the lowest stretching length and lowest energy costs for reformation. We conclude that the observation of rebinding events for ferrocene is on the one hand due to the higher off-rate of ferrocene and on the other hand due to the lower rupture force compared to azobenzene and adamantane. For adamantane and azobenzene, the higher rupture forces suppress the reformation of broken bonds.

The pull-off forces for all connector molecules are rate dependent. The overall appearance of the rate dependence is in good agreement with the simulations of Guerra et al. in Ref.[31] (see Fig.7.7). The simulations are performed in response to the results in chapter 3 which was published in 2015 and refer directly to our molecular system. The simulations reveal to a rate dependence of the pull-off force for different ratios of on- and off-rates. Two regimes are observed: (i) at low pulling rates the pull-off force is low and almost constant, (ii) at high loading rates, the pull-off force increases with scanning speed. The shape of the rate dependence is similar for all ratios but the transition point from regime (i) to regime (ii) is dependent on the off-rates of the individual bonds. It was found that the pull-off force is predominantly determined by the off-rate and the on-rate has a minor effect due to the high energy costs for bond reformation.

In our experiment, the on-rate is similar for all connector molecules. The ferrocene connector exhibits the highest off-rate  $k_{\text{off,fe}} = 16$  kHz of the investigated connector molecules. The highest off-rate leads to the lowest pull-off force. The pull-off force of ferrocene exceeds the force of unspecific contributions at a unloading rate of 100 nN/s in Fig.7.2(a). At this loading rate, the pull-off force transfers from regime (i) to regime (ii) which is in good agreement with the simulations in Fig.7.7(b) when considering an off-rate of ferrocene.

The azobenzene connector exhibits a lower off-rate than ferrocene  $k_{\text{off,azo}}^{\text{eff}} = 12$  kHz causing a higher overall pull-off force. The transition from the constant regime (i) to the rate dependent regime (ii) is not visible in the investigated range of unloading rates but can be estimated to occur at an unloading rate of 1 nN/s. We did not expect such a significant difference in the rate dependence of the pull-off force since the off-rates do not vary much

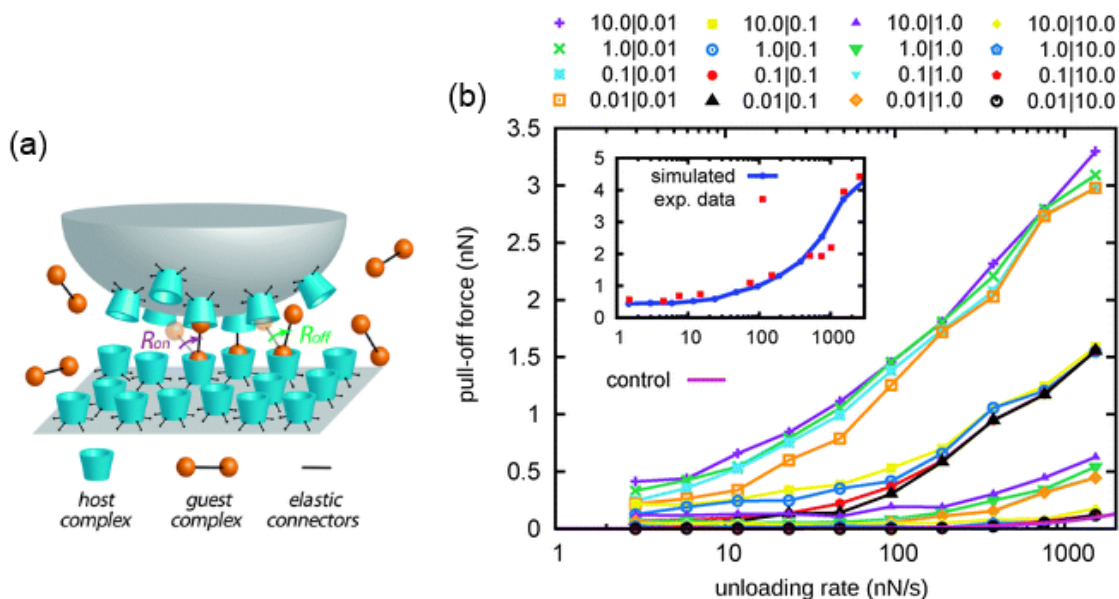


Figure 7.7: (a) Sketch of model system; (b) pull-off force as a function of unloading rate for different  $R_{on}^0 | R_{off}^0$  values in kHz. The control curve is simulated for a free tip which is subject only to viscous damping. The inset shows the best fit to the experimental data in chapter 3 with  $R_{on}^0 = 100$  kHz,  $R_{off}^0 = 25$  kHz,  $x_\beta = 2.3$  Å and  $k_1 = 0.0036$  N/m. The Figure is obtained from Ref.[31].

for ferrocene and azobenzene. From the simulation we would expect such changes in rate dependence if the off-rates differ by a factor of ten.

Adamantane exhibits the lowest off-rate  $k_{off,ad}^{eff} = 8$  kHz leading to the highest overall pull-off force. Interestingly, the rate dependence is not as prominent as it is the case for the other two connector molecules although the off-rate is only slightly lower. The high pull-off force at low unloading rates suggests that a high number of bonds contributes already at low pulling velocities. This phenomenon was also observed for the friction force and is not yet fully understood. It is unlikely that the weak rate dependence is caused by a higher on-rate since the simulations reveal that the on-rate have a minor effect on the pull-off force.

In summary, the pull-off forces of the three different connector molecules is rate dependent in the range of investigated unloading rates which is in good agreement with the simulations by Guerra et al. [31]. The agreement of experiment and simulations reveal that the different rate dependence is caused by the different binding kinetics of the individual complexes. However, the rate dependence of the pull-off forces of the three connector molecules are surprisingly different although the off-rates differ only slightly indicating that



additional effects contribute which are not included in the model.

### 7.4.3 Velocity dependence of friction

In line with adhesion, the friction force increases with sliding velocity. We observe a different velocity dependence and different rupture characteristics for the different connector molecules. The friction loops of azobenzene and ferrocene exhibits a transition from smooth sliding to a beginning stick-slip characteristic. Our observation is in line with recent theoretical studies which predict the transition from uncorrelated thermal unbinding to a correlated rupture characteristic with increasing sliding speed. In the following the rate dependence of friction for the three connector molecules is discussed in relation to sliding velocity and bond kinetics.

Recent theoretical studies exhibit three different sliding regimes distinguished by a characteristic sliding time scale  $\tau = k_B T / (k_l v x_\beta)$  [33] where  $k_l$  is the molecular linker stiffness,  $v$  the sliding velocity and  $x_\beta$  the energy barrier width of the bond potential. The slow sliding regime ( $\tau \ll 1/k_{\text{off}}$ ) is characterized by a smooth sliding where the bonds thermally un- and rebind so that the average number of attached bonds is constant. Sliding faster, the thermal unbinding competes with force-induced rupture resulting in the intermediate regime ( $\tau \geq 1/k_{\text{off}}$ ) where stick-slip is observed. Higher sliding speeds ( $\tau \gg 1/k_{\text{on}}^{\text{eff}}$ ) lead to a reduced friction force because only a small number of bonds survive and the friction force is mainly caused by viscous damping of the surrounding liquid [31].

The different sliding regimes provide further understanding of our experimental data. In our experiment, the characteristic sliding time scale varies from  $\tau = 2$  ms for the lowest velocity to  $\tau = 20.5$   $\mu\text{s}$  for the highest velocity with the parameters  $x_\beta = 2.3$   $\text{\AA}$  obtained from chapter 5 and  $k_l = 1$  N/m obtained from chapter 4. Cyclodextrin inclusion complexes are characterized by a high on-rate at the surface which is diffusion limited and similar for all connector molecules. The high on-rate leads to a low minimum bond formation time  $1/(k_{\text{on}} C_{\text{eff}}) = 45$  ns which is three orders of magnitude lower than the lowest characteristic sliding time scale of our experiment. Due to the high on-rate we are well below the high velocity regime, i.e. we expect a constant rebinding of broken bonds.

For azobenzene and ferrocene, a linear increase of the friction force is observed above a critical velocity of  $v_c \approx 200$  nm/s. At this velocity, the characteristic sliding time scale  $\tau_c = k_B T / (k_l v_c x_\beta) = 50$   $\mu\text{s}$  is close to the life time of the individual bonds of azobenzene  $1/k_{\text{off,azo}}^{\text{eff}} = 80$   $\mu\text{s}$  and ferrocene  $1/k_{\text{off,fe}}^{\text{eff}} = 60$   $\mu\text{s}$ . Above the critical velocities, an irregular stick-slip characteristic emerges in the friction loop indicating a correlated bond rupture.

For lower sliding speeds, the thermal unbinding of the bonds leads to a smooth sliding and the friction force does not exceed the level of unspecific contributions.

Interestingly, a plateau is observed for ferrocene in an intermediate sliding regime in the range of 60 nm/s to 300 nm/s. It is conceivable that there is an intermediate regime, where a significant stress is applied to the bonds but the sliding speed is so low that broken bonds can rebind resulting in a force plateau. For higher speeds, the stick-slip movement indicates a cooperative interaction of several bonds which result in a larger stretching length and a suppression of the rebinding of broken bonds. Experimental evidence for the rebinding is provided by force curves recorded with high resolution where force jumps indicate the detachment and rebinding of several bonds. For adamantane and azobenzene no such jumps were observed although azobenzene exhibits a similar binding energy. The reason for the difference between azobenzene and ferrocene lies probably in the chemical structure of the connecting chain between the hydrophobic ends. The ferrocene connector molecules contain a positively charged amino group close to the hydrophobic group. This charge is assumed to interact with the hydrophilic hydroxyl plane of the CD molecule by forming hydrogen bonds resulting in an attractive interaction between the ferrocene connector and the CD molecules. There is a specific attractive interaction although the ferrocenyl end group does not enter the cyclodextrin cavity. This attractive interaction probably affects the binding kinetics of the ferrocene-cyclodextrin complex leading to a different rate dependence than observed for azobenzene although both molecules exhibit a similar binding affinity and constant.

Adamantane exhibits an exceptionally weak rate dependence although the binding affinity is only a factor of two larger than the binding affinity of ferrocene. A stick-slip movement in the friction loop is observed for all sliding speeds so that we assume that the rupture mechanisms are the same within the investigated range of sliding speeds. The weaker rate dependence may be caused by a contact ageing effect. During the “stick” phase of a stick-slip pattern, the contact could be strengthened by a rearrangement of  $\beta$ -CD molecules enlarging the number of connected bonds as it was observed for the pull-off force in chapter 4. The lateral distance of the “stick” phase is about 1 nm leading to a contact time of  $\Delta t = 125 \mu\text{s}$  for the highest velocity and  $\Delta t = 100 \text{ms}$  for the lowest velocity. Within this range, a logarithmic increase in the pull-off force was observed in chapter 4 which is in the order of several hundreds of piconewton and could lead to higher friction forces for low sliding velocities. This ageing effect increases the friction force for lower sliding speeds and is likely to counteracts the other rate effect.

The ageing effect is visualized in the force trace recorded at slow sliding velocities. Prominent force peaks are observed with a height comparable to the events observed in the high velocity regime. At high velocities, the force increase during the “stick” phase is followed by a sudden force drop, the “slip” phase. No force drop is observed at slow sliding velocities. Instead of a “slip” phase, several small force peaks are observed indicating that multiple bonds are ruptured subsequently. The ruptured bonds can rebind due to the slow movement of the cantilever. For azobenzene and ferrocene the ageing effect is negligible because of the raw and less pronounced stick-slip events.

## 7.5 Conclusion

In conclusion, we investigated the effects of supramolecular binding kinetics on dynamic friction and adhesion. A remarkable difference in the rate dependence of adhesive friction is observed for the three different connector molecules adamantane, azobenzene and ferrocene. The friction force and the shape of the friction loops of azobenzene and ferrocene are velocity dependent. We attribute the velocity dependence of the friction loops to the varying relation of sliding velocity and binding rates leading to a change in the rupture characteristics. With increasing sliding speed, the rupture of bonds changes from an uncorrelated thermally activated unbinding to a correlated rupture. The velocity dependence of the friction force and the friction loop are in good agreement with the simulations in Ref.[33, 31]. For adamantane, the friction loop exhibits a stick-slip characteristic for all investigated sliding speeds and a weak velocity dependence of the friction force was observed. We attribute the different rate dependence of adamantane to a combined effect of its high binding affinity and contact ageing effects. The high binding affinity compared to ferrocene and azobenzene leads to a lower off-rate resulting in continuous stick-slip events in the friction loop for all sliding speeds. During the stick-phase the contact can age by a rearrangement of the CD molecules. The duration of the “stick” phase increases with decreasing sliding speed leading to an inverse rate dependence which is likely to diminish the rate effect. The quantitative agreement between friction and adhesion demonstrates that adhesive friction in our system is predominantly caused by the rupture and reformation of supramolecular bonds formed between the AFM tip and surface.

## 8 Conclusions

A new surface functionalization was applied for controlling adhesive interactions and investigating the molecular mechanisms underlying adhesive friction. The interactions of single and multiple bonds were probed by the asperity of an AFM tip in aqueous environment. Connector molecules with two hydrophobic end groups form inclusion complexes with cyclodextrin molecules on the tip and at the surface. By varying the connector molecules the dynamics of friction and adhesion were tuned. Significant differences in the rate dependence of friction and adhesion were observed which could be attributed to the relation between complexation kinetics and sliding speed as proposed by Filippov et al. [33]. The transition from thermally activated unbinding to the collective bond rupture was observed as a change in the shape of the friction characteristic from smooth sliding to stick-slip movement of the AFM tip.

The flexibility of the attachment was demonstrated to have a remarkable effect on the adhesive interaction. Higher flexibility increases the number of bonds between AFM tip and surface leading to higher forces. Higher flexibility also leads to a stronger rate dependence of adhesion whereas in friction it results in a constant friction force over more than three orders of magnitude of sliding speed. The absence of a rate dependence of friction is attributed to a contact ageing effect which balances the rate effect. On a stiff molecular attachment, friction and adhesion forces are quantitatively in good agreement, providing evidence that adhesive friction is mainly caused by the rupture of molecular bonds. In conclusion, the compliance of the interacting surface layer has to be considered when answering the fundamental question if friction and adhesion are alike or not.

Single supramolecular complexes were probed in thermodynamic equilibrium due to their fast complexation kinetics compared to the time scale of an AFM experiment [2]. The molecular linker stiffness has no impact on the rupture force of single bonds in thermal equilibrium. This surprising contradiction to the Bell-Evans model was attributed to the fast complexation time of inclusion complex compared to the relaxation time of the AFM cantilever. The single bond rupture force increases proportional to the square root of the

cantilever stiffness, meaning that the rupture force is determined by the potential energy stored in the cantilever spring and its direct relation to the binding free energy of the inclusion complex.

To demonstrate one application of the new surface functionalization, friction and adhesion were switched by using photoresponsive connector molecules. In light-activated experiments, the binding between cyclodextrin and azobenzene derivatives were reversibly switched by UV and VIS light [1].

A further step towards application was taken by attaching the CD molecules onto a stiff polymer chain and attaching the polymers to the surfaces. The flexibility induced by the polymers enhances the adhesive interaction compared to stiffly bound CD monolayers by increasing the numbers of bonds. Depending on the attachment geometry, the stiff polymers exhibit a clear contrast between peeling and shearing mechanisms leading to a significant contrast in work of separation. The length distribution of the polymers allows to adjust the surface functionalization to more realistic contacts which exhibits a certain roughness. Finally, continuous wavelet transform has been demonstrated to be an effective tool for studying the attachment process of polymers to a surface.

In conclusion, the different chapters address different aspects of the dynamic effects in adhesive friction and provide a deep understanding of the underlying molecular mechanisms. The five most important results are as follows:

- Adhesive friction is caused by the cooperative rupture of supramolecular bonds.
- The dynamics in adhesion and friction can be tuned by changing the kinetics of the individual bonds.
- Adhesion and friction force can be switched by external light stimuli.
- The relation between adhesion and friction depends on the compliance of the molecular surface attachment.
- The rupture force of single bonds in thermal equilibrium is determined by the force probe stiffness and not by the stiffness of the molecular linker.



# Bibliography

- [1] J. Blass, B. L. Bozna, M. Albrecht, J. A. Krings, B. J. Ravoo, G. Wenz, and R. Bennewitz. Switching adhesion and friction by light using photosensitive guest–host interactions. *Chemical Communications*, 51(10):1830–1833, 2015.
- [2] J. Blass, M. Albrecht, B. L. Bozna, G. Wenz, and R. Bennewitz. Dynamic effects in friction and adhesion through cooperative rupture and formation of supramolecular bonds. *Nanoscale*, 7(17):7674–7681, 2015.
- [3] C. R. Martin and L. A. Baker. Expanding the molecular electronics toolbox. *Science*, 309(5731):67–68, 2005.
- [4] M. Pita, M. Krämer, J. Zhou, A. Poghossian, M. J. Schoning, V. M. Fernandez, and E. Katz. Optoelectronic properties of nanostructured ensembles controlled by biomolecular logic systems. *ACS nano*, 2(10):2160–2166, 2008.
- [5] V. Wagner, A. Dullaart, A. Bock, and A. Zweck. The emerging nanomedicine landscape. *Nature biotechnology*, 24(10):1211–1217, 2006.
- [6] D. A. Pippig, F. Baumann, M. Strackharn, D. Aschenbrenner, and H. E. Gaub. Protein–dna chimeras for nano assembly. *ACS nano*, 8(7):6551–6555, 2014.
- [7] H. Lee, N. F. Scherer, and P. B. Messersmith. Single-molecule mechanics of mussel adhesion. *Proceedings of the National Academy of Sciences*, 103(35):12999–13003, 2006.
- [8] E. Evans and P. Williams. Dynamic force spectroscopy. In *Physics of bio-molecules and cells. Physique des biomolécules et des cellules*, pages 145–204. Springer, 2002.
- [9] P. Ball. Natural strategies for the molecular engineer. *Nanotechnology*, 13(5):R15, 2002.

- 
- [10] J. Bacharouche, M. Degardin, L. Jierry, C. Carteret, P. Lavalle, J. Hemmerlé, B. Senger, R. Auzély-Velty, F. Boulmedais, D. Boturyn, et al. Multivalency: influence of the residence time and the retraction rate on rupture forces measured by afm. *Journal of Materials Chemistry B*, 3(9):1801–1812, 2015.
- [11] J. D. Badjic, A. Nelson, S. J. Cantrill, W. B. Turnbull, and J. F. Stoddart. Multivalency and cooperativity in supramolecular chemistry. *Accounts of Chemical Research*, 38(9):723–732, 2005.
- [12] C. Fasting, C. A. Schalley, M. Weber, O. Seitz, S. Hecht, B. Kokschi, J. Dervede, C. Graf, E. Knapp, and R. Haag. Cover picture: Multivalency as a chemical organization and action principle (angewandte chemie international edition 42/2012). *Angewandte Chemie International Edition in English*, 51(42):10419–10419, 2012.
- [13] M. Mammen, S. Choi, and G. M. Whitesides. Polyvalent interactions in biological systems: implications for design and use of multivalent ligands and inhibitors. *Angewandte Chemie International Edition*, 37(20):2754–2794, 1998.
- [14] F. Vögtle and F. Alfter. *Supramolecular chemistry: an introduction*. Wiley, 1993.
- [15] A. Harada, R. Kobayashi, Y. Takashima, A. Hashidzume, and H. Yamaguchi. Macroscopic self-assembly through molecular recognition. *Nature chemistry*, 3(1):34–37, 2010.
- [16] F. Herbst, D. Döhler, P. Michael, and W. H. Binder. Self-healing polymers via supramolecular forces. *Macromolecular rapid communications*, 34(3):203–220, 2013.
- [17] A. Gomez-Casado, H. H. Dam, M. D. Yilmaz, D. Florea, P. Jonkheijm, and J. Huskens. Probing multivalent interactions in a synthetic host–guest complex by dynamic force spectroscopy. *Journal of the American Chemical Society*, 133(28):10849–10857, 2011.
- [18] G. Wenz. Cyclodextrins as building blocks for supramolecular structures and functional units. *Angewandte Chemie International Edition in English*, 33(8):803–822, 1994.
- [19] M. V. Rekharsky and Y. Inoue. Complexation thermodynamics of cyclodextrins. *Chemical reviews*, 98(5):1875–1918, 1998.



- 
- [20] K. Huang, S. Gast, C. D. Ma, N. L. Abbott, and I. Szlufarska. Comparison between free and immobilized ion effects on hydrophobic interactions: A molecular dynamics study. *The Journal of Physical Chemistry B*, 119(41):13152–13159, 2015.
- [21] G. Wenz, C. Strassnig, C. Thiele, A. Engelke, B. Morgenstern, and K. Hegetschweiler. Recognition of ionic guests by ionic  $\beta$ -cyclodextrin derivatives. *Chem. Eur. J.*, 14(24):7202–7211, 2008.
- [22] M. Smoluchowski et al. Versuch einer mathematischen theorie der koagulationskinetik kolloider lösungen. 1917.
- [23] H. Schönherr, M. W. J. Beulen, J. Bügler, J. Huskens, F. C. J. M. van Veggel, D. N. Reinhoudt, and G. J. Vancso. Individual supramolecular host-guest interactions studied by dynamic single molecule force spectroscopy. *Journal of the American Chemical Society*, 122(20):4963–4967, 2000.
- [24] G. I. Bell. Models for the specific adhesion of cells to cells. *Science*, 200(4342):618–627, 1978.
- [25] J. Zlatanova, S. M. Lindsay, and S. H. Leuba. Single molecule force spectroscopy in biology using the atomic force microscope. *Progress in biophysics and molecular biology*, 74(1):37–61, 2000.
- [26] P. Hinterdorfer and Y. F. Dufrêne. Detection and localization of single molecular recognition events using atomic force microscopy. *Nature methods*, 3(5):347–355, 2006.
- [27] E. M. Puchner and H. E. Gaub. Force and function: probing proteins with AFM-based force spectroscopy. *Current opinion in structural biology*, 19(5):605–614, 2009.
- [28] R. W. Friddle, P. Podsiadlo, A. B. Artyukhin, and A. Noy. Near-equilibrium chemical force microscopy. *The Journal of Physical Chemistry C*, 112(13):4986–4990, 2008.
- [29] R. W. Friddle, A. Noy, and J. J. De Yoreo. Interpreting the widespread nonlinear force spectra of intermolecular bonds. *Proceedings of the National Academy of Sciences*, 109(34):13573–13578, 2012.
- [30] P. M. Williams. Analytical descriptions of dynamic force spectroscopy: behaviour of multiple connections. *Analytica Chimica Acta*, 479(1):107–115, 2003.

- [31] R. Guerra, A. Benassi, A. Vanossi, M. Ma, and M. Urbakh. Friction and adhesion mediated by supramolecular host-guest complexes. *Physical Chemistry Chemical Physics*, 18:9248–9254, 2016.
- [32] M. H. Müser. Velocity dependence of kinetic friction in the prandtl-tomlinson model. *Physical Review B*, 84(12):125419, 2011.
- [33] A. E. Filippov, J. Klafter, and M. Urbakh. Friction through dynamical formation and rupture of molecular bonds. *Physical Review Letters*, 92(13):135503, 2004.
- [34] Q. Li, T. E. Tullis, D. Goldsby, and R. W. Carpick. Frictional ageing from interfacial bonding and the origins of rate and state friction. *Nature*, 480(7376):233–236, 2011.
- [35] I. Barel, M. Urbakh, L. Jansen, and A. Schirmeisen. Multibond dynamics of nanoscale friction: the role of temperature. *Physical review letters*, 104(6):066104, 2010.
- [36] G. Binnig, C. F. Quate, and C. Gerber. Atomic force microscope. *Physical review letters*, 56(9):930, 1986.
- [37] E. Meyer, H. J. Hug, and R. Bennewitz. *Scanning probe microscopy: the lab on a tip*. Springer Science & Business Media, 2013.
- [38] E. Meyer, T. Gyalog, R. M. Overney, and K. Dransfeld. *Nanoscience: friction and rheology on the nanometer scale*. World Scientific, 1998.
- [39] C. P. Green, H. Lioe, J. P. Cleveland, R. Proksch, P. Mulvaney, and J. E. Sader. Normal and torsional spring constants of atomic force microscope cantilevers. *Review of scientific instruments*, 75(6):1988–1996, 2004.
- [40] H. Wang and M. L. Gee. AFM lateral force calibration for an integrated probe using a calibration grating. *Ultramicroscopy*, 136:193–200, 2014.
- [41] John E Sader. Frequency response of cantilever beams immersed in viscous fluids with applications to the atomic force microscope. *Journal of applied physics*, 84(1):64–76, 1998.
- [42] M. Varenberg, I. Etsion, and G. Halperin. Crosstalk problems in scanning-by-probe atomic force microscopy. *Review of scientific instruments*, 74(7):3569–3571, 2003.

- 
- [43] E. Tocha, J. Song, H. Schönherr, and G. J. Vancso. Calibration of friction force signals in atomic force microscopy in liquid media. *Langmuir*, 23(13):7078–7082, 2007.
- [44] J. Lahann, S. Mitragotri, T. Tran, H. Kaido, J. Sundaram, I. S. Choi, S. Hoffer, G. A. Somorjai, and R. Langer. A reversibly switching surface. *Science*, 299(5605):371–374, 2003.
- [45] Y. F. Dufrêne, W. R. Barger, J.-B. Green, and G. U. Lee. Nanometer-scale surface properties of mixed phospholipid monolayers and bilayers. *Langmuir*, 13(18):4779–4784, 1997.
- [46] D. J. Díaz, J. E. Hudson, G. D. Storrier, H. D. Abruña, N. Sundararajan, and C. K. Ober. Lithographic applications of redox probe microscopy. *Langmuir*, 17(19):5932–5938, 2001.
- [47] M. Lemieux, D. Usov, S. Minko, M. Stamm, H. Shulha, and V. V. Tsukruk. Reorganization of binary polymer brushes: Reversible switching of surface microstructures and nanomechanical properties. *Macromolecules*, 36(19):7244–7255, 2003.
- [48] V. Kolivoška, M. Mohos, I. V. Pobelov, S. Rohrbach, K. Yoshida, W. J. Hong, Y. C. Fu, P. Moreno-García, G. Mészáros, P. Broekmann, et al. Electrochemical control of a non-covalent binding between ferrocene and beta-cyclodextrin. *Chemical Communications*, 50(79):11757–11759, 2014.
- [49] T. Kobayashi, E.O. Degenkolb, and P.M. Rentzepis. Picosecond spectroscopy of 1-phenylazo-2-hydroxynaphthalene. *Journal of Physical Chemistry*, 83(19):2431–2434, 1979.
- [50] I. K. Lednev, T. Ye, R. E. Hester, and J. N. Moore. Femtosecond time-resolved uv-visible absorption spectroscopy of trans-azobenzene in solution. *The Journal of Physical Chemistry*, 100(32):13338–13341, 1996.
- [51] W. R. Browne and B. L. Feringa. Light switching of molecules on surfaces. *Annual Review of Physical Chemistry*, 60:407–428, 2009.
- [52] K. G. Yager and C. J. Barrett. Novel photo-switching using azobenzene functional materials. *Journal of Photochemistry and Photobiology A: Chemistry*, 182(3):250–261, 2006.

- 
- [53] Z. Liu and M. Jiang. Reversible aggregation of gold nanoparticles driven by inclusion complexation. *Journal of Materials Chemistry*, 17(40):4249–4254, 2007.
- [54] J. Voskuhl, S. Sankaran, and P. Jonkheijm. Optical control over bioactive ligands at supramolecular surfaces. *Chemical communications*, 50(96):15144–15147, 2014.
- [55] N. B. Holland, T. Hugel, G. Neuert, A. Cattani-Scholz, C. Renner, D. Oesterhelt, L. Moroder, M. Seitz, and H. E. Gaub. Single molecule force spectroscopy of azobenzene polymers: switching elasticity of single photochromic macromolecules. *Macromolecules*, 36(6):2015–2023, 2003.
- [56] S. K. M. Nalluri and B. J. Ravoo. Light-responsive molecular recognition and adhesion of vesicles. *Angewandte Chemie International Edition*, 49(31):5371–5374, 2010.
- [57] S. Zapotoczny, T. Auletta, M. R. de Jong, H. Schönherr, F. C. J. M. van Veggel, J. Huskens, D. N. Reinhoudt, and G. J. Vancso. Chain length and concentration dependence of  $\beta$ -cyclodextrin-ferrocene host-guest complex rupture forces probed by dynamic force spectroscopy. *Langmuir*, 18(18):6988–6994, 2002.
- [58] T. Auletta, B. Dordi, A. Mulder, A. Sartori, S. Onclin, C. M. Bruinink, M. Peter, C. A. Nijhuis, H. Beijleveld, H. Schönherr, et al. Writing patterns of molecules on molecular printboards. *Angewandte Chemie*, 116(3):373–377, 2004.
- [59] O. Kaftan, S. Tumbiolo, F. Dubreuil, R. Auzély-Velty, A. Fery, and G. Papastavrou. Probing multivalent host-guest interactions between modified polymer layers by direct force measurement. *The Journal of Physical Chemistry B*, 115(24):7726–7735, 2011.
- [60] A. Samanta and B. J. Ravoo. Metal ion, light, and redox responsive interaction of vesicles by a supramolecular switch. *Chemistry—A European Journal*, 20(17):4966–4973, 2014.
- [61] A. Mulder, T. Auletta, A. Sartori, S. Del Ciotto, A. Casnati, R. Ungaro, J. Huskens, and D. N. Reinhoudt. Divalent binding of a bis(adamantyl)-functionalized calix[4]arene to  $\beta$ -cyclodextrin-based hosts: An experimental and theoretical study on multivalent binding in solution and at self-assembled monolayers. *Journal of the American Chemical Society*, 126:6627–6636, 2004.

- 
- [62] E. Gnecco, R. Bennewitz, T. Gyalog, and E. Meyer. Friction experiments on the nanometre scale. *Journal of Physics: Condensed Matter*, 13(31):R619, 2001.
- [63] S. K. M. Nalluri, J. B. Bultema, E. J. Boekema, and B. J. Ravoo. Photoresponsive molecular recognition and adhesion of vesicles in a competitive ternary supramolecular system. *Chemistry-A European Journal*, 17(37):10297–10303, 2011.
- [64] F. P. Bowden and D. Tabor. *The friction and lubrication of solids*. Clarendon Press, Oxford, 2008.
- [65] S. Raman, T. Utzig, T. Baimpos, B. R. Shrestha, and M. Valtiner. Deciphering the scaling of single-molecule interactions using jarzynski's equality. *Nature communications*, 5:1–7, 2014.
- [66] X. L. Qui, G. Li, G. Wu, J. Zhu, L. Zhou, P. L. Chen, A. R. Chamberlin, and W. H. Lee. *J. Med. Chem.*, 52:1757–1767, 2009.
- [67] T. Yamamoto, A. Terada, T. Muramatsu, and K. Ikeda. Synthesis of alkyl isothiocyanates from primary alkyl amines using dicyandiamide as a dehydrosulfurizing agent. *Organic preparations and procedures international*, 26(5):555–557, 1994.
- [68] M. V. Rekharsky and Y. Inoue. Complexation thermodynamics of cyclodextrins. *Chemical Reviews*, 98:1875–1917, 1998.
- [69] J. N. Kinkel, B. Anspach, K. K. Unger, R. Wieser, and G. Brunner. Separation of plasma membrane proteins of cultured human fibroblasts by affinity chromatography on bonded microparticulate silicas. *Journal of Chromatography A*, 297:167–177, 1984.
- [70] A. Embrechts, H. Schönherr, and G. J. Vancso. Forced unbinding of individual urea-aminotriazine supramolecular polymers by atomic force microscopy: A closer look at the potential energy landscape and binding lengths at fixed loading rates. *The Journal of Physical Chemistry B*, 116(1):565–570, 2011.
- [71] M. Novo, D. Granadero, J. Bordello, and W. Al-Soufi. Host-guest association studied by fluorescence correlation spectroscopy. *Journal of Inclusion Phenomena and Macrocyclic Chemistry*, 70(3-4):259–268, 2011.
- [72] D. Pussak, D. Ponader, S. Mosca, T. Pompe, L. Hartmann, and S. Schmidt. Specific adhesion of carbohydrate hydrogel particles in competition with multivalent inhibitors evaluated by AFM. *Langmuir*, pages 6142–6150, 2014.

- [73] P. Silberzan, L. Leger, D. Ausserre, and J. J. Benattar. Silanation of silica surfaces. a new method of constructing pure or mixed monolayers. *Langmuir*, 7(8):1647–1651, 1991.
- [74] V. V. Naikrant, M. Crobu, N. V. Venkataraman, and N. D. Spencer. Multiple transmission-reflection ir spectroscopy shows that surface hydroxyls play only a minor role in alkylsilane monolayer formation on silica. *The Journal of Physical Chemistry Letters*, 4(16):2745–2751, 2013.
- [75] S. Onclin, B. J. Ravoo, and D. N. Reinhoudt. Engineering silicon oxide surfaces using self-assembled monolayers. *Angewandte Chemie International Edition*, 44(39):6282–6304, 2005.
- [76] A. Ulman. Formation and structure of self-assembled monolayers. *Chemical reviews*, 96(4):1533–1554, 1996.
- [77] P. Silberzan, L. Leger, D. Ausserre, and J. J. Benattar. Silanation of silica surfaces. a new method of constructing pure or mixed monolayers. *Langmuir*, 7(8):1647–1651, 1991.
- [78] T. Vallant, H. Brunner, U. Mayer, H. Hoffmann, T. Leitner, R. Resch, and G. Friedbacher. Formation of self-assembled octadecylsiloxane monolayers on mica and silicon surfaces studied by atomic force microscopy and infrared spectroscopy. *The Journal of Physical Chemistry B*, 102(37):7190–7197, 1998.
- [79] Y. Wang and M. Lieberman. Growth of ultrasMOOTH octadecyltrichlorosilane self-assembled monolayers on sio<sub>2</sub>. *Langmuir*, 19(4):1159–1167, 2003.
- [80] Y. Liu, L. K. Wolf, and M. C. Messmer. A study of alkyl chain conformational changes in self-assembled n-octadecyltrichlorosilane monolayers on fused silica surfaces. *Langmuir*, 17(14):4329–4335, 2001.
- [81] M Lessel, O Bäumchen, M Klos, H Hähl, R Fetzer, M Paulus, R Seemann, and K Jacobs. Self-assembled silane monolayers: an efficient step-by-step recipe for high-quality, low energy surfaces. *Surface and Interface Analysis*, 47(5):557–564, 2015.
- [82] Y. Xie, C. A. S. Hill, Z. Xiao, H. Miltz, and C. Mai. Silane coupling agents used for natural fiber/polymer composites: A review. *Composites Part A: Applied Science and Manufacturing*, 41(7):806–819, 2010.

- 
- [83] V. V. Naik, R. Städler, and N. D. Spencer. Effect of leaving group on the structures of alkylsilane sams. *Langmuir*, 30(49):14824–14831, 2014.
- [84] E. B Walton, S. Lee, and K. J. Van Vliet. Extending bell’s model: how force transducer stiffness alters measured unbinding forces and kinetics of molecular complexes. *Biophysical journal*, 94(7):2621–2630, 2008.
- [85] Z Tshiprut, J Klafter, and M Urbakh. Single-molecule pulling experiments: When the stiffness of the pulling device matters. *Biophysical journal*, 95(6):L42–L44, 2008.
- [86] O. K. Dudko, A. E. Filippov, J. Klafter, and M. Urbakh. Beyond the conventional description of dynamic force spectroscopy of adhesion bonds. *Proceedings of the National Academy of Sciences*, 100(20):11378–11381, 2003.
- [87] B. Heymann and H. Grubmüller. Elastic properties of poly (ethylene-glycol) studied by molecular dynamics stretching simulations. *Chemical Physics Letters*, 307(5):425–432, 1999.
- [88] J. Y. Wong, T. L. Kuhl, J. N. Israelachili, N. Mullah, and S. Zalipsky. Direct measurement of a tethered ligand-receptor interaction potential. *Science*, 275(5301):820–822, 1997.
- [89] T. Auletta, M. R. de Jong, A. Mulder, F. C. van Veggel, J. Huskens, D. N. Reinhoudt, S. Zou, S. Zaopotoczny, H. Schönherr, G. J. Vancso, and L. Kuipers.  $\beta$ -cyclodextrin host-guest complexes probed under thermodynamic equilibrium: Thermodynamics and AFM force spectroscopy. *Journal of the American Chemical Society*, 126:1577–1584, 2004.
- [90] M. Evstigneev and P. Reimann. Force dependence of energy barriers in atomic friction and single-molecule force spectroscopy: critique of a critical scaling relation. *Journal of Physics: Condensed Matter*, 27(12):125004, 2015.
- [91] B. L. Bozna, J. Blass, M. Albrecht, F. Hausen, G. Wenz, and R. Bennewitz. Friction mediated by redox-active supramolecular connector molecules. *Langmuir*, 31(39):10708–10716, 2015.
- [92] K. Lindner and W. Saenger.  $\beta$ -cyclodextrin dodecahydrate: Crowding of water molecules within a hydrophobic cavity. *Angewandte Chemie International Edition in English*, 17(9):694–695, 1978.

- 
- [93] W. C. Cromwell, K. Bystrom, and M. R. Eftink. Cyclodextrin-adamantanecarboxylate inclusion complexes: studies of the variation in cavity size. *The Journal of Physical Chemistry*, 89(2):326–332, 1985.
- [94] A. Karmakar and A. Chandra. Water in hydration shell of an iodide ion: structure and dynamics of solute-water hydrogen bonds and vibrational spectral diffusion from first-principles simulations. *The Journal of Physical Chemistry B*, 119(27):8561–8572, 2015.
- [95] G. V. Dubacheva, T. Curk, B. M. Mognetti, R. Auzély-Velty, D. Frenkel, and R. P. Richter. Superselective targeting using multivalent polymers. *Journal of the American Chemical Society*, 136(5):1722–1725, 2014.
- [96] S.K. Kufer, E.M. Puchner, H. Gump, T. Liedl, and H.E. Gaub. Single-molecule cut-and-paste surface assembly. *Science*, 319(5863):594–596, 2008.
- [97] M. J. Ludden, D. N. Reinhoudt, and J. Huskens. Molecular printboards: versatile platforms for the creation and positioning of supramolecular assemblies and materials. *Chemical Society Reviews*, 35(11):1122–1134, 2006.
- [98] M. Rief, M. Gautel, and H. E. Gaub. Unfolding forces of titin and fibronectin domains directly measured by afm. In *Elastic Filaments of the Cell*, pages 129–141. Springer, 2000.
- [99] N. Thewes, A. Thewes, P. Loskill, H. Peisker, M. Bischoff, M. Herrmann, L. Santen, and K. Jacobs. Stochastic binding of staphylococcus aureus to hydrophobic surfaces. *Soft matter*, 11(46):8913–8919, 2015.
- [100] S. Maier, Y. Sang, T. Filleter, M. Grant, R. Bennewitz, E. Gnecco, and E. Meyer. Fluctuations and jump dynamics in atomic friction experiments. *Physical Review B*, 72(24):245418, 2005.
- [101] G. Malegori and G. Ferrini. Tip-sample interactions on graphite studied using the wavelet transform. *Beilstein journal of nanotechnology*, 1(1):172–181, 2010.
- [102] A. R. Bizzarri. Energy landscape investigation by wavelet transform analysis of atomic force spectroscopy data in a biorecognition experiment. *Journal of biological physics*, 42(1):167–176, 2016.



- 
- [103] B. T. Marshall, K. K. Sarangapani, J. Wu, M. B. Lawrence, R. P. McEver, and C. Zhu. Measuring molecular elasticity by atomic force microscope cantilever fluctuations. *Biophysical journal*, 90(2):681–692, 2006.
- [104] H. J. Butt and M. Jaschke. Calculation of thermal noise in atomic force microscopy. *Nanotechnology*, 6(1):1, 1995.
- [105] M. Farge. Wavelet transforms and their applications to turbulence. *Annual review of fluid mechanics*, 24(1):395–458, 1992.
- [106] C. Torrence and G. P. Compo. A practical guide to wavelet analysis. *Bulletin of the American Meteorological society*, 79(1):61–78, 1998.
- [107] Y. Deng, C. Wang, L. Chai, and Z. Zhang. Determination of gabor wavelet shaping factor for accurate phase retrieval with wavelet-transform. *Applied Physics B*, 81(8):1107–1111, 2005.
- [108] R.W. Fearick. Wavelet script. webpage of Yale University, 04 2016. ©2012, R.W. Fearick, University of Cape Town. <http://senselab.med.yale.edu/modeldb/showmodel.cshtm>.
- [109] A. Ptak, H. Gojzewski, M. Kappl, and H. Butt. Quantitative analysis of the interaction between an atomic force microscopy tip and a hydrophobic monolayer. *The Journal of Physical Chemistry C*, 114(49):21572–21578, 2010.
- [110] S. P. Pujari, Y. Li, R. Regeling, and H. Zuilhof. Tribology and stability of organic monolayers on crn: a comparison among silane, phosphonate, alkene, and alkyne chemistries. *Langmuir*, 29(33):10405–10415, 2013.
- [111] E. Gnecco, R. Bennewitz, T. Gyalog, C. Loppacher, M. Bammerlin, E. Meyer, and H-J H. Güntherodt. Velocity dependence of atomic friction. *Physical Review Letters*, 84(6):1172, 2000.
- [112] W. V. Gerasimowicz and J. F. Wojcik. Azo dye- $\alpha$ -cyclodextrin adduct formation. *Bioorganic Chemistry*, 11(4):420–427, 1982.
- [113] J. Huskens, A. Mulder, T. Auletta, C. A. Nijhuis, M. J. W. Ludden, and D. N. Reinhoudt. A model for describing the thermodynamics of multivalent host-guest interactions at interfaces. *Journal of the American Chemical Society*, 126(21):6784–6797, 2004.



# Publications

In the context of this work at the INM - Leibniz Institute for New Materials, Saarbücken, Germany the following contributions were published:

## Peer reviewed articles

- J. Blass, M. Albrecht, B. L. Bozna, G. Wenz, R. Bennewitz. Dynamic effects in friction and adhesion through cooperative rupture and formation of supramolecular bonds. *Nanoscale* 7 17, 7674-7681, 2015.  
<http://dx.doi.org/10.1039/C5NR00329F>
- B. L. Bozna, J. Blass, M. Albrecht, F. Hausen, G. Wenz, R. Bennewitz. Friction mediated by redox-active supramolecular connector molecules. *Langmuir* 31 39, 10708-10716, 2015.  
<http://dx.doi.org/10.1021/acs.langmuir.5b03026>
- J. Blass, B. L. Bozna, M. Albrecht, J. Krings, B. J. Ravoo, G. Wenz, R. Bennewitz. Switching adhesion and friction by light using photosensitive guest-host interactions. *Chemical Communications* 51 10, 1830-1833, 2015.  
<http://dx.doi.org/10.1039/C4CC09204J>

## Talks

- *Invited*: Controlling friction and adhesion by supramolecular assemblies. J. Blass, B. L. Bozna., M. Albrecht, G. Wenz, and R. Bennewitz. *6th European Nanomanipulation Workshop, September 23, 2015, Gießen.*
- *Invited*: AFM study on dynamic friction and adhesion mediated by supramolecular bonds. J. Blass, M. Albrecht, G. Wenz, and R. Bennewitz. *Harvard Medical*

*School, Seminar, Department of Biological Chemistry and Molecular Pharmacology, December 18, 2015, Boston.*

- Molecular toolkit for surface materials with switchable tribological functions. J. Blass, M. Albrecht, G. Wenz, and R. Bennewitz. *McGill University, Seminar talk, Department of Physics, August 03, 2015, Montreal.*
- Friction and adhesion on cyclodextrin assemblies for different connector molecules. J. Blass, M. Albrecht, B. L. Bozna, G. Wenz, and R. Bennewitz. *International Conference on Understanding and Controlling Nano and Mesoscale Friction, June 21-27, 2015, Istanbul.*
- Single host-guest interactions of self-assembled monolayers on activated silicon. J. Blass, F. Hausen, M. Albrecht, G. Wenz, and R. Bennewitz. *PhD Student's Day, April 25-26, 2013, Saarbrücken.*

## Posters

- Dynamic effects in friction and adhesion mediated by supramolecular bonds. J. Blass, M. Albrecht, B. L. Bozna, G. Wenz, and R. Bennewitz. *GRC Science of Adhesion, July 29, 2015, Holyoke.*
- Molecular toolkit for surface materials with switchable tribological functions. J. Blass, B. L. Bozna, F. Hausen, M. Albrecht, G. Wenz, and R. Bennewitz. *Soft Matter+ Day, University of Twente, June 04, 2015, Enschede.*
- Anisotropy of dynamic friction and adhesion force on cyclodextrin assemblies mediated by ditopic guest molecules. J. Blass, B. L. Bozna, F. Hausen, M. Albrecht, G. Wenz, and R. Bennewitz. *Gordon Research Conference on Tribology, Bentley University, July 19-20, 2014, Waltham.*
- A molecular toolkit based on cyclodextrin polymers for surface materials with switchable tribological functions. B. L. Bozna, J. Blass, F. Hausen, M. Albrecht, Krings, Jennifer A., G. Wenz, Ravoo, Bart Jan, and R. Bennewitz. *17th International Cyclodextrin Symposium (ICS17), May 29-31, 2014, Saarbrücken.*

- Single host-guest interactions on self-assembled monolayers mediated by ditopic guest molecules. J. Blass, B. L. Bozna, F. Hausen, M. Albrecht, G. Wenz, and R. Bennewitz. *International Nanotribology Forum, January 06-10, 2014, Kochi.*
- Single host-guest interactions on self-assembled monolayers mediated by ditopic guest molecules. J. Blass, B. L. Bozna, F. Hausen, M. Albrecht, G. Wenz, and R. Bennewitz. *Soft Control Conference, September 22-24, 2013, Darmstadt.*
- Scanning Force Microscopy applied to protein adhesion and nano-assemblies. J. Blass, F. Hausen, M. Albrecht, A. Hermsdörfer, O. Köhler, C. Müller, G. Wenz, C. Ziegler, and R. Bennewitz. *XV. Annual Linz Winter Workshop, February 15-18, 2013, Linz.*



# Danke!

An dieser Stelle möchte ich allen Danken, die mich während meiner Promotionsphase unterstützt haben. Mein besonderer Dank gilt Roland Bennewitz für die interessante Themenstellung, die vielen Anregungen und Diskussionen und die immer offene Tür. Des Weiteren danke ich Karin Jacobs für die Übernahme des Zweitgutachtens. Für die gute Zusammenarbeit möchte ich der Arbeitsgruppe von Gerhard Wenz danken. Mein Dank gilt besonders Gerhard Wenz, Marcel Albrecht, Jessica Brunke und Yan Nan Zhang, die mit ihren "Kochkünsten" die in dieser Arbeit verwendeten Makromoleküle synthetisiert, mich in die chemischen Grundlagen eingeführt und mit vielen Ideen zu dieser Arbeit beigetragen haben.

Franziska Emmerich danke ich für die mutige Arbeit mit denen uns vorher recht unbekannt Polymeren und die immer gute Laune auch wenn die Silane nicht immer das gemacht haben was wir wollten. Florian Hausen danke ich für die Einführung in das Thema und die Unterstützung besonders in der Anfangsphase. Felix Wählich möchte ich für die Erarbeitung eines Auswertungsskripts und die Einführung in Python danken. I would like to thank Bianca Liliana Bozna who successfully implemented the electrochemistry in our project and contributed with valuable suggestions to this work.

Mein großer Dank gilt der ganzen Arbeitsgruppe Nanotribologie für die gute Zusammenarbeit, große Hilfsbereitschaft und schöne Arbeitsatmosphäre. Ich möchte meinen Bürokollegen Thomas Kister, Susanne Selzer, Balakrishna Soorali Ganeshamurthy, Florian Hausen und Arzu Colak danken, sowie allen Kollegen am INM, die mir die Saarländische Kultur näher gebracht und während der Arbeit für die manchmal nötige Abwechslung gesorgt haben!

Ganz besonders danke ich meiner Familie für das große Interesse und die liebevolle Unterstützung. Vielen Dank an meinen Patenonkel Dieter und meine Schwester Katharina für das Korrekturlesen dieser Arbeit. Mein ganz besonderer Dank gilt Ulrich für seine Unterstützung, die Korrekturen, seine unermüdete Geduld und die Erinnerung daran, dass es Wichtigeres im Leben gibt als zu promovieren.

VIELEN DANK!